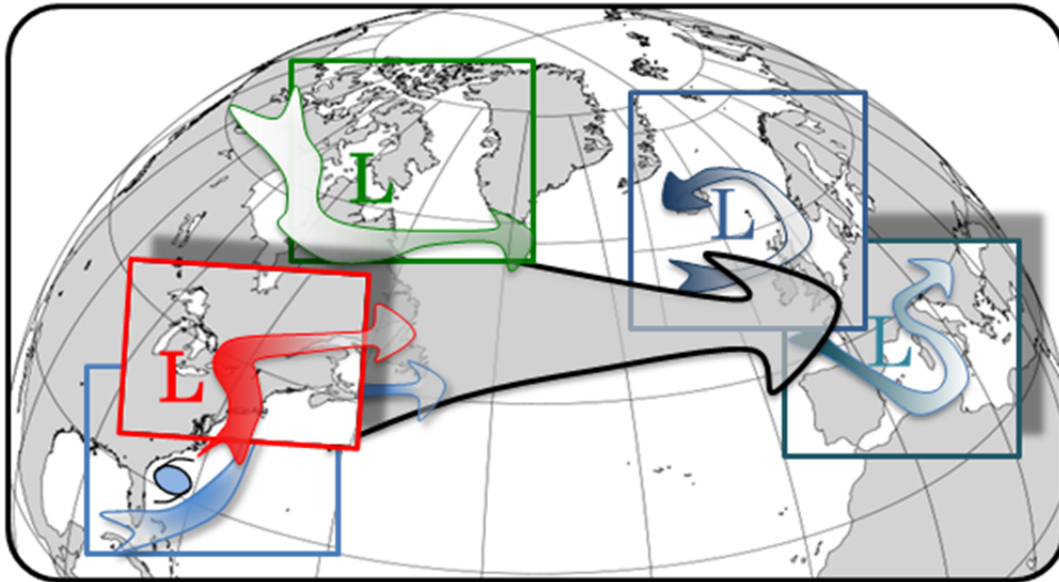


Campaign Implementation Plan

for the deployment of HALO and Falcon in

NAWDEX



North Atlantic Waveguide and Downstream Impact Experiment

Number of pages:	78	
Prepared by	Schäfler Andreas (DLR) Böttcher Maxi (ETH) Craig George (LMU) Dörnbrack Andreas (DLR) Ehrlich André (U Leipzig) Hagen Martin (DLR) Hirsch Lutz (MPI)	Mech Mario (U Köln) Quinting Julian (ETH) Rautenhaus Marc (TU Munich) Reitebuch Oliver (DLR) Wirth Martin (DLR) Groß Silke(DLR) Wernli Heini (ETH)
Last change	19 February 2016	



1	Introduction and Purpose of Document	4
2	Objectives	4
2.1	The mission	4
2.2	Scientific background	4
2.3	Planned observations	6
2.4	National and International network	7
3	Science Questions	9
3.1	International Science Hypotheses	9
3.1.1	Overarching hypothesis	9
3.1.2	Diabatic processes and impact on the potential vorticity	9
A)	Diabatic processes affecting Rossby wave packets (upscale effect):	9
B)	Diabatic processes directly implied in high-impact weather events (downscale influence)	10
3.1.3	Potentially misrepresented diabatic processes in models and impact on the circulation	10
A)	Rossby wave packets	10
B)	High-impact weather, and downscale influence of Rossby wave packets	11
3.2	Primary Objectives	12
3.2.1	Moisture Structure in the Boundary layer	12
3.2.2	Mixed phase clouds	13
3.2.3	Upper level PV	14
3.2.4	Diabatic effects on cyclonic systems	15
3.2.5	Impacts of tropopause waveguide uncertainty on HIW events	16
3.2.6	Moisture and Cloud Structure in Tropopause Region	17
3.2.7	Quantification of analysis errors	17
3.2.8	Lagrangian Tracking of disturbances	18
3.2.9	Initial condition sensitivity and predictability of high-impact weather downstream	18
3.2.10	Overview of strategies	20
3.3	Secondary Objectives	21
3.3.1	Earth Care Preparation	21
3.3.2	ADM Preparation	21
3.3.3	Turbulence observations near jet-streams	22
3.4	Priorities of the objectives	22
3.5	Contribution of NAWDEX instrumentation to the objectives	23
4	Aircraft Platforms & Instrumentation	24
4.1	HALO	24
4.1.1	Aircraft properties	24
4.1.2	Instrumentation	25
4.1.3	HAMP (HALO Microwave Package):	25
4.1.4	WALES	29
4.1.5	HALO-SR	31
4.1.6	specMACS	33
4.1.7	Dropsondes	34
4.2	Dassault Falcon 20-E5	35
4.2.1	Aircraft properties	35
4.2.2	Instrumentation	35
5	Logistics	38
5.1	General information	38

5.2	Flight operation.....	38
5.3	Mission Operation (for FX, to be iterated)	40
5.4	Schedule	40
5.5	Personnel	40
5.6	Flight restrictions	41
5.6.1	Operation in transatlantic air-space	41
5.6.2	Operation in European airspace	42
5.6.3	Planning process	43
5.6.4	Ideal setup	44
5.7	Pilots working hours	44
6	Data handling.....	45
7	Preparation	46
7.1	Previous cases in the campaign period.....	46
7.1.1	Extratropical transition of TC Rafael (2012) – the western North Atlantic case.....	46
7.1.1	The central North Atlantic case.....	52
7.2	Observation examples.....	54
7.2.1	Radar observations near frontal clouds	54
7.2.2	Humidity observations in the outflow of a WCB	55
7.2.3	Jet stream wind observations during WindVal	55
7.3	Climatology.....	58
7.4	Dry run	59
7.4.1	Summary of NAWDEX dry run cases (28 September to 9 October 2015).....	60
7.4.2	Summary	71
8	Forecasting products	73
8.1	NWP Forecasts	73
8.1.1	Mission support system (MSS)	73
8.1.2	Met 3D	74
8.1.3	Trajectory calculations and additional products	74
8.2	Satellite products.....	75
8.3	Additional links to forecast products	75
9	References.....	76

1 Introduction and Purpose of Document

The North Atlantic Waveguide and Downstream Impact Experiment (NAWDEX) is an international field experiment with a major German/Swiss component. This contribution to NAWDEX is led by the Ludwig-Maximilians-Universität (LMU) Munich and the Deutsches Zentrum für Luft- und Raumfahrt (DLR) Oberpfaffenhofen in cooperation with the Eidgenössische Technische Hochschule (ETH) Zurich and the Office of Naval Research in the USA.

NAWDEX is scheduled for 19 September to 16 October 2016. The German research aircraft HALO and DLR Falcon will be deployed to generate new knowledge in the field of mid-latitude atmospheric dynamics and predictability.

This document provides an overview on the scientific background and aims of NAWDEX, the available aircraft and instruments, and logistic aspects. For the campaign preparation several case studies and a catalogue of forecast products are presented.

This campaign implementation plan is a living document that reflects the current status in the preparation of NAWDEX. Additional information can be found at <http://www.pa.op.dlr.de/nawdex/>

2 Objectives

2.1 The mission

NAWDEX is a field experiment that emerged from the WMO THORPEX programme and contributes to the World Weather Research Programme WWRP in general and to the High Impact Weather (HIW) project in particular. An international consortium from the US, Canada, UK, France, Switzerland and Germany has applied for funding of a multi-aircraft campaign, supported by enhanced surface observations, over the North Atlantic and European region.

The German/Swiss/US contribution to NAWDEX aims at locating and quantifying errors in the numerical representation of midlatitude Rossby waves and weather systems that are related to diabatic processes. Therefore remote sensing measurements on board HALO and DLR Falcon will be carried out to obtain a comprehensive picture of the thermodynamic and flow structure near midlatitude jet streams and to quantify the impact of diabatic processes for the weather evolution over Europe. NAWDEX aims at observing the physical processes that are responsible for the triggering and modification, propagation and downstream impact of Rossby waves on a transatlantic scale over several days in a quasi-Lagrangian experiment. The observation period in September and October 2016 is climatologically ideal to observe many relevant weather systems characterized by strong diabatic activity.

2.2 Scientific background

Although the skill of numerical weather prediction has continuously improved over the last years (Richardson et al., 2012), there remain a serious number of forecast busts. Beside extreme forecast errors with a complete loss of predictability of the large-scale flow pattern, also less severe forecast errors, especially of high impact weather systems, i.e., weather with an immediate socioeconomic relevance (costs and damage of properties) can have substantial consequences. High impact weather arises on different scales and varies from large-scale heat waves, flooding events and wind storms to

small-scale and rapidly-developing convective systems, locally producing heavy rain, flash floods, severe winds and hail.

Therefore, uncertainty in the detailed knowledge about the intensity, timing and location of intense surface winds and heavy precipitation is crucial, e.g., if one thinks about storms affecting Europe. However, an accurate prediction of these aspects of high impact weather systems is still challenging (Zhang et al., 2007).

The predictability of weather systems that affect Europe is often linked to the evolution, propagation and breaking of North Atlantic Rossby waves. On tropopause intersecting isentropic surfaces, the Rossby waves are guided by longitudinally elongated bands of strong meridional gradients of potential vorticity (PV) coinciding with the meandering jet stream (Rossa and Davies, 1998; Martius et al., 2010). The strong PV gradient serves as waveguide for the propagating Rossby waves (Schwierz et al., 2004). Disturbances of the waveguide can amplify and propagate downstream, and errors in these processes can cause large forecast errors over Europe.

Rodwell et al. (2013) showed that a common initiator of large forecast errors over Europe are insufficiently represented mesoscale convective systems (MCSs) over the eastern US. The study highlighted that diabatic processes, such as in MCSs, are crucial for the evolution of the synoptic-scale flow. Several studies corroborate the major relevance of upstream diabatic processes for the evolution of the downstream weather. It is well known that the release of latent heat caused by cloud condensation affects the structure and evolution of cyclones (e.g., Kuo et al., 1991; Davis et al., 1993; Rossa et al., 2000). Error growth experiments in numerical models show that perturbations grow most rapidly where condensation is occurring before expanding in scale to affect the synoptic-scale weather pattern (Zhang et al. 2007, Selz and Craig 2015). A majority of the condensational processes in extratropical cyclones is controlled by saturated air ascending in a coherent airstream referred to as the warm conveyor belt (WCB). A WCB denotes an ascending airflow carrying warm and moist air from the southern midlatitude boundary layer to the northern midlatitude upper troposphere in 1-2 days (Browning et al., 1973; Carlson, 1980; Wernli and Davies, 1997). Condensation processes in the coherently ascending airstream produce a positive PV anomaly in the lower troposphere below the level of maximum latent heating (Wernli and Davies, 1997). Above the level of maximum latent heating, PV is reduced by cloud diabatic processes leading to negative PV anomalies in the upper tropospheric WCB outflow region (Wernli, 1997; Pomroy and Thorpe, 2000; Madonna et al., 2014).

The modification of upper tropospheric PV at the level of the midlatitude jet stream can significantly influence the wavelength and amplitude of the downstream Rossby wave development by modifying the upper level ridge (e.g., Knippertz and Martin, 2005). Grams et al. (2011) showed that cloud diabatic processes occurring in cyclones can interact with the North Atlantic jet stream and influence the amplification of Rossby waves by cross-isentropic transport of low PV air into WCB outflows. Massacand et al. (2001) showed that latent heating caused the downstream formation of PV streamers, i.e., Rossby wave breaking. In both studies diabatically amplified Rossby waves triggered high impact weather in the form of heavy precipitation over Europe.

Gray et al. (2014) investigated systematic errors in Rossby waves and found that underrepresented diabatic processes reduce Rossby wave amplitude. Dirren et al. (2003) investigated forecast errors and found amplitude and phase errors of Rossby waves. They showed negative PV biases at the end of the Atlantic storm track during winter. Davies and Didone (2013) quantified forecast errors in terms of PV on synoptic to subsynoptic scales. Their study refers to moist processes, radiative effects or a misspecification of location and structure of the jet stream in the initial conditions as possible error sources. Several studies corroborated the importance of realistic parameterizations of diabatic processes in general (Martínez-Alvarado and Plant, 2013), specifically microphysical processes (Joos and Wernli, 2012) and low-level humidity (Schäfler and Harnisch, 2015) to correctly predict the upper-level flow. In addition to moist processes, the distribution of PV at the tropopause can be modified by radiative effects, i.e., due to radiative heating/cooling anomalies near ice clouds in the vicinity of the tropopause (Zierl and Wirth, 1997; Chagnon et al., 2013) and turbulent mixing.

Extratropical cyclones are not the only weather systems that lead to diabatic processes that interact with the midlatitude flow. In addition to cloud processes in WCBs, also convective storms are able to impact the large-scale flow (Done et al., 2006). Tropical cyclones that transit into the extratropics can enhance anticyclonic flow at upper levels and excite Rossby waves (e.g., Agusti-Panareda et al., 2004; Riemer and Jones, 2010). Tropopause polar vortices, which are radiatively driven positive PV anomalies above the tropopause (Cavallo and Hakim, 2010, 2012; Kew et al. 2010), are likely to trigger disturbances of the jet stream.

A systematic evaluation and identification of insufficiently represented diabatic processes in midlatitude cyclones and their interaction with the jet stream are essential for improving forecast models. Although numerical weather prediction models have improved significantly during the last decades (Richardson et al., 2012), forecasts remain uncertain even on synoptic scales, especially in the medium range. The quality of the initial conditions, that indeed has improved by advancing assimilation methods and increasing the availability of observations (Zhu and Thorpe, 2006; Magnusson and Källén, 2013), is still a limiting factor causing uncertainty in forecasts. In addition, model errors due to, e.g., unavoidable simplifications in the subgrid-scale parameterizations, lead to increased forecast uncertainty. A systematic validation requires independent observations (i.e., observations that are not incorporated in the operational data assimilation). NAWDEX offers a fantastic opportunity to obtain high-quality measurements specifically aimed at the quantification of errors near the extratropical Rossby waveguide.

The study of diabatic processes affecting the extratropical waveguide, motivated so far primarily by the potential benefit for numerical weather prediction in general, and of high impact weather events in particular, will also be directly relevant for current initiatives in the climate community. WCRP recently issued a set of “Grand Challenges” on Clouds, Circulation and Climate Sensitivity. As one of the challenges Bony et al. (2015) identified the not well-known processes that control the position, strength and variability of storm tracks. Here too, observations taken during NAWDEX will likely make an important contribution.

2.3 Planned observations

NAWDEX aims at quantifying errors of the thermodynamic structure near Rossby waves and their relation to diabatic processes. The aim is to obtain a comprehensive and unprecedented data set in a region that, so far, was not accessible with smaller research platforms. HALO is the ideal aircraft as it provides the required flight range to reach the central and eastern North Atlantic and Europe and the altitude to perform remote sensing observations from above cloud systems. With the help of the established instrument combination of the WALES differential absorption lidar, the cloud radar of the Hamburg Microwave Package (HAMP), different radiometers and the dropsonde device the three-dimensional structure of water vapour, wind, temperature and cloud properties will be observed. Additionally to HALO, DLR will deploy its research aircraft Falcon with a wind lidar payload which allows a detailed observation of jet-level winds.

The collected data inside and outside clouds allows to investigate the relevance of different diabatic processes and related weather systems for the Rossby wave evolution by validating different numerical models. Beside upper-level observations, the humidity structure in the lower troposphere is of interest for diabatic processes. HALO and Falcon will operate over the eastern North Atlantic with the operation base in Iceland to guarantee optimal flight range and proximity to the regions of interest. The observation period in September and October is chosen as the above described weather systems characterized by strong diabatic activity and forecast busts are likely to occur. 100 flight hours from Iceland are envisaged with HALO. 50 flight hours are planned with the DLR Falcon. For a three-dimensional characterization of wind, temperature and moisture at jet level elongated high-level cross-sections across the jet stream and in regions where diabatically modified air masses interact with the wave-guide will be designed depending on the flow field.

For the first time it will be possible to follow the evolution of Rossby waves along the wave guide and to observe weather systems ranging from synoptic to cloud scales. Lagrangian tracking of diabatically modified air masses is planned. This will be tried with consecutive HALO/Falcon flights and by coordinating flights with the international partners. French colleagues have applied for the use of the French Safire Falcon to perform measurements in downstream developing weather systems. The airborne observations will be supplemented by an extensive network of ground-based observations in the UK, France, Germany and other European countries that will link the larger-scale atmospheric processes to specific high impact weather events.

2.4 National and International network

To maximize the scientific impact of the data set, NAWDEX is jointly performed by institutions both on a national and an international level.

The national NAWDEX consortium is led by the Meteorological Institute of the LMU Munich, and consists of six university partners (LMU Munich, University of Leipzig, University of Mainz, University of Cologne, University of Hamburg, Karlsruhe Institute of Technology) plus the DLR Institute for Atmospheric Physics and the Max Planck Institute for Meteorology in Hamburg. The consortium of the NAWDEX campaign is completed by the Eidgenössische Technische Hochschule Zürich (ETH), Switzerland and the Office of Naval Research in the USA. ETH Zürich supports NAWDEX financially thanks to a generous offer of the former ETH president, who was fascinated by the unique opportunities to identify physical processes in the atmosphere with new observational facilities. The group of Prof Heini Wernli at ETH led the T-NAWDEX Falcon pre-campaign and will contribute their expertise and unique forecast products to NAWDEX operations. An additional financial support comes from the Naval Research Laboratory (NRL) Monterey. Dr James Doyle will provide access to specialized forecast products such as adjoint sensitivities. A successful EUFAR proposal from Prof John Methven of the University of Reading, UK supports additional Falcon flight hours and provides access to forecast products and expertise.

Analysis and exploitation of the campaign data will be conducted in collaboration with the international campaign partners but also with the theoretical meteorology community and this collaboration will continue through the operational phase and in the analysis and exploitation of the data. Central to this is the recently funded DFG CRC “Waves to Weather”, connecting universities in Munich, Mainz and Karlsruhe. NAWDEX and W2W perfectly complement each other as the NAWDEX measurements of dynamical and physical processes that affect the limits of predictability of different weather systems over a broad range of scales are also the central topic of W2W, where the topic is addressed from a theoretical and modelling perspective. The new and unique observational NAWDEX data set will be an outstanding possibility to synergistically apply theoretical methods and diagnostics with the reality being observed by a multitude of state-of-the art remote sensing instruments.

Downstream measurements are planned over the eastern Atlantic and European continent in addition to the observations along the Rossby Waveguide in the central Atlantic, to take advantage of ground-based instruments and provide information on the development of high impact weather events. A proposal for the deployment of the UK ground-based measurement facility (led by John Methven) is currently under review, while Dr Gwendal Rivière of the Laboratoire de Météorologie Dynamique (LMD), Paris France is leading an effort to obtain funding for measurements with the Safire Falcon. Additional observations are planned including enhanced radiosonde ascents from Reykjavik, Iceland, and tropopause level measurements with the MST radars in Aberystwyth, UK and Andøya, Norway. The international NAWDEX website <http://nawdex.org/> is updated regularly with information about these efforts.

NAWDEX has a strong link to the HIWeather (high-impact weather project). This new activity of the WWRP has the objective to “Promote cooperative international research to achieve a dramatic

increase in resilience to high impact weather, worldwide, through improving forecasts for timescales of minutes to two weeks and enhancing their communication and utility in social, economic and environmental applications". NAWDEX is part of the HIWeather implementation plan that states: "Many of the research and cross-cutting activities (of HIWeather) will converge on field campaigns ... like the planned North Atlantic Waveguide and Downstream development Experiment ..."

The instrumentation and deployment of the aircraft over the Atlantic will also allow to pursue a number of side objectives, e.g. by combining radar and lidar data, observations of cirrus clouds, clouds and radiation and water vapour at the tropopause. The wind lidar payload is comparable to the future satellite mission Atmospheric Dynamics Mission (ADM) by the European Space Agency (ESA). The collected data will be valuable for the preparation of future ADM validation flights. The combined radar and lidar payload onboard HALO allows preparatory investigations for the future satellite mission EarthCare.

NAWDEX cooperates with the NARVAL II field experiment (PI: Prof. Bjorn Stevens, MPI Hamburg), i.e. a HALO campaign using the same payload to investigate trade wind clouds in the southern North Atlantic in August 2016. The cooperation provides a link to the climate community. The investigation of the role of cloud effects on the large scale dynamics is a cross-cutting topic for both weather and climate community. Within the World Climate Research Programme (WCRP) Grand Challenge on Clouds, Circulation and Climate sensitivity (Bony et al., 2015) it is stated that "... a deeper understanding of how clouds and moist processes interact with the circulation might help us think about largescale dynamics. We believe that this shift in thinking is a priority for our science, as we endeavour to help a society in urgent need of information about the Earth's changing climate."

3 Science Questions

Since NAWDEX is an international project, there are overarching scientific questions, developed over the years with colleagues worldwide, and the more specific primary and secondary objectives, which are particularly relevant for the operations with the aircraft HALO and DLR Falcon. The latter will be discussed in detail in sections 3.2 and 3.3, but first are listed the overarching NAWDEX goals taken from the NAWDEX Science plan (version 2, 30 July 2015):

3.1 International Science Hypotheses

3.1.1 Overarching hypothesis

"Diabatic processes over North America and the North Atlantic have a major influence on jet stream meanders, the downstream development of Rossby waves on the tropopause, and high impact weather phenomena and predictability over Europe."

3.1.2 Diabatic processes and impact on the potential vorticity

A) Diabatic processes affecting Rossby wave packets (upscale effect):

Warm conveyor belt / latent heating / ridge building

The air in the warm sector of each cyclone flows poleward and ascends in a warm conveyor belt (WCB) from the boundary layer into the ridge at tropopause level. For North Atlantic cyclones, climatologically the most frequent inflow region of WCBs is along the U.S. East Coast whereas the outflow spreads over the entire central North Atlantic (Madonna et al., 2014). Diabatic processes, such as turbulent fluxes, cloud microphysics and convection in the WCB influence the net heating, the level of the outflow layer and the direction taken by outflow air masses (Martinez-Alvarado et al., 2014). The effect of the heating on the PV is to strengthen the negative PV anomaly (compared with its surroundings in that layer) in the shallow outflow layer which tends to intensify the upper-level downstream ridge. If the outflow layer is higher, the negative PV anomaly is stronger and more mass enters the anti-cyclonic branch of the WCB flowing into the downstream ridge. The latent heating in WCBs is strong both in the early phase of the ascent when condensation dominates and later when mixed-phase clouds are formed and vapour deposition on snow becomes important (Joos and Wernli, 2012).

Long wave radiation / trough reinforcement

A sharp peak in longwave radiative cooling immediately below the tropopause and associated with a step change in water vapour creates a reinforcement of the upper troughs on the stratospheric side in Rossby wave packets (Chagnon et al., 2013). Radiation has also been proposed as an essential process for the formation of so-called tropopause polar vortices (high amplitude cyclonic PV anomalies) in the lower stratosphere (Cavallo and Hakim, 2012), which can disturb the Rossby waveguide from the polar side.

PV gradient

The combined effects of the low PV in the WCB outflow, the displacement of the tropopause, and increased PV due to radiative effects on the stratospheric side of the tropopause lead to the creation of a diabatic PV dipole (positive above and negative below), and a reinforcement of the horizontal PV gradient between the troughs and ridges (Chagnon et al., 2013).

B) Diabatic processes directly implied in high-impact weather events (downscale influence)

Rossby wave breaking

Rossby wave breaking leads to PV filamentation forming smaller-scale PV anomalies such as PV streamers and (isolated) cut-off PV vortices. The eastern North Atlantic and Europe are regions where the formation of PV streamers and cut-offs is particularly frequent (e.g., Wernli and Sprenger, 2007), and several studies reported the relevance of these flow features for triggering high-impact weather, in particular heavy precipitation (e.g., Martius et al., 2006; Chaboureaud and Claud, 2006).

Advection of moisture

Large-scale advection by persistent PV vortices of existing mesoscale humidity anomalies in the lower troposphere may lead to heavy precipitation events (e.g., Martius et al., 2006). Moisture advection is also important, e.g., in the inflow region of WCBs. Studies by Schäfler et al. (2011) and Schäfler and Harnisch (2015) have shown that low-level humidity in WCB inflows can be poorly constrained by observations, and that errors in the low-level moisture can influence the outflow level of WCBs and thereby the waveguide disturbance and downstream flow evolution.

Frontogenesis, frontolysis, conditional symmetric instability

Extratropical cyclogenesis is accompanied by generation of mesoscale structure by frontogenesis, frontal instability and banding through mechanisms such as conditional symmetric instability initiated in saturated air. Such processes are invoked to explain the occurrence of sting jets that are damaging winds occurring in the frontal fracture region in Shapiro-Keyser type cyclones (Clark et al., 2005; Gray et al., 2011)

3.1.3 Potentially misrepresented diabatic processes in models and impact on the circulation

A) Rossby wave packets

Intensity of the negative PV anomaly and PV gradient

The amplitude of ridges seems to be systematically underestimated in current NWP models (Davies and Didone, 2013). Gray et al (2014) show that ridge amplitude erroneously decays with lead time in the operational forecasts from the Met Office and ECMWF. Similarly, the PV gradients decrease with lead time suggesting that models cannot maintain the sharpness of the observed waveguide. One possible explanation is that the PV gradient at the tropopause is smoothed by numerical dissipation in NWP models (via the advection scheme) and this has a systematic effect acting to slow down Rossby waves and decrease amplitude. Another origin of the too weak PV gradient in models might come from the representation of long wave radiative cooling, which is sensitive to the vertical profile of water vapour and cirrus clouds near the tropopause. This has ramifications for forecasts of downstream development, since theory tells us that although both the jet stream maximum and westward

propagation rate decrease if the PV gradient lessens, the jet effect is stronger and Rossby wave phase speed decreases. Perhaps more importantly, Rossby wave packets disperse too rapidly downstream. Therefore, non-conservative processes, often operating on small scales, can have important consequences for large-scale forecast error. However, the relative importance of the mechanisms outlined above is not known and the aim of the experiment is to quantify the effects using a combination of new observations and model simulations.

Vertical structure of the negative PV anomaly

The negative PV anomaly in a WCB outflow resembles a thin lens dominated by a static stability anomaly. It is hypothesised that forecast models misrepresent the vertical structure of the PV lens which has consequences for the flow “induced” and associated Rossby wave propagation along the waveguide.

Displacement of the PV gradient

Ascent, amplified by heating, is associated with horizontal divergence at the outflow level. On each isentropic surface, the divergent flow has a strong component normal to the tropopause PV gradient, resulting in poleward advection of the tropopause. This acts as a “Rossby wave source” and can initiate Rossby wave packets that propagate downstream. Because the divergent flow reaches higher levels than the diabatic heating itself, this process can extend the impact of diabatic processes to levels above the level of the WCB outflow and can thus be regarded as an indirect diabatic effect.

B) High-impact weather, and downscale influence of Rossby wave packets

Synoptic-scale upper-level forcing of precipitation events

The advection of mesoscale humidity by upper-level PV anomalies gives rise to strong sensitivity of forecasts to the moisture field. A better knowledge of the low-level moisture field is required for forecast improvements.

Jet streaks

The positive part of the diabatic PV dipole can form a local PV maximum on the poleward, stratospheric side of the tropopause. These maxima constitute jet streaks and tropopause polar vortices that can have a direct impact on severe weather through strong baroclinic interaction with the lower troposphere.

Relation between near-surface strong winds and PV anomalies

It is not clear how near-surface strong winds are connected to PV anomalies and how balanced these winds are.

Role of evaporation in the formation of strong wind gusts

The role of evaporation of precipitating bands in the formation of strong winds like sting jets is not clear yet (Baker et al., 2014).

Connection between lower-tropospheric winds and boundary-layer processes

Destabilization of the boundary layer and weak static stability is required to facilitate downward mixing by convective plumes (Parton et al., 2009). But it is rather difficult to reproduce such a downward transfer of momentum in NWP models under both a real or idealized framework (Parton et al., 2009; Baker et al., 2014). Generally speaking, the interaction between boundary-layer processes and extratropical cyclones still raises open questions, and it is not clear yet how synoptic conditions organize the boundary layer.

3.2 Primary Objectives

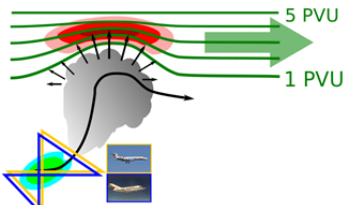
3.2.1 Moisture Structure in the Boundary layer

Comparisons of observations with model analyses showed overestimated specific humidity values in ECMWF's boundary layer (Schäfler et al., 2010, 2011). Most likely these errors are associated to insufficiently parameterized boundary layer processes. The current observational system lacks high-resolution observations of moisture as ground observations are sparse over the oceans and satellite observations have insufficient vertical resolution, especially close to the ground.

As diabatic processes related to the lifting of moist air masses can strongly influence the dynamics of the extratropics an accurate representation of the boundary layer humidity can be crucial. Schäfler and Harnisch (2015) showed that initial condition errors in the low-level moisture supply of a WCB deteriorate the forecast quality. Doyle et al. (2014) found forecasts of extratropical cyclone Xynthia, which had a severe impact on western Europe, were very sensitive to the initial moisture, particularly in the lower levels that influenced the moisture supply in a WCB. In some unstable flow situations, e.g. baroclinic cyclones, the small-scale errors can grow rapidly and impact the large-scale flow and propagate downstream (Doyle et al. 2014).

The observation of horizontal moisture transport also provides a link to "atmospheric rivers" (filaments of strong WV transport). These particularly strong exports of tropical moisture can have substantial impact by causing intense rain in the mid-latitudes (e.g. Cordeira et al. 2013)

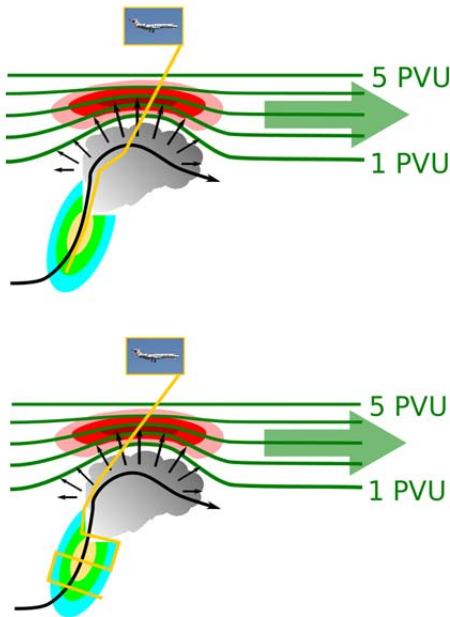
The collocated deployment of wind and water vapour lidar instruments has shown to be a valuable instrument combination to observe both horizontal (Schäfler et al. 2010) and vertical transport of humidity (Kiemle et al. 2011).

Moisture Structure in the Boundary layer	
Research questions:	<ul style="list-style-type: none"> ➤ How does the moisture structure at lower levels evolve? ➤ What is the vertical and horizontal structure in the inflow regions? ➤ Sharp transition from smooth boundary layer to synoptically forced region? ➤ What is the impact of moisture uncertainties on high impact weather forecasts?
Planned Observations:	<ul style="list-style-type: none"> ➤ HALO and Falcon (dropsondes, DIAL, wind lidar, radar)
Observation Strategy:	<ul style="list-style-type: none"> ➤ several transects in pre-saturated environment where lifting starts, e.g. the inflow region of WCBs before the ascent starts and clouds develop ➤ HALO water vapour with lidar and dropsondes (T, u, v) ➤ for the case that moisture source regions are within the range of the DLR Falcon coordinated flights to measure moisture transport (horizontal and vertical) are possible ➤ atmospheric river situation would be of high interest ➤ radar observations to observe changing cloud structures in different regimes ➤ observations of moisture and water vapor flux in regions of high sensitivity
Schematic flight plan:	

3.2.2 Mixed phase clouds

Cloud processes including water phase transitions need to be parameterized in global NWP models. Martínez-Alvarado and Plant (2013) investigated the importance of the large-scale precipitation parameterization (cloud microphysics parameterization) and the convection parameterization for the evolution of a WCB. They highlighted a sensitivity of the large-scale dynamics to both, the type of parameterization scheme but also the interaction of the large-scale and convection parameterization. Joos and Wernli (2012) illustrated that different microphysical processes along the WCB ascent contribute to latent heat release and PV-changes within a cyclone. A large uncertainty exists in the model representation of mixed-phase clouds; comparison of heating rates along WCB (Joos and Forbes, in preparation).

Martínez-Alvarado et al. (2014) showed that diabatic processes can determine the WCB outflow height and in turn impact the Rossby wave evolution. They demonstrate that differences in the Rossby wave structure can be attributed to differences in the parameterization schemes affecting WCBs. Interactions between cloud microphysics and small-scale dynamics such as gravity wave motions and embedded convection may also have an influence on WCB evolution. High resolution trajectories have shown that a significant fraction of air parcels in the WCB experience periods of rapid ascent, either in cold frontal line convection or mid-level embedded cells (Rasp 2015). Regions of rapid ascent in WCBs have been shown to correlate well with areas of large initial condition sensitivity (e.g., Doyle et al. 2014), providing a potential key link to predictability.

Mixed phase clouds	
Research questions:	<ul style="list-style-type: none"> ➤ Representation of clouds along WCB (freezing level, IWC, LWC)? ➤ Where is latent heating and cooling taking place in and below the WCB? ➤ Slantwise ascent vs. embedded convective?
Planned Observations:	<ul style="list-style-type: none"> ➤ HALO (dropsondes, radar, in-situ, radiometer)
Observation Strategy:	<ul style="list-style-type: none"> ➤ Along and across WCB variations of liquid, cloud snow and rain water path + integrated vapour transport
Schematic flight plan:	

3.2.3 Upper level PV

Potential vorticity, with its property of being conserved in adiabatic motions, is a key quantity to investigate the diabatic influence on the dynamic structure at upper levels. Despite its outstanding dynamical importance, PV is difficult to measure in the atmosphere as this requires the simultaneous observation of horizontal wind and vertical potential temperature gradients, which is a large challenge for available observing systems. Chagnon et al. (2013) investigated diabatic PV production and showed that both negative PV in warm conveyor belt outflows related to latent heating and positive PV on the stratospheric side of the tropopause related to radiative processes, i.e. LW cooling impact the tropopause PV structure. These processes can change the PV gradient, which in turn is highly relevant for the downstream propagation of Rossby waves. Since significant uncertainties exist in the representation of diabatic processes affecting these PV gradients in numerical models, it is highly desirable to confront model-derived PV structures with those estimated from direct wind and temperature observations.

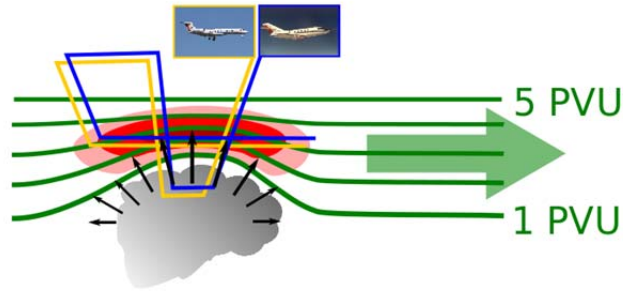
Several earlier studies have estimated PV from aircraft data (e. g., Shapiro, 1978; Hartmann et al., 1989; Vaughan et al., 1996). They used in-situ wind observations to calculate along-track wind gradients. To gather vertical temperature information, the in-situ wind observations had to be combined with lapse-rate data from dropsondes or a microwave temperature profiler. However, these observations were limited to PV estimates along the flight track. Information about PV at different altitudes could only be obtained by flying the aircraft at different vertical levels. This limits the possibility of temporally collocated measurements and only very limited vertical resolution can be achieved with flight legs at different altitudes.

During NAWDEX range-resolved temperature and wind profiles will be observed by a dropsondes and a wind lidar. Unlike the earlier studies, this new effort will use range resolved remote sensing to estimate PV in a 2-dimensional cross-section. The range resolved temperature profiles allow determining lapse rates at different altitudes and the scanning wind-lidar that measures the wind vector beneath the aircraft allows to estimate horizontal wind gradients in flight direction.

Under the assumption that variations of winds along the jet are small compared to across-jet variations PV can be approximated as $Q \cong \left(\frac{1}{\rho} \left(f - \frac{\partial u}{\partial y} \right) \frac{\partial \theta}{\partial z} + \frac{\partial u}{\partial z} \frac{\partial \theta}{\partial y} \right)$ where f is the Coriolis parameter. The y-coordinate points in the across-jet direction and x-coordinate points along the jet. This allows a PV estimation solely based on observed quantities.

Upper level PV	
Research questions:	<ul style="list-style-type: none"> ➤ How much of the total PV is reproduced by approximated PV determined from observations? ➤ How much information is contained in the wind field versus thermodynamic gradients? ➤ Can diabatically generated PV features be tracked to evaluate model (non) conservation?
Planned Observations:	<ul style="list-style-type: none"> ➤ HALO & Falcon (wind lidar, dropsondes & radiometer temperatures)
Observation Strategy:	<ul style="list-style-type: none"> ➤ repeated across-jet flight legs perpendicular to the wind direction ➤ enter a region of divergent WCB outflow ➤ along-jet control leg to investigate the assumption of small variation ➤ flight in region where dropsondes are allowed, drop at high frequency

Schematic flight plan:



3.2.4 Diabatic effects on cyclonic systems

Diabatic processes not only modify the upper-level Rossby waves, they also have a strong impact on the structure, intensity and evolution of the weather system (e.g., MCS, ET, extratropical cyclone). For extratropical cyclones, a climatological study (Campa and Wernli, 2012) has shown that deep cyclones have systematically stronger, diabatically produced, low-tropospheric cyclonic PV anomalies in their centre.

Certain categories of extratropical cyclones, so-called diabatic Rossby waves (DRWs) (e.g., Parker and Thorpe, 1995; Wernli et al., 2002; Moore et al., 2010; Boettcher and Wernli, 2011) only exist because of continuous diabatic low-level PV production. These systems are potentially highly relevant, as they can explosively intensify via interaction with an upper-level trough, not unlike the re-intensification of ET systems. During NAWDEX, a horizontal setup with a set of vertical profiles of winds and temperature in the vicinity of cyclonic systems (e.g., from dropsondes) could reveal novel insight into the structure of the diabatic intensification of these systems. Additionally, regions of diabatic heating may have important links to initial state sensitivity and uncertainty, and can lead to rapid perturbation growth that impacts the predictability of downstream high-impact weather (Doyle et al. 2014).

Cyclonic systems

Research questions: (to be discussed)

- How well do analyses and forecasts represent the vertical structure and wind, humidity and temperature in diabatically intensified cyclonic systems?
- Are there distinct features of clouds associated with diabatic Rossby waves?
- How do regions of diabatic heating relate to forecast sensitivity and predictability?

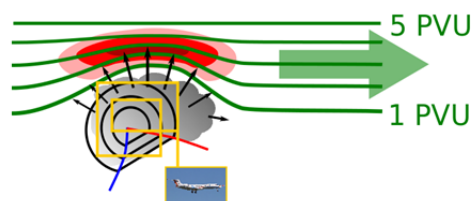
Planned Observations:

- HALO (dropsondes, in-situ, cloud radar)

Observation Strategy:

- Circular flight paths around centre of cyclonic system
- Repeated observations along track of cyclonic system
- DRW systems are expected to develop far south and may be out of range of the aircraft, for a northward propagating system DRW, observations would be similar as for "normal" cyclones
- Lidar or dropsonde observations in regions of forecast sensitivity

Schematic flight plan:

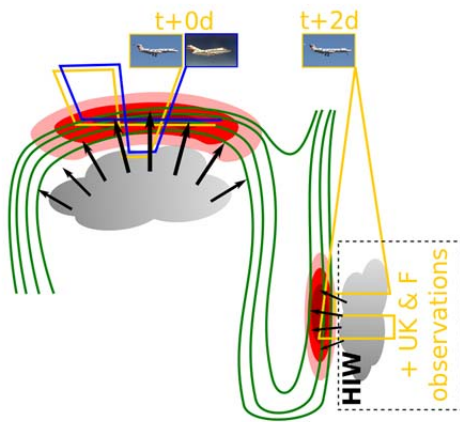


3.2.5 Impacts of tropopause waveguide uncertainty on HIW events

Tropopause PV features have been regularly linked to HIW events such as heavy precipitation (e.g., Martius et al., 2006; Chaboureaud and Claud, 2006). An analysis of high-resolution ensemble forecasts from the DWD COSMO-DE system showed that the synoptic structure was often the dominant source of ensemble spread (Keil et al. 2013). However the same study showed that in some cases, uncertainty in local small-scale processes can play an equally large role. Chaboureaud et al. (2012) showed that intense Mediterranean cyclone forced by combination of large scale ascent and surface-driven instability.

During NAWDEX, precursors of high impact weather events will be identified and their errors and uncertainty as represented in the NWP analysis ensemble will be evaluated using the aircraft observations. Adjoints of nonlinear forecasts can be used to identify upstream regions of sensitivity (e.g., Doyle et al. 2014). Ensemble forecasts will be used to relate these errors to HIW events downstream. Ground-based observations will provide detailed verification of the physical processes linking the precursors at the level of the Rossby waveguide to local extremes in wind and precipitation.

An important factor for achieving this objective will be coordinate the aircraft observations planned here with surface and lower tropospheric observations in the UK, France and other countries. An overview of these activities is provided in the international NAWDEX science plan.

Impacts of tropopause waveguide uncertainty on HIW events	
Research questions:	<ul style="list-style-type: none"> ➤ Does amplification of small errors at tropopause level lead to significant uncertainty in surface weather such as wind gusts and heavy precipitation? ➤ Can changes in surface weather be causally connected to precursors, or does local amplification lead to intrinsic unpredictability? ➤ Is the representation of diabatic processes in NWP models adequate to represent the impact of waveguide disturbances on HIW?
Planned Observations:	➤ HALO and Falcon
Observation Strategy:	<ul style="list-style-type: none"> ➤ wind lidar, dropsondes ➤ upstream-downstream flights
Schematic flight plan:	

3.2.6 Moisture and Cloud Structure in Tropopause Region

In addition to microphysical processes, the distribution of PV at the tropopause is also influenced by radiative effects, i.e., due to radiative heating/cooling anomalies in the vicinity of the tropopause, induced by the presence of ice clouds and/or strong vertical humidity gradients (Zierl and Wirth, 1997; Chagnon et al., 2013). Also within the lower stratosphere can radiative effects modify PV and contribute to the formation of intense mesoscale cyclonic PV anomalies, so-called TPOs (Cavallo and Hakim, 2010; Kew et al., 2010). And clearly, for the climate community understanding the processes that influence radiation in the upper troposphere and lower stratosphere is of central importance, also because in this region changes in water vapour strongly affect surface climate and decadal variability of surface temperatures (Forster and Shine, 1997).

High resolution observations of the thermodynamic structure near the tropopause, in and around clouds, will enable the assessment of the model representation of these processes, which can be interpreted with the aid of sensitivity tests using simulations where cloud and radiative parameters are varied.

Moisture and Cloud Structure in Tropopause Region	
Research questions:	<ul style="list-style-type: none"> ➤ Heating and cooling rates from lw radiation ➤ Role of latent heating vs. radiative effects ➤ How well represented are moisture and temperature gradients at the tropopause?
Planned Observations:	<ul style="list-style-type: none"> ➤ Moisture, temperature profiles and radiation
Observation Strategy:	<ul style="list-style-type: none"> ➤ Upstream and downstream flights in situation of predicted downstream wave breaking, airborne and ground obs of international partners ➤ Downstream flights with predicted HIW over northern France, UK, Benelux in coordination with international partners
Schematic flight plan:	

3.2.7 Quantification of analysis errors

The NAWDEX data set will be compared with NWP analysis fields to study the magnitude of initial condition errors. By comparing all observations of wind and water vapor with NWP output, statistics of errors will be computed.

A special focus is put on the relation of errors to the dynamic structure of the midlatitude flow. It will be verified how well the strong wind gradients around the jet stream are represented in the vicinity of positive and negative PV anomalies. Errors will be related to the waveguide location and to the tropopause position and structure to identify possible regions of misrepresentation in upper level PV anomalies driven by diabatic processes. It will be investigated whether the especially strong errors are related more to the type or the strength of diabatic processes.

The Ensemble analyses differ by perturbations to the atmospheric observations, sea-surface temperature and model physics. It will be investigated whether the observed analysis errors relative to the campaign observations are within the initial condition uncertainty of the NWP system provided by Ensemble Data Assimilation (EDA, Isaksen et al., 2010).

Quantification of analysis errors	
Research questions:	<ul style="list-style-type: none"> ➤ How well represented are static stability and moisture, wind and PV at the tropopause in regions of divergent wind in diabatic outflow? ➤ Where do the analysis errors of the wind field occur with respect to the location of the tropopause, the jet stream and the Rossby wave? ➤ Do dynamic features like WCBs, tropical cyclones or tropopause polar vortices contribute exceptionally strong to the formation of forecast errors?
Planned Observations:	➤ All wind, temperature and moisture data
Observation Strategy:	➤ Use all HALO and Falcon observations

3.2.8 Lagrangian Tracking of disturbances

Diabatic processes lead to material modification of air mass properties, so that additional insight can be obtained by observing the same air mass multiple times over a period of several days. Incorporating this observational strategy will potentially add value to all scientific objectives. A tracking of air masses allows the quantification of changes to PV and other properties along the flow and gives direct insight into physical processes, e.g. by the ability to assess the cloud microphysical evolution in WCB air parcel.

However the tracking of air masses is challenging as it requires highly complex flight planning. It needs trajectory forecasts from first flight leg to determine path of the next flight. Especially, since flight planning needs to be finalized 1-3 days in advance, the forecast might be incorrect. In addition, the “forward projected flight path” may not be technically/administratively feasible. Schäfler et al. (2014) provide examples of these difficulties and the tools available to overcome them.

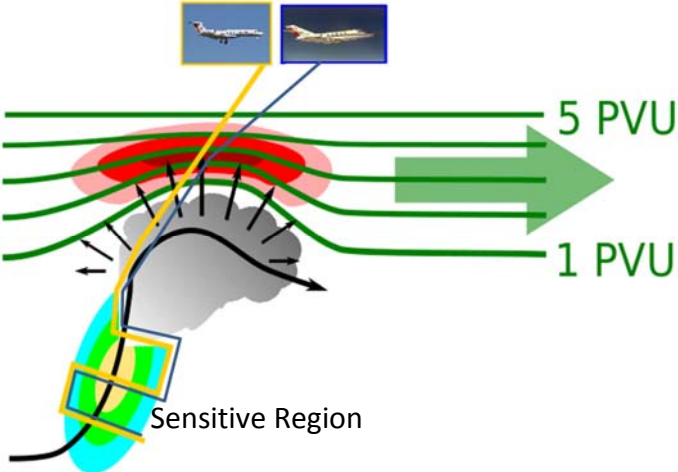
Lagrangian Tracking of disturbances	
Observation strategy:	<ul style="list-style-type: none"> ➤ It is generally favourable if the above described aims can be connected and commonly addressed during the evolution of a weather system ➤ If possible the transport of airmasses will be observed with consecutive flights ➤ e.g. observation of upstream moisture and clouds and upper-tropospheric outflow or divergent outflow and downstream local weather

3.2.9 Initial condition sensitivity and predictability of high-impact weather downstream

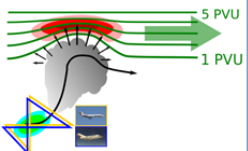
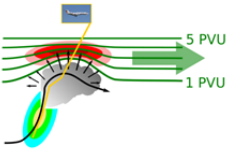
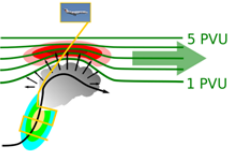
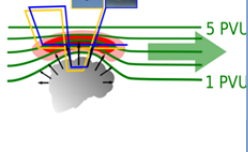

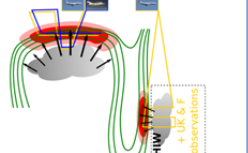
The predictability of high-impact weather events over Europe is often inherently linked to the rapid forecast error growth that can occur over the N. Atlantic and propagate downstream in the Rossby waveguide. Poorly predicted high-impact weather events are often linked to the nature of the disturbances that perturb the waveguide, such as tropical or sub-tropical disturbances, polar PV

anomalies, atmospheric rivers, WCBs, and regions of diabatic heating (e.g., Doyle et al. 2014). Many key questions related to predictability are closely tied to aspects of sensitivity. An adjoint model (e.g., Errico 1997) [or ensemble (e.g., Torn and Hakim 2009)] provides quantitative information on the influence of each component of an earlier model state on a later forecast metric (such as kinetic energy, moisture flux etc.).

The adjoint applied to high impact extratropical cyclones, such as Xynthia (2010), Klaus (2009), Nina (2015), highlight regions of maximum sensitivity in the waveguide and in the vicinity of moist filaments associated with atmospheric rivers and and at times coinciding with WCBs, low- and mid-level PV anomalies, and regions of diabatic heating/cooling (e.g., Doyle et al. 2014; Langland et al. 1995; Langland et al. 2002). Sensitive regions appear to be similar to DRWs in some cases, To improve the prediction of these high-impact weather events, NAWDEX observations within and outside of these sensitive regions will be used to test sensitivity and predictability hypotheses. A special focus will be on observing sensitive regions that are coincident with dynamically and thermodynamically active regions in WCBs, atmospheric rivers, tropopause features, and PV anomalies.

Initial Condition Sensitivity and Predictability	
Research questions: (to be discussed)	<ul style="list-style-type: none"> ➤ How do observations within and outside of sensitive regions influence the predictability of downstream high-impact weather? ➤ What is the relationship between diabatic heating, WCBs, frontal features, tropopause processes and forecast sensitivity as well as downstream predictability of HIW? ➤ What is the relationship between DRWs and optimal adjoint perturbations?
Planned Observations:	<ul style="list-style-type: none"> ➤ Moisture, temperature, wind profiles using Falcon (wind lidar, in-situ), and HALO (dropsondes, in-situ, cloud radar)
Observation Strategy:	<ul style="list-style-type: none"> ➤ Lawnmower pattern of observations covering key sensitive regions and dynamically/thermodynamically active regions ➤ Upper-air soundings near regions of upstream sensitivity ➤ Lidar and/or dropsonde observations in regions of forecast sensitivity ➤ Downstream flights with predicted HIW over northern France, UK, Benelux in coordination with international partners
Schematic flight plan: (need to modify figure)	

3.2.10 Overview of strategies

Aim	Planned observations	Flight strategy
Moisture Structure in the Boundary layer	<ul style="list-style-type: none"> • HALO observations of winds, water vapor and temperature (dropsondes, DIAL, HAMP radiometers) • Falcon observation of winds (wind lidar) 	<ul style="list-style-type: none"> • several transects in the pre-saturated environment where lifting starts, e.g. the inflow region of WCBs before the ascent starts and clouds develop • for the case that moisture source regions are within the range of the DLR Falcon, coordinated flights to measure moisture transport (horizontal and vertical) are possible • radar observations to observe changing cloud structures in different forcing regimes 
Mixed phase clouds	<ul style="list-style-type: none"> • HALO (dropsondes, radar, in-situ, radiometer, imager) 	<ul style="list-style-type: none"> • Along and across WCB variations of liquid cloud, snow and rain water path + integrated vapor transport  
Upper level PV	<ul style="list-style-type: none"> • HALO temperature profiles (dropsondes & radiometer temperatures) • Falcon wind profiles (wind lidar) 	<ul style="list-style-type: none"> • repeated across-jet flight legs perpendicular to the wind direction • enter a region of divergent WCB outflow along-jet control leg to investigate the assumption of small variation • flight in region where dropsondes are allowed, drop at high frequency 
Cyclonic systems	<ul style="list-style-type: none"> • HALO (dropsondes, in-situ, cloud radar) 	<ul style="list-style-type: none"> • Circular flight paths around center of cyclonic system • Repeated observations along track of cyclonic system • diabatic Rossby wave systems may be investigated with a similar strategy if far enough north to be in aircraft range 
Impacts of tropopause waveguide uncertainty on HIW events	<ul style="list-style-type: none"> • HALO and Falcon 	<ul style="list-style-type: none"> • wind lidar, dropsondes • upstream-downstream flights 
Moisture and Cloud Structure in Tropopause Region	<ul style="list-style-type: none"> • HALO (Moisture, temperature profiles and radiation, radar reflectivity, heating rates) 	<ul style="list-style-type: none"> • Upstream and downstream flights in situation of predicted downstream wave breaking, airborne and ground observations of international partners • Downstream flights with predicted HIW over France, UK, Benelux in coordination with international partners
Quantification of analysis errors	<ul style="list-style-type: none"> • All wind, temperature and moisture data 	<ul style="list-style-type: none"> • Use all HALO and Falcon observations
Initial Condition Sensitivity and Predictability	<ul style="list-style-type: none"> • Moisture, temperature, wind profiles using Falcon (wind lidar, in-situ), and HALO (dropsondes, in-situ, cloud radar) 	<ul style="list-style-type: none"> • Lawnmower pattern of observations covering key sensitive regions and dynamically/thermodynamically active regions • Upper-air soundings near regions of upstream sensitivity • Lidar and/or dropsonde observations in regions of forecast sensitivity • Downstream flights with predicted HIW over northern France, UK, Benelux in coordination with international partners

3.3 Secondary Objectives

The link to climate and space research is also a significant motivation for NAWDEX. In the DLR project KliSAW, the data will be used to improve the understanding of physical and chemical processes, including those affecting cloud and humidity, in a changing climate system. The combination of radar and lidar onboard HALO will be used in preparatory studies for the earth observation satellite missions EarthCARE and MERLIN. This synergy will be examined in detail by the research group (DLR-NWG) by Dr. Silke Groß. In addition DLR is involved in the preparation of the Atmospheric Dynamics Mission (ADM) which will be the first wind lidar in space with the launch scheduled for 2017. DLR developed the airborne demonstrator instrument A2D that is part of the DLR Falcon payload, and data taken in NAWDEX will be used to prepare for future validation missions for ADM. With increasing interest in storm track changes in future climates, it is expected that the NAWDEX data set will be a valuable resource for climate, earth observation, and weather prediction researchers in the coming years.

3.3.1 Earth Care Preparation

Some background will follow soon

Earth Care Preparation	
Research questions:	<ul style="list-style-type: none"> ➤ Determination of optimal overlap of Radar und Lidar observations onboard HALO ➤ Implementation and adjustment of synergistic analysis methods to retrieve information about microphysical cloud properties ➤ Investigation of horizontal cloud structure ➤ Ableitung der Wolkenphase (Wolkenmaske) durch synergistische Betrachtung von Radar und Lidar
Planned Observations:	<ul style="list-style-type: none"> ➤ Combined Radar & Lidar observations
Observation Strategy:	<ul style="list-style-type: none"> ➤ Use high level observations performed by HALO of Ice Clouds

3.3.2 ADM Preparation

The Atmospheric Dynamics Mission ADM Aeolus from European Space Agency (ESA) will be the first European lidar and the first wind lidar in space worldwide with a planned launch in 2017. Significant improvements for weather forecasts are expected, because Aeolus fills the gap in the global observing system for wind profile observations. IPA plans to provide key contributions to Aeolus after launch with the development of retrieval algorithms and processors, by validation of the Aeolus wind and aerosol products and by scientific use of its observations.

IPA is strongly involved in algorithm studies and the development and use of the airborne prototype of Aeolus – the ALADIN airborne demonstrator A2D that will be installed onboard Falcon together with the 2-µm Doppler wind lidar, which serves as a reference instrument. This payload was already flown during pre-launch validation campaign in May 2015 called WindVal together with two other wind lidars on the NASA-DC8. The objectives and implementation of this campaign are summarized in Reitebuch (2015). All of the main objectives of the WindVal campaign could be met, but there were a number of secondary objectives, which could be not fully tackled. In addition some of the main objectives of

WindVAI could be approached again during NAWDEX to extend the dataset before launch of Aeolus during different seasons (September/October instead of May) and weather conditions.

ADM Preparation	
Research questions:	<ul style="list-style-type: none"> ➤ Extend dataset on Response Calibration over Ice ➤ Extend dataset on satellite underpasses, e.g. ASCAT, TDS-1 ➤ Derivation of aerosol products from A2D
Planned Observations:	<ul style="list-style-type: none"> ➤ A2D Wind Lidar in calibration mode ➤ Wind Lidar on Falcon flights under satellite tracks ➤ Perform flights with sufficient aerosol amount in atmosphere with Falcon, collocated HSRL observations from HALO to quantify aerosol backscatter, extinction and de-polarisation
Observation Strategy:	<ul style="list-style-type: none"> ➤ Circle Flights with Falcon over Greenland ➤ Satellite underpass of Metop-A/B, TDS-1, CALIPSO and others ➤ Combined flights of Falcon and HALO over distinct aerosol layers

3.3.3 Turbulence observations near jet-streams

Some background will follow soon

Turbulence	
Research questions:	<ul style="list-style-type: none"> ➤ Which part of the turbulence spectrum spreads and propagates to the mesosphere? ➤ Insufficient explanation of the development of non-orographic gravity waves, partly related to turbulence e.g. in deformed jet stream ➤ Tropopause inversion layer influenced by turbulence (internal friction)
Planned Observations:	<ul style="list-style-type: none"> ➤ 100 Hz Bahamas data of T, u, q
Observation Strategy:	<ul style="list-style-type: none"> ➤ Flights in area of increased turbulence and gravity wave excitation

3.4 Priorities of the objectives

Priorities and decision making will be discussed and tested during the NAWDEX dry run

3.5 Contribution of NAWDEX instrumentation to the objectives

	HAMP	HAMP	WALEs	HALO-SR	specMACS	Dropsonde	Bahamas	Wind Lidar
Moisture structure in the boundary layer	X		X			X	X	X
Mixed phase clouds	X	X		X	X	X	X	
Upper level PV	X		X			X	X	X
Diabatic effects on cyclonic systems	X	X		X	X	X	X	X
Impacts of tropopause waveguide uncertainty on HIW events		X	X		X	X	X	X
Moisture and cloud structure in tropopause region	X	X	X	X	X	X	X	
Quantification of analysis errors	X	X	X	X		X	X	X

4 Aircraft Platforms & Instrumentation

4.1 HALO

4.1.1 Aircraft properties

The following information can be found at: www.halo.dlr.de and <http://www.dlr.de/fb/>

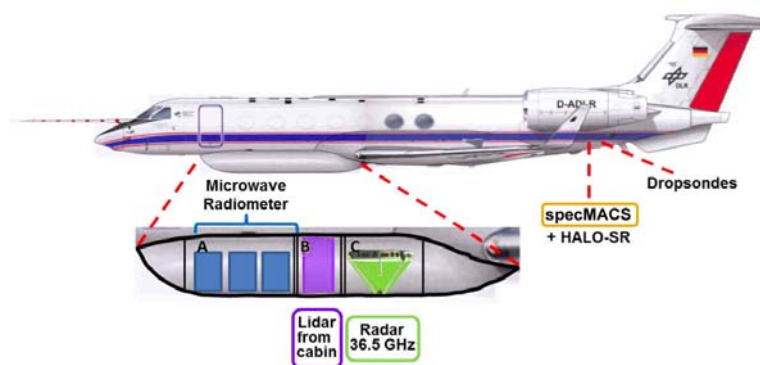


Figure 4.1 HALO instrumentation for NAWDEX (and NARVAL-II)

The High Altitude and Long Range Research Aircraft (HALO) research aircraft is based on a Gulfstream G 550 ultra long-range business jet. HALO was funded by the Federal Ministry of Education and Research, the Helmholtz-Gemeinschaft and the Max-Planck-Gesellschaft. The main strengths of HALO are its long range and endurance, high ceiling altitude and large instrument load capacities, which are not available in such combination on any other research aircraft in Europe.

Length:	31 metres (including 1.6 metre nose boom)
Height:	7.9 metres
Wingspan:	28.5 metres
Seating capacity:	19 (normally 3 crew members and 5 to 8 scientists and engineers, depending on the instrumentation)
Range:	over 8000, depending on the mission profile and payload
Flight altitude:	maximum 15.5 kilometres (51,000 feet)
Speed:	maximum 340 KCAS / Mach 0.885 / 1054 kilometres per hour
Fuel capacity:	18.73 tonnes (41,300 pounds)
DLR Flight Facility:	Oberpfaffenhofen

Table 4.1 Information about HALO

4.1.2 Instrumentation

HALO will be equipped with a payload that was originally assembled for the Next-generation Aircraft Remote Sensing for Validation Studies (NARVAL I, Klepp et al. 2014) field campaign in 2013/2014. The profiling payload with remote-sensing instruments and dropsondes will be employed to measure three-dimensional structure of water vapor, wind, temperature and cloud properties. For NAWDEX and NARVAL-II the established instrument combination of the WALES differential absorption lidar, the cloud radar of the Hamburg Microwave Package (HAMP), different radiometers and the dropsonde device is slightly changed by adding a cloud spectrometer (specMACS) and a revised version of the HALO-SR instrument (see Figure 4.1).

Instrument	Institution	Measured parameters/data products
HAMP	MPI-M Hamburg, Univ. Hamburg, Univ. Cologne, DLR-PA	<ul style="list-style-type: none"> liquid water path, temperature + humidity profiles cloud snow + rain water path profiles of radar reflectivity, depolarization ratio + vertical velocity
WALES	DLR-PA	Profiles of <ul style="list-style-type: none"> water vapour, backscatter coefficient (532/1064 nm), colour ratio of backscatter (532/1064 nm), particle linear depolarization ratio (532/1064 nm), particle extinction coefficient at 532 nm
HALO-SR	Univ. Leipzig	<ul style="list-style-type: none"> spectral nadir radiance (300-2200 nm), spectral upward and downward irradiance (300-2200 nm), cloud top albedo cloud thermodynamic phase liquid and water path cloud optical thickness, effective radius
dropsondes	DLR-PA	<ul style="list-style-type: none"> relative humidity profiles temperature profiles horizontal wind profiles
Bahamas	DLR-FX	In-situ observations of T, q, u, v, w 100 Hz data, GPS
specMACS	LMU Munich	<ul style="list-style-type: none"> spectral radiance (400-2500 nm), push-broom imaging, nadir and +/- 17° across track cloud thermodynamic phase liquid and ice optical thickness particle size cloud cover

Table 4.2 Overview of instruments onboard HALO during NAWDEX

4.1.3 HAMP (HALO Microwave Package):

HAMP provides an advanced suite of microwave cloud remote sensing instruments for operation onboard HALO. The package consists of microwave radiometers with 26 channels that in addition to HAMSr frequencies also include the low-frequency channels along the 22GHz water vapor line (K band) for better estimation of rain and cloud liquid water, together with the thermodynamic environment (temperature and humidity profiles).



Figure 4.2 Left image: Cloud radar 35 GHz. Right image: Microwave radiometer 90/119, 22/58, 183 GHz mounted in Belly-Pod beneath the aircraft.

In addition to its unique frequency combination, HAMP also includes a high-sensitivity cloud radar at 35.2 GHz (~ 38 dBZ at 5 km and 1 s avg.), making it a versatile tool for studying both clouds and precipitation in different regions of the world that are difficult to assess with ground-based instrumentation.

The radar MIRA-36 (Görsdorf et. al, 2015), owned by University of Hamburg and manufactured by METEK, is a monostatic, pulsed, magnetron, Ka band, Doppler radar that operates at 35.2GHz. The advantage of the Ka band as compared to the more common 94 GHz, or W band, is its reduced attenuation in the presence of condensate. The radar has two receivers to provide a co- and cross-polarization channel. The output parameters are the radar reflectivity (Z), the Doppler spectra, the Doppler velocity or line of sight velocity of targets (V), the spectral width, and the linear depolarization ratio (LDR). An advantage of the monostatic, pulsed magnetron is that it captures strong gradients in the reflectivity precisely. This is especially important to avoid problems with ground reflection in nadir-looking instruments. The radar's transmitter and receiver are initially calibrated using external sources and internal references sources are continually used to achieve a permanent calibration of the system.

Cloud Radar MIRA-36	
Frequency	35,2 GHz Ka-band (8 mm), nadir pointing
Peak power	30 kW
Resolution	30 m range, 1 s temporal
Antenna	in belly pod, 1 m diameter, 0.6° beam width (\triangleq 130 m at 13 km)
Parameters	Radar reflectivity Z, Doppler velocity V, Depolarization ratio LDR
Sensitivity (airborne operation)	-38 dBZ @ 5km with 1s avg. -30 dBZ @ 13km with 1s avg.

Table 4.3 Cloud radar properties

Compared to ground-based cloud radar, two additional effects have a major influence on the retrieved Doppler velocities. The first effect is the contribution of the aircraft speed to the mean Doppler velocity in the case that the radar is not pointing exactly nadir (see more detailed discussion in Lee et al., 1994). With a typical aircraft speed of 210 m/s and a forward pitch angle of 2 deg, this offset accounts for -7.33 m/s (negative means towards the aircraft).



In the case of vertical shear of the horizontal wind between the measurement height and the height of the aircraft, an additional offset by the projection of the horizontal wind vector on the flight direction has to be considered. The second effect of the aircraft motion is the broadening of the Doppler spectrum due to the beam width. Even in the case of an antenna pointing exactly nadir, part of the radar beam is pointing forward and backward, thus seeing an offset in Doppler velocity. In total this results in a broadening of the velocity distribution in the radar measurement volume. While the power peak of the original monodisperse spectrum might be above the noise level, the power peak of the broadened spectrum could be below the noise level. This has an effect on the ability to detect clouds with low reflectivity. Software algorithms are able to diminish this reduction in sensitivity to 8–9 dB. The resulting sensitivity for airborne operation has been found to be in agreement with the expected values to be in the range of -38 dBZ at 5km with 1s average or -30 dBZ at 13km also with 1s average.

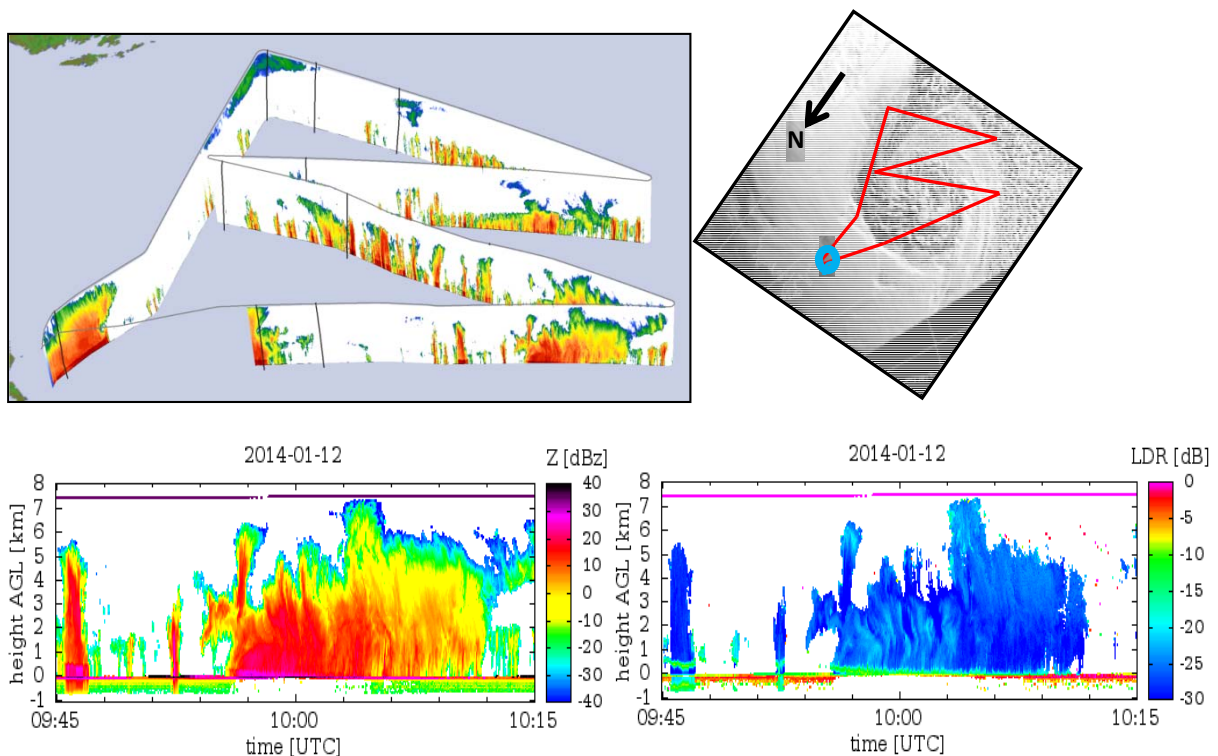


Figure 4.3 Example of radar observations close to a cyclone being located in the Northern Atlantic on 12 January 2014 with reflectivity Z (left column) and Linear Depolarization ratio LDR (lower right panel). The NARVAL mission flight started and ended in Keflavik (Iceland, see upper right panel with a VIS satellite image at the time of the flight)

The HAMP microwave radiometers are owned by the Max Planck Institute and were custom-manufactured for HALO by Radiometer Physics GmbH (RPG). They are separated into three nadir-pointing modules mounted in the belly pod underneath HALO.

Microwave Radiometers	
Frequency	5 radiometers in 3 modules
	<ul style="list-style-type: none">22 GHz K-band (H₂O channel)58 GHz V-band (O₂ channel)90 GHz W-band (window channel)118 GHz F-band (O₂ channel)183 GHz G-band (H₂O channel)
Resolution	1 s temporal, field of view 1.2-0.6 km @ 14 km flight altitude



Parameters	Brightness temperatures, temperature and humidity profile, integrated water vapour, liquid water path, ice/snow water path, rain rate
Noise-equivalent delta temperatures (NeDT)	0.1 @ K-band 0.2 @ V-band 0.25 @ 90 GHz 0.6 @ 118 GHz 0.6 @ 183 GHz
Absolute accuracy (Acc.)	0.5 @ K & V-band 1.5 @ 90, 118 & 183 GHz

Table 4.4 HAMP microwave radiometer properties

The first module contains two independent packages with parallel antenna axis for the K and V bands. Both units are direct detection filter bank receivers similar in design to the one within the ground-based Humidity and Temperature Profiler (HATPRO; Rose et al., 2005) that is used at several locations worldwide for automatic thermodynamic profiling and measurements of the liquid water path (LWP).

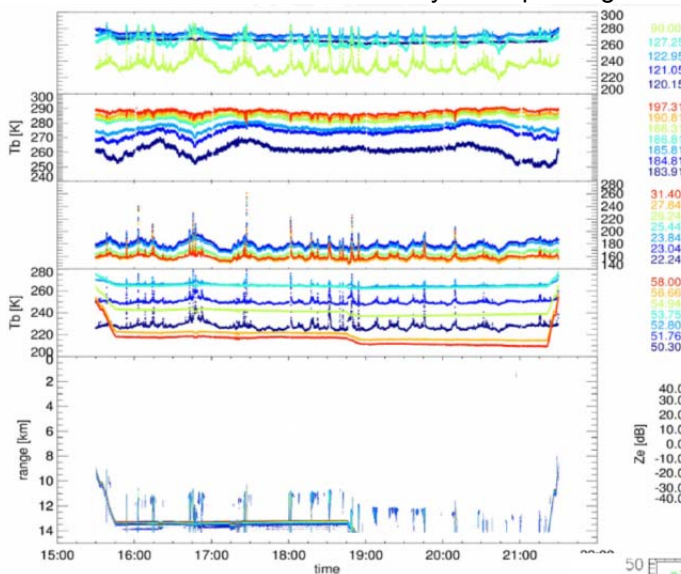
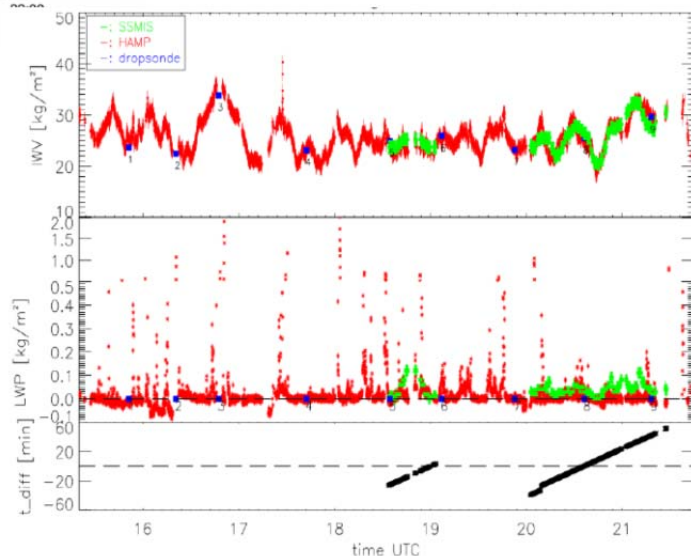


Figure 4.4 Example of HAMP radiometer observations (temperatures) at different frequency channels compared to radar observations for a NARVAL north flight. Courtesy Mario Mech (University Cologne)

Figure 4.5 Integrated Water Vapor (IWV) and Liquid Water Path (LWP) derived from radiometer observations in comparison with SSMIS satellite observations and dropsonde profiles. Courtesy Sabrina Schnitt (University Cologne).



The second module consists of two independent receiver packages: one direct detection radiometer at a window channel at 90 GHz and one heterodyne receiver in double-sideband mode with four channels along the 118.75 GHz O₂ line from ± 1.4 to ± 8.5 GHz. The third module contains a single heterodyne receiver providing seven channels along the 183.31 GHz H₂O line (± 0.6 to ± 12.5 GHz, double side-band). The radiometers view the atmosphere through existing apertures in the belly pod, which are covered by window material with low microwave attenuation.

The frequencies for the three modules of passive microwave radiometers were selected to cover the main spectral signatures in the microwave spectral range similarly to currently operated Advanced Microwave Sounding Unit (AMSU)-A and -B, SSM/I, Microwave Humidity Sounder (MHS) and forthcoming satellite instruments like the GPM Microwave Imager or the Microwave Imager (MWI) on MetOp-SG, covering attenuation and window regions of the microwave spectrum.

The accuracy of the measured brightness temperatures (TB) is determined by the quality of the calibration and by the noise component. During flight the radiometer channels are continuously calibrated using two reference loads. The noise-equivalent delta temperatures (NeDT) and the absolute accuracies (Acc.) are given in the table above.

Operational constraints HAMP	
<ul style="list-style-type: none"> - One operator for cloud radar + radiometers possible - Quicklooks during flight available (radar moments and TB's) - real-time processing of radar moments and spectra during flight - pre-flight: <ul style="list-style-type: none"> - radiometers: heat up of approx 2 hours before take off (desirable) - radiometers: calibration before each take off with liquid nitrogen - radar: pre-heating: 5 minutes after take-off - in-flight: <ul style="list-style-type: none"> - radiometers: one clear sky dropsonde per flight desirable - radar: minimum flight height: FL 200 (6 km) for operation (because of saturation of receiver by sea (earth) surface) - radar: maximum flight height: FL 450 (13.7 km) (because of maximum range 15 km, but ground echo preferred and forward pitch considered) radar: frequency permission required (DE valid till 2022, IS+GL available temporary by email, UK available temporary (50 £), NL available temporary (225 €), IR (unresolved responsibilities, to be clarified), CA (was not necessary for NARVAL-North, exact flight track within Canadian EEZ would have been required) 	

Table 4.5 HAMP operational constraints

4.1.4 WALES

The Water Vapour Lidar Experiment in Space (WALES) airborne demonstrator is an airborne four-wavelength Differential Absorption Lidar DIAL that was developed at DLR (Wirth et al., 2009). The water vapour concentration can be deduced by comparing returned signals of two spectrally narrow laser pulses that were emitted to the atmosphere. WALES instrument allows to measure profiles over the whole range of water vapour concentrations, often varying by up to four orders of magnitude between the ground and the flight level in the upper troposphere/lower stratosphere region.

Parameter	Water Vapour	Aerosol
Wavelength	4 wavelengths ~935 nm	532 nm and 1064 nm
Laser energy	40 mJ	
Pulse repetition rate	200 Hz	
Telescope diameter	48 cm	

Observed parameter	Water Vapour mixing ratio, Relative humidity (in combination with external temperature data (e.g. ECMWF or dropsonde))	Backscatter coefficient (532 nm and 1064 nm), Color ratio (532 nm/1064 nm) of backscatter, aerosol depolarization (532 nm and 1064 nm), Aerosol extinction (532 nm – HSRL)
Vertical resolution	~200m	15 m
Temporal resolution	25s (2.6 – 2.9 km)	1s (0.22 – 0.24 km)

Table 4.6 WALES instrument characteristics

The observation of water vapour up to the tropopause succeeds by comparing the returned signal of three wavelengths that are sensitive at different water vapour concentrations, i.e., different altitudes, to the reference wavelength at a non-absorbing wavelength. The four wavelengths are located in the water vapour absorption band at 935 nm (Wirth et al., 2009). The error is evaluated to be less than 5–7% (Kiemle et al., 2007; Bhawar et al., 2011),

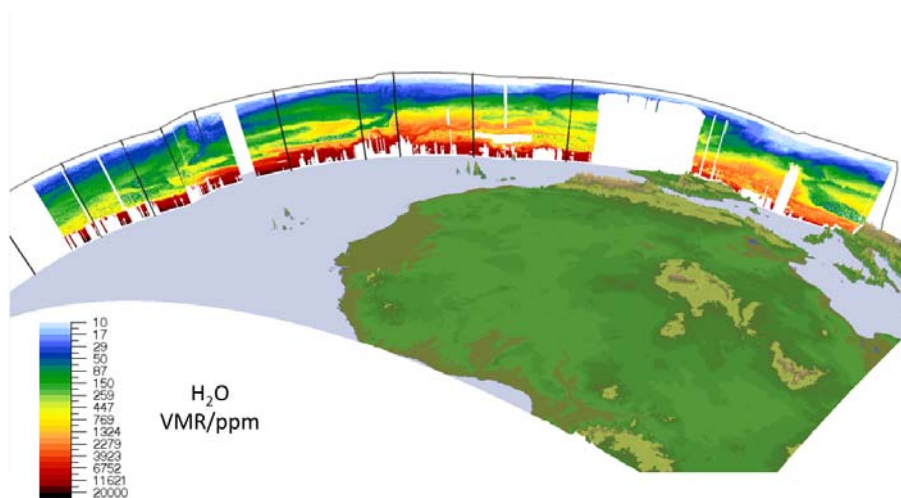


Figure 4.6 Example of Water Vapor Volume Mixing ratio on a large scale transect from Oberpfaffenhofen to Barbados with HALO during NARVAL
Courtesy of M. Wirth

Operational constraints WALES	
-	Best performance if 2 km distance to cloud top is ensured <ul style="list-style-type: none"> • Saturation effects at cloud top for closer distances • Higher random error for larger distances
-	No data for flight legs within cloud
-	System is not frost-proof
-	System about 1 h to warm up, before the lasers can be started and one hour of laser operation for full performance (esp. H ₂ O).

Table 4.7 WALES operational constraints



4.1.5 HALO-SR

HALO-SR provides spectral solar radiation measurements with sampling frequency of about 2 Hz. HALO-SR has been operated on HALO during three missions (HALO-TECHNO, Fricke et al., 2014, NARVAL-I, Klepp et al., 2014, and OMO) to detect spectral nadir radiance. During ML-CIRRUS and ACRIDICON another set of spectral solar radiation sensors was applied including irradiances (on stabilized platforms), the SMART (Spectral Modular Airborne Radiation Measurement System, Wendisch et al. 2015, Ehrlich et al. 2008) albedometer.

For NAWDEX the capabilities of HALO-SR will be extended to spectral irradiances looking upward and downward using existing components of the SMART. All quantities measured by HALO-SR are obtained for the wavelength range of 0.3–2.2 μm with spectral resolution of 2-16 nm full width of half maximum (FWHM), which is sufficient to analyze the spectral characteristics of spectral absorption bands of ice and liquid water. While the irradiance sensors provide spectral albedo at flight level representative for a specific area, the measurement frequency of 2 Hz and the 2.1° field of view of the radiance sensor allows identifying cloud inhomogeneities (about 200 m footprint for cloud top at 5 km and flight altitude of 10 km).



Figure 4.7 Images and illustrations of HALO-SR as mounted on HALO.

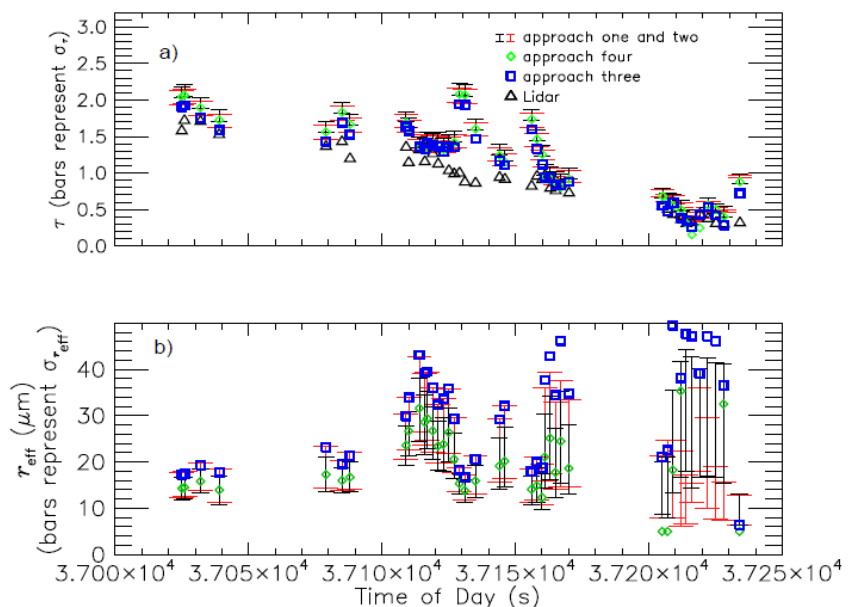
Measurement uncertainties range at about 5% dominated by the uncertainty of the radiometric standards. The optics used to measure nadir radiance have a field of view of about 2.1° which allows to resolve cloud inhomogeneities in horizontal dimensions down to 100 m. For the narrow view, the footprint is mostly determined by the flight velocity. In contrast, the actinic flux density measurements have a maximum $4\pi\text{-sr}$ field of view also covering the combined influence of clouds in a complex cloud field.

Module	Nadir Radiance (LIM)
Wavelength	300-1000 nm (1024 pixel) 1000-2200 nm (256 pixel)
Spectral resolution	2-3 nm and 9-16 nm
Temporal resolution	2 Hz
Field of view	2.1 °
Derived parameter	<ul style="list-style-type: none"> spectral nadir radiance (300-2200 nm), spectral upward and downward irradiance (300-2200 nm), cloud top albedo cloud thermodynamic phase liquid and water path cloud optical thickness, effective radius

Table 4.8 HALO-SR specifications

From the radiance observations, cloud properties such as cloud thermodynamic phase, cloud optical thickness and cloud particle effective size can be derived. An example of retrieval results for a relatively homogeneous cirrus cloud observed during the TECHNO mission is given in Figure 4.8 (Fricke et al., 2014). The retrieved optical thickness were compared to independent lidar observations onboard of HALO. Good agreement was found only if aggregate ice crystals are assumed while other crystals shapes caused significant differences. Further, it was found, that for cloud optical thickness the surface albedo does not significantly affect the results, but uncertainties in the assumed albedo introduce up to 50 % uncertainties in the retrieved effective ice crystal sizes.

Figure 4.8 Cloud optical thickness (a) and particle effective radius (b) derived from HALO-SR during the TECHNO mission on 3 November 2010. Different approaches for representing the surface albedo were used and compared to cloud optical thickness observed by WALES (Fricke et al. 2014).



Similar investigations comparing passive and active remote sensing of different cloud types are done for ML-CIRRUS and NARVAL where in addition the HAMP package was operated. An example of how HAMP and HALO-SR data can be merged is shown in Figure 4.9.

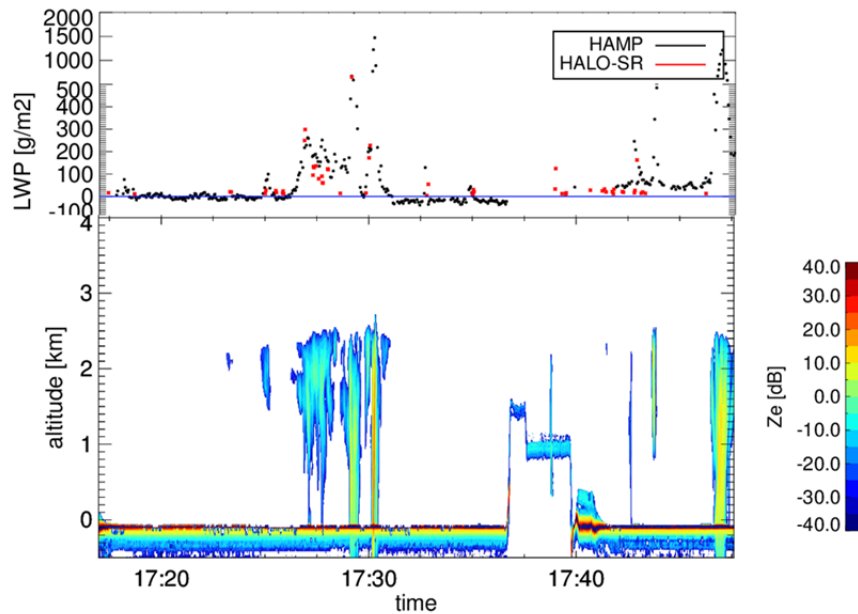


Figure 4.9 Comparison of liquid water path (LWP) derived from spectral radiance measurements with HALO-SR and observations by HAMP during a NARVAL flight on 11 Dec 2013. Courtesy of F. Werner (LIM) and E. Orlandi (University Cologne).

For the liquid clouds observed in the NARVAL sequence, LWP derived from HAMP and HALO-SR agree well. Having comparable fields of view and sampling frequencies, retrieval algorithms combining the other remote sensing techniques of the NAWDEX instrumentations will be developed.

Another aspect of HALO-SR measurements is the comparison with satellite observations, which in general apply similar measurements and techniques for cloud retrieval but have a lower spatial and spectral resolution. Good agreement between HALO-SR nadir radiance and MODIS radiance in the centre pixel were found during dedicated flights of the ML-Cirrus mission (not shown here). Therefore, the data analysis of NAWDEX will benefit from a synchronization with satellite overpasses, when airborne remote sensing can be used to validate satellite observations.

Operational constraints HALO-SR

- Requires illumination by the Sun, only daytime measurements
 - Avoid low solar zenith angles $> 80^\circ$ ($< 10^\circ$ sun altitude)
 - Higher random error for larger distances
- High flight levels are preferred (at least 500 ft above clouds)
 - Clear sky above flight level is needed for proper cloud retrieval
 - No cloud retrieval for measurements inside clouds
- Regular calibration at ground (typically in between flights) ~ 1 hour
- HALO cabin should not heat up, 20-25°C are preferred (high temperatures = increased signal noise and dark current). Depend also on Rack configuration.

Table 4.9 HALO-SR operational constraints.

4.1.6 specMACS

The cloud spectrometer of the Munich Aerosol Cloud Scanner (specMACS) is an imaging cloud spectrometer for the solar spectral range. It consists of two spectral camera systems covering the spectral range 400-2500 nm combined with fast data acquisition and flexible in-flight camera control software. A detailed description of the system with spectral and spatial imaging characteristics is given in Ewald et al. (2015). The instrument provides multi-spectral images of calibrated radiances with a spectral resolution between 3 nm and 10 nm in a spatial swath of 34° across the flight direction.

specMACS was already successfully flown on HALO at the ACRIDICON campaign 2014 where it measured radiance reflected by convective clouds' sides through a side view-port. Data examples of the imaging and spectral capabilities, detailed lab calibration, and the ACRIDICON HALO setup of specMACS can be found in Ewald et al. (2015). An additional commercial video camera looking through the same window will allow to provide real-time imagery of the flight path and facilitate a derivation of cloud geometry from stereo evaluation combined with absorption spectra (O₂A) measured with specMACS. Derived products will be cloud thermodynamic phase and droplet size which have already been derived from ACRIDICON data.

4.1.7 Dropsondes

The dropsonde device to observe vertical profiles of temperature, pressure, relative humidity, horizontal wind. It consists of data acquisition rack and a release unit both installed in the baggage compartment.



Figure 4.10 Left: Dropsonde data acquisition rack. Middle: release unit in HALO baggage compartment. Right: release pipe as seen from outside the aircraft.

4.2 Dassault Falcon 20-E5

4.2.1 Aircraft properties

The DLR research aircraft Dassault Falcon 20-E5 will be operated from Keflavik Iceland. The well experienced airborne platform for atmospheric research was deployed during several field campaigns over Iceland

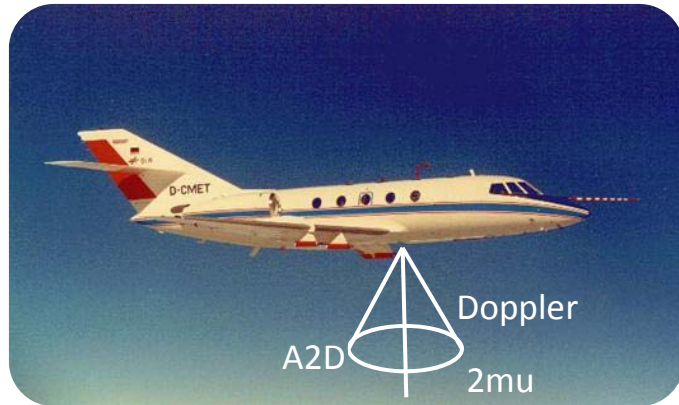


Figure 4.11 DLR Falcon instrumentation

Altitude [ft]	10 000	20 000	31 000	41 000
max. Range [NM]	1150	1500	1700	2000
max. Endurance [h:min]	04:10	04:15	04:45	05:00
max. Altitude			42 000 ft	12 800 m
max. Speed (VMO / MMO)			380 KCAS	0,865 Mach
Long Range Speed			410 KTAS	0,720 Mach
Takeoff Distance (MTOM, ISA, MSL)			2000 m	6562 ft

Table 4.10 DLR Falcon performance data

4.2.2 Instrumentation

The following description of the Falcon instrumentation is taken from the Campaign Implementation plan of the WindVAL campaign 2015 (Reitebuch 2015)

The payload of the DLR Falcon aircraft will consist of the A2D (Reitebuch et al. 2009, Paffrath et al. 2009) and the 2- μ m Doppler wind lidar (DWL, Weissmann et al. 2005) Two seats are available on the Falcon aircraft, which will be shared among the operators for the A2D and 2- μ m DWL (Figure 4.12).

The A2D and the 2- μ m lidar will be pointing in the same line-of-sight LOS direction to the right side of the aircraft (in flight direction) with a nadir angle of 20°. The instruments are mounted as follows:

- the A2D aircraft frame is mounted with a pitch angle of -6° (pointing to the back) along the aircraft axis; the telescope is mounted such that it points towards the right with a roll angle of 20° and pointing back by -4°; thus the A2D telescope points backwards by -2° and 20° to the right side.



- the 2- μ m is mounted with a pitch angle of -2° (pointing to the back) along the aircraft axis. It is equipped with a double-wedge scanner, which allows to point towards -6° and a roll angle of 20° . Small offsets in the order of 0.1° of the 2- μ m pointing direction will be determined in flight.

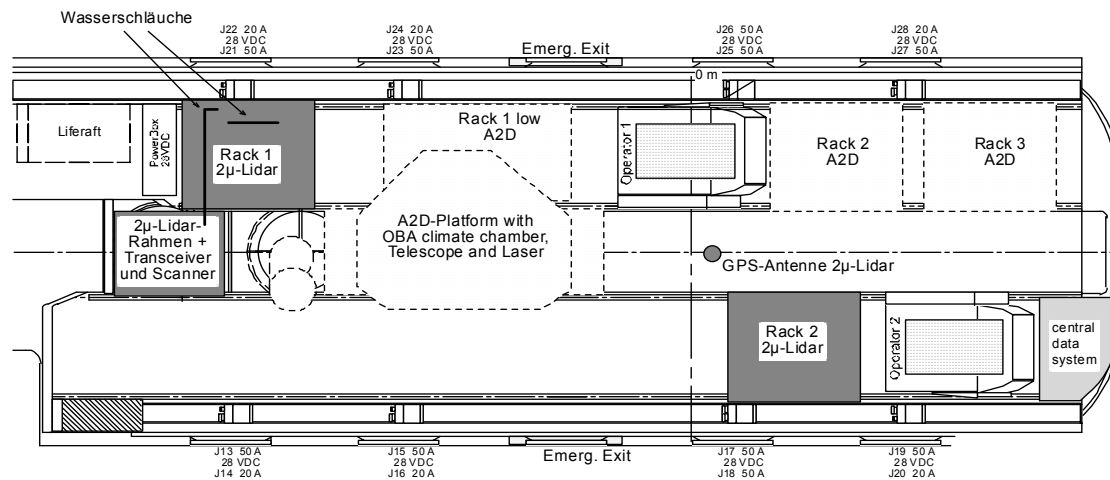


Figure 4.12 Cabin layout of the DLR Falcon aircraft with the A2D and the 2- μ m lidar

The nominal operation of the 2- μ m lidar will be the measurement of the LOS wind and conical step-stare scans will be performed in order to measure the horizontal wind vector during flight. The vertical sampling of the A2D will be set such, that the ground layers are sampled with highest vertical resolution (2.1 μ s, 315 m range).

The 2- μ m DWL will measure time series of raw signal with a sampling rate of 500 MHz, which corresponds to a range resolution of 0.3 m for each emitted laser shot with a repetition rate of 500 Hz. This amounts to rather high raw-data rates of up to 60 GByte/hour depending on maximum range. The data will be processed on-ground to range-gates of 100 m resolution and temporal resolution of 1 s (500 shots).

Standard meteorological parameters (pressure, horizontal wind vector, vertical wind speed, temperature, humidity (relative humidity, mixing ratio)) will be measured by in-situ sensors inside the Falcon nose-boom with a temporal resolution of up to 100 Hz and processed with resolution of 1 Hz. Thus vertical profile data are available for ascent and descent and flight-level data from cruising altitude. First quick-look data from these sensors will be available about 1 day after each flight during the campaign.

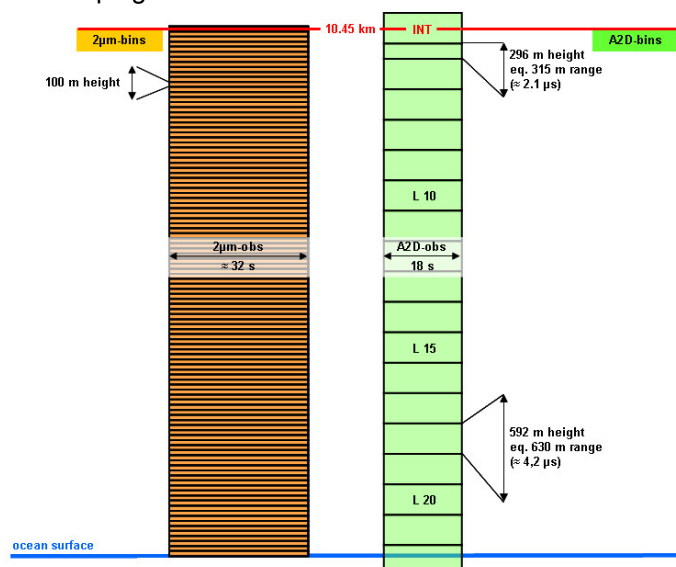


Figure 4.13 Principle of vertical and horizontal sampling for 2- μ m wind lidar with 100 m range gates and a duration of 32 s for 1 scan and A2D with vertical sampling of 592 m, which will be adapted for each flight; horizontal distance of each A2D profile is 18 s and averaging time is 14 s; 4 s are needed for data transfer

Parameter	DLR A2D	DLR 2-µm DWL
Wavelength	354.89 nm	2022.54 nm
Laser energy	50 mJ	1-2 mJ
Pulse repetition rate	50 Hz	500 Hz
Pulse length	20 ns (FWHM)	400-500 ns (FWHM)
Telescope diameter	20 cm	10.8 cm
Vertical resolution	300 m – 2.4 km	100 m
Temporal averaging raw data (horizontal)	20 laser shots = 0.4 s	single shot = 2 ms
Temporal averaging product (horizontal)	14 s (+4 s data gap)	1 s LOS, 32 s scan (20-22 LOS)
Horizontal resolution @ 200 m/s=720 km/h = 12 km/min.	3.6 km (18 s)	0.2 km LOS, 6.4 km scan
Scanning capabilities	No, fixed 20° off nadir	Yes, double wedge, conical scan, fixed LOS and vertical
Precision (random error)	1.5 m/s Mie wind 2.5 m/s Rayleigh wind	< 1 m/s wind speed

Table 4.11 Main specifications and products from the 2 different direct-detection wind lidars



5 Logistics

5.1 General information

- **Experiment phase:** 19 September – 16 October 2016
- **Operation Centre:** Keflavik Iceland
 - ICAO code: KEF
 - Position: 63° 59' 55.06" N, 22° 33' 58.85" W

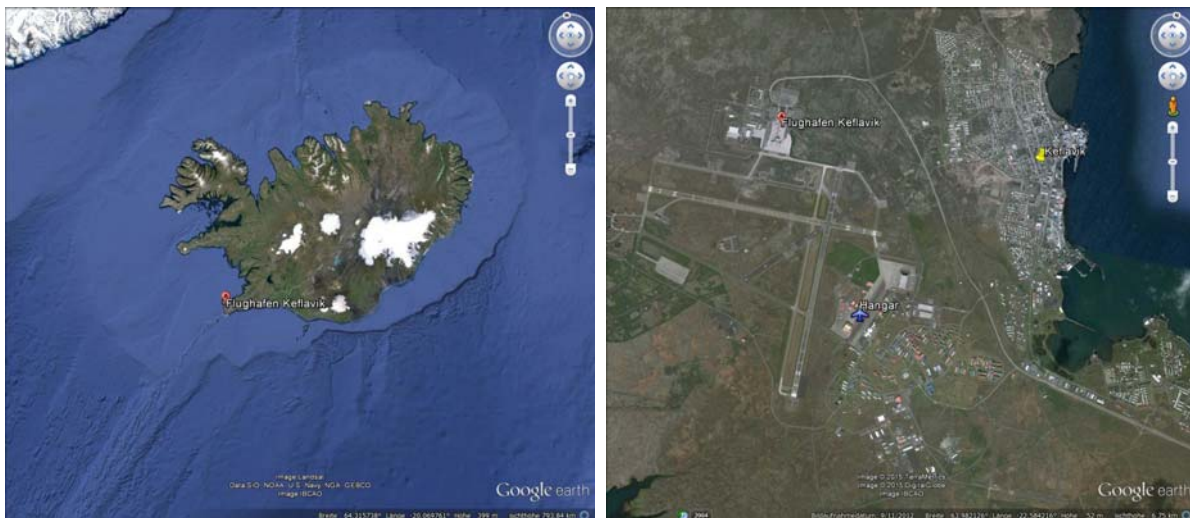


Figure 5.1 Left: Iceland with location of Keflavik in the southwest of the Island. Zoom to the international airport Keflavik with its perpendicular

5.2 Flight operation

Both aircraft will be located in Iceland. The table below lists the planned operation within the capabilities of the aircraft. Depending on the aim coordinated flights are planned. Both joint flights in the same region and consecutive flights to track airmasses are envisaged. Therefore two separate crews are requested.

	<u>HALO</u>	Falcon
Flight hours total:	100 (incl. Ferry-flight)	50 h
Typical flight duration:	6-8h	3-4 h
Number of flights:	tbd	tbd
Mission period:	depends on funding, 4-7 weeks	depends on funding, 4 weeks
Night operation:	yes	yes
Weekend operation:	yes	yes

Table 5.1 Overview of planned aircraft operation during NAWDEX

Figure 5.2 shows the range of the two aircraft when flying out of Keflavik. For coordinated flights of both aircraft a region from Greenland to Norway and Northern UK is available. The region could be enlarged when the DLR Falcon would refuel at an external airport (e.g. Kangerlussuaq (Greenland) or Shannon (Ireland))

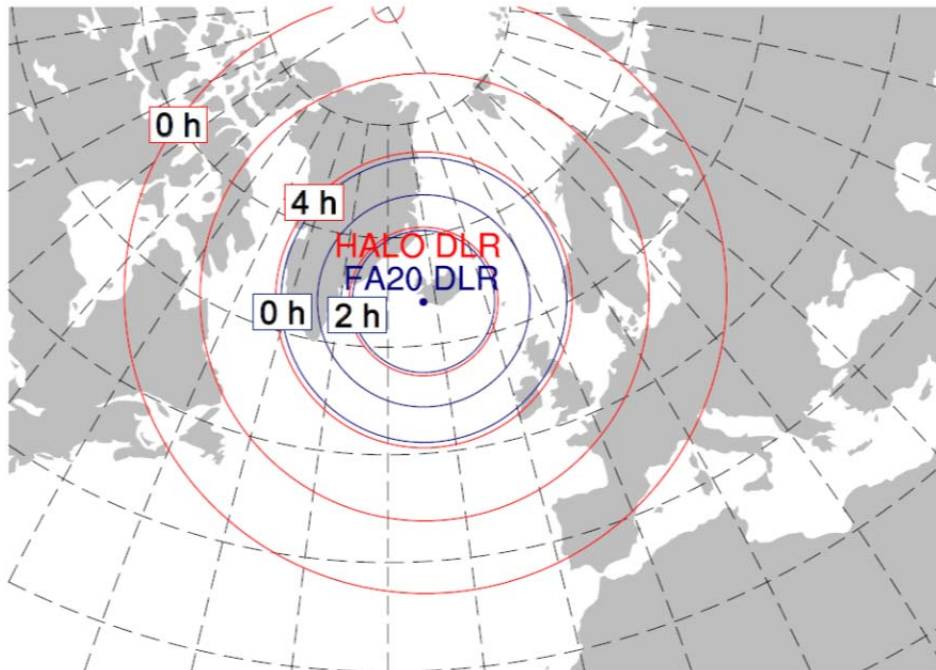


Figure 5.2 Range of the two aircraft when flying out of Keflavik. The indicated times show remaining time for local operation before returning to Keflavik.

For the NAWDEX campaign, measurement permission (aerial permit to operate away from airways and dropsondes) will be requested for an area comprising the North Atlantic, Greenland, Iceland, UK, Ireland, Norway, France, Germany, Poland, Benelux, Austria, Italy, Spain and Denmark.

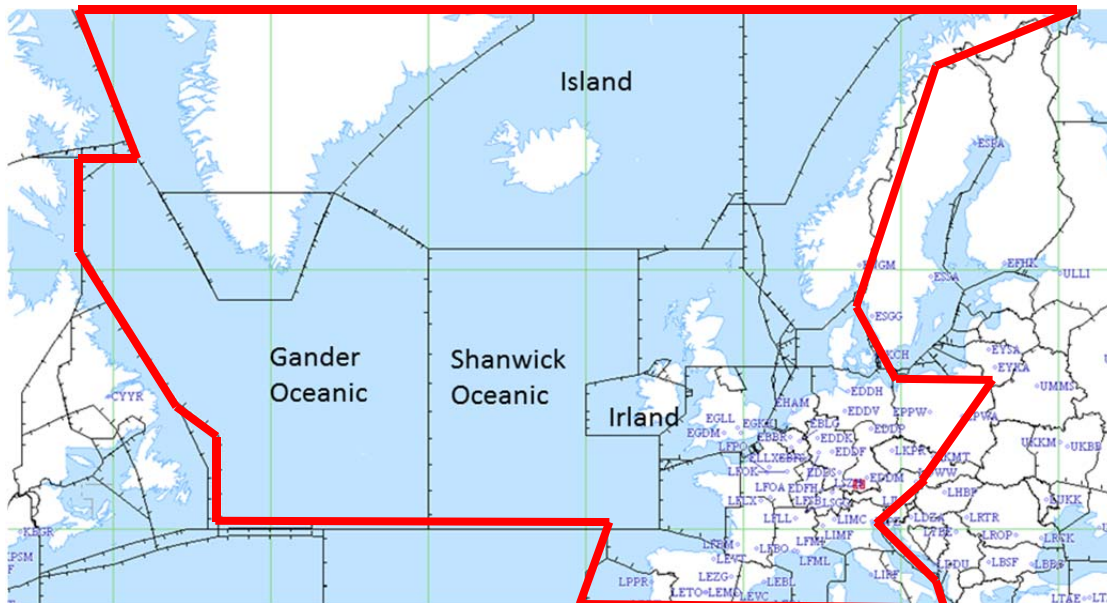


Figure 5.3 Air Spaces over the North Atlantic and Europe. Red area shows countries where measurement permissions are requested for NAWDEX.

5.3 Mission Operation (for FX, to be iterated)

- Hangar required for both aircraft
- GPU shipped with container or local rent has to be checked (has to be discussed with NARVAL II)
- Storage: as during NARVAL/WindVAL
- Time in advance and after the flight for work at the aircraft:
 - HALO: 3h before the flight, 2 h after the flight (can possible be reduced)
 - Falcon:
- Working hours during preparation: regular, Mon-Fri
- Nr of scientists in Iceland: XX
 - Planning team XX
 - Operators XX
- Operation Centre: for XX persons
- Meeting room: for XX persons
- Freight:
 - HALO (as for NARVAL North 2014):
 - Air freight in kg: 650 kg
 - Nr of container for sea freight: 0
 - Falcon: as during WindVAL
 - Air freight in kg:
 - Nr of container for sea freight: 1

5.4 Schedule

5.5 Personnel

5.6 Flight restrictions

This chapter summarizes the experience from a number of campaigns that were taken out over the North Atlantic, NARVAL North with HALO in January 2014, ML-CIRRUS with HALO in 2014, T-NAWDEX-Falcon in 2012 with Falcon and WindVal with the Falcon in 2015). We list experiences with flight planning and flight restrictions.

This list has to be updated in the preparation phase of NAWDEX. Several points have to be adapted and discussed with the aim to improve communication with ATC to facilitate the planning process and to achieve best flexibility for scientific flights during NAWDEX.

5.6.1 Operation in transatlantic air-space

North Atlantic tracks (information taken from <http://occ.iviao.aero/index.php?site=airspace>):

- The North Atlantic airspace is controlled by the Gander Oceanic Flight information region (FIR) and Shanwick FIR. It comprises an area from 44° North to 61° North and partly up to 64° North (see Figure 5.3). This airspace has virtually no land-based navigational aids or communication relays.
- Dynamic flight routes so called North Atlantic tracks (NATs) for commercial transatlantic traffic are defined depending on wind situation
- Flight routes cover FL 285- FL 420
- The hours of validity of the two Organized Track Systems (OTS) are normally: day-time OTS (westbound): 1130z – 1900z night-time OTS (eastbound): 0100z – 0800z
- NATS are defined only about 17 h in advance. As the flight plan had to be submitted already the day before, it was complicated to consider location and timing for the flight planning so far. There was no discussion with ATC about operation in consideration of NATS (also not FL > 430)

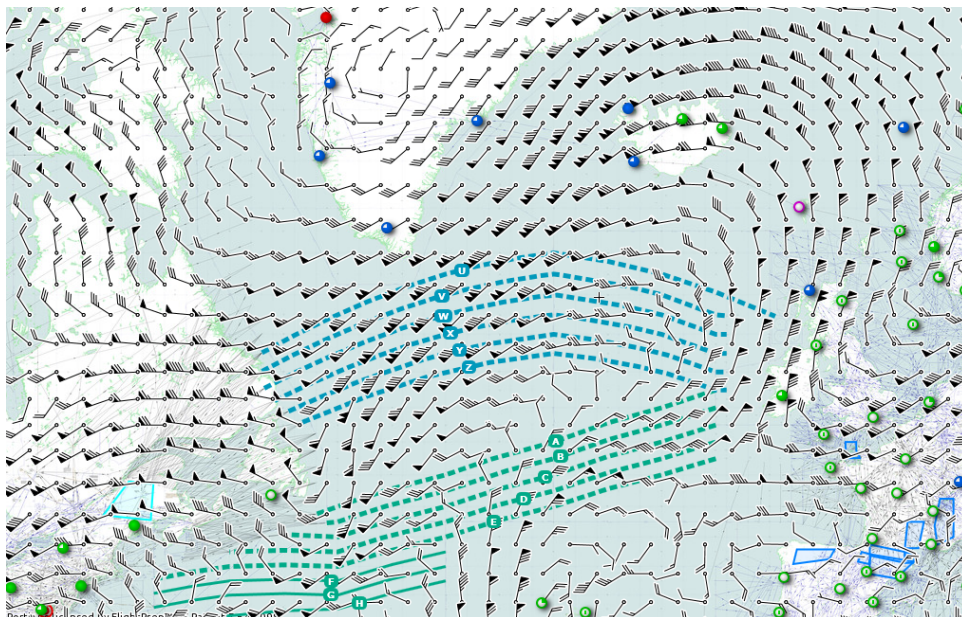


Figure 5.4
Example of NAT tracks on 8 July 2015. U-Z show eastbound traffic, A-H westbound flight routes, wind barbs at 300 hPa, figure taken from skyvector.com

Operation above FL 270:

- Envisaged transfers at high altitudes (FL 400 and higher) above main commercial air traffic with a subsequent descend in a target region could not be realized and were not tried.
- height changes and flight pattern above FL 270 were commented by ATC with „may or may not be possible“. Flights between FL 270 and FL 430 in NAT altitudes were judged as impossible.
- Height changes were only possible in radar controlled airspace (Gander, Iceland, Shannon) or regions of little traffic (Greenland)
- We did not perform complicated observation flights in altitudes above FL 430. ATC considered flights above FL 430 as possible under optimal conditions. However, in case of air traffic they left open to cancel the flight on short notice. One direct flight from Ireland to Iceland at FL 430 was conducted during NARVAL.

Flights below FL270 (<8 km altitude)

- FL 270 and below offered higher planning reliability. On the day before a measurement flight we were able to define a large-scale operation area that was reserved only for HALO. This was possible in the NAT airspaces of Shanwick und Gander. Inside these areas it was possible to flexibly perform desired flight pattern that could be adapted to changing weather conditions. Also moderate adaptations during flight were possible.
- Entry and exit points to the defined boxes as well as coordinates with overflight times had to be defined. Within one FIR a change of entry and exit points to the reserved box were changeable on the flight day.

Dropsondes

- Dropsonde release in Icelandic air space and Gander and Shanwick below FL 270 were possible (NOTAM required)
- Gander and Shannwick above FL 270 impossible
- Greenland (Denmark) gave no permission (no established procedure). During WindVAL NASA DC-8 dropped sondes!?
- The drift of the dropsondes was taken into account so that they do not leave the predefined areas

5.6.2 Operation in European airspace

The following experiences with flight planning refer to the T-NAWDEX-Falcon Campaign in 2012 (Schäfler et al. 2014): “There were many different restrictions the scientists had to deal with during the preparatory phase of this campaign and also when planning the flight routes. The execution of research flights in European air space demands intensive logistical preparation.

Air traffic over Europe is generally very dense and a number of authorities need to be contacted and asked for permissions to operate freely away from airways (aerial work permit) and to release dropsondes. To reach the scientific objectives it was crucial to perform measurements away from airways as the shape and location of WCBs is very variable and forecast uncertainty was expected to be high.

Figure 5.5 gives an overview of the achieved permissions from the different countries. The regulations of Air Traffic Controls (ATCs) varied from country to country in terms of lead time for the submission of

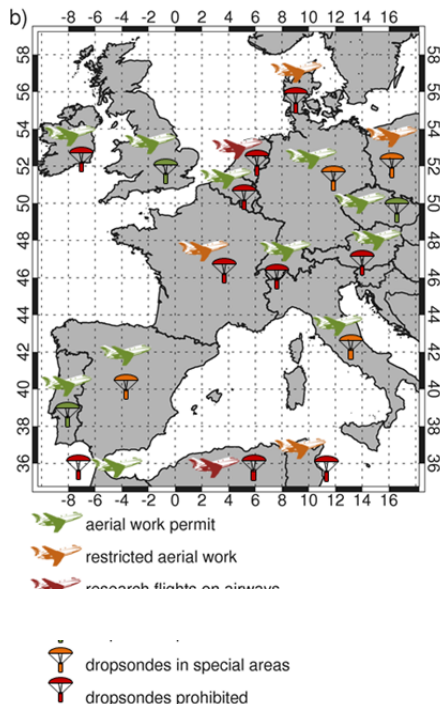


Figure 5.5 Overview of the permission status for aerial work and dropsonde releases during T-NAWDEX Falcon.

the flight patterns, and in terms of the area where free operation was permitted. Some countries refused aerial work and required the definition of generic flight patterns with fixed flight routes and altitudes that could be activated during the campaign.

Generally the first announcement to the relevant ATCs had to be made already 2-4 days in advance. In several countries military trainings were announced which blocked parts of the airspace.

It was even more complicated to obtain permission to release dropsondes (see Figure 5.5). In many countries laws of aviation forbid the release of any object from an aircraft. Although the danger for beneath flying aircraft and the population is very low, a remaining risk is unavoidable. Permission was granted over British territorial waters, in some German and Italian restricted areas, in some Spanish regions, mainly over sea, and over international waters of the Malta airspace. Slovakia and Portugal generally allowed the use of dropsondes. We tried to adjust flight routes such that dropsondes could be released whenever possible. Further limitations for the flight planning were airport opening hours and crew duty times, which partly constrained options for sequential flights in a developing WCB."

5.6.3 Planning process

In summary the current regulations have to be followed:

- ATCs need a notification of measurement flights as early as possible. A submission of the detailed flight plans on the day before was sufficient.
- Confirmation of flight plans within 24h before the flight when ATC is able to estimate air traffic.
- For trans-Atlantic air spaces flights were requested and coordinated by EUCARF (European Central Altitude Reservation Facility, Ramstein), EUCARF is closed on weekends and public holidays, ARE (ALTITUDE RESERVATIONS EAST, NAVCANADA Altitude Reservation Unit) is closed on week-end, Shanwick limited
- Flight plans for Saturday, Sunday and Monday have to be submitted on Friday at noon (more planning flexibility on weekend if Gander is not affected).

The following points to improve the performance of flight over the North Atlantic during NAWDEX have to be discussed together with DLR-FX-operations in the preparation phase:

- Can we consider location and timing of the NAT region: simple flight pattern (east west oriented and clearly north of the NAT, outside peak of main traffic)
- Are there options to get better planning reliability for high level flights (>FL 430)?
- Would it help to work out scenarios and visit ATC for personal exchange?
- Contact to ATCs was complicated on week-ends. Could this somehow be improved?

5.6.4 Ideal setup

Under current ATC regulations an ideal setup would be a Rossby wave amplifying north so that the diabatic outflow and Jetstream are located close to Iceland. This would allow an early flight in the evolution stage of the cyclone with HALO below the main air traffic and an observation at maximum altitudes with both aircraft when the outflow interacts with the waveguide around Iceland.

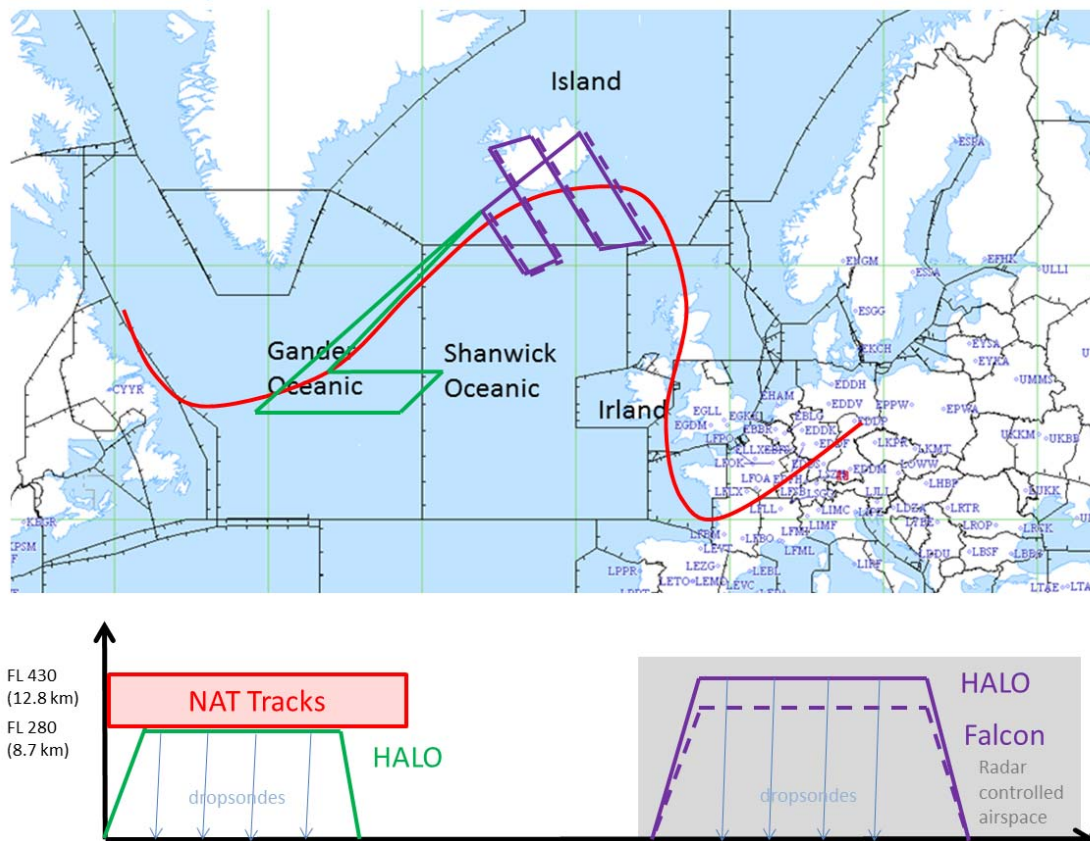


Figure 5.6 Schematic for coordinated flights under current regulations as planned for NAWDEX.

5.7 Pilots working hours

6 Data handling

Aircraft data will be archived in the HALO database which is operated at DLR-IPA (<https://halo-db.pa.op.dlr.de/>) and which allows optimal access to data. Data usage will follow accepted best practices as defined in the usual HALO Data Protocols. These protocols treat data analysis, deadlines for data storage to the data base and access to the data. Typically data protocols are coordinated between the campaign partners and follow the rules of good scientific practice defined by DFG. To our knowledge a template version is currently discussed in the HALO scientific steering committee (WLA)

7 Preparation

For the preparation of NAWDEX a number of case studies are performed with the aim improve the flight strategies, optimize the use of instruments and train flight planning. In the following the cases from previous years which showed suitable NAWDEX scenarios are described. Additionally some cases from previous measurement campaigns (with different research focus) are shown. In September and October 2015

7.1 Previous cases in the campaign period

7.1.1 Extratropical transition of TC Rafael (2012) – the western North Atlantic case

a) Synoptic setup

Hurricane Rafael (labelled as “TC” in Figure 7.1) became extratropical at 40N, 60W on 17 October 2012. Rafael moved northeastward to the south of an extratropical low (L1) which was located over the Gulf of St Lawrence at that time (Figure 7.1a). It is suggested that diabatic processes in the region of the occlusion of L1 contributed to a northward deflection of the midlatitude waveguide (R1).

The ex-Rafael moved northeastward into R1 until 18 October (Figure 7.1b). A dry intrusion to the south of Rafael, cold frontal structures and an extended cloud shield to the north showed that an interaction with the midlatitude baroclinic flow was in progress. WCB-like ascent east of Rafael into R1 potentially contributed to an anew amplification of R1 over the central North Atlantic until 19 October (Figure 7.1c). The northern part of R1 evolved into a cut-off anticyclone until 21 October.

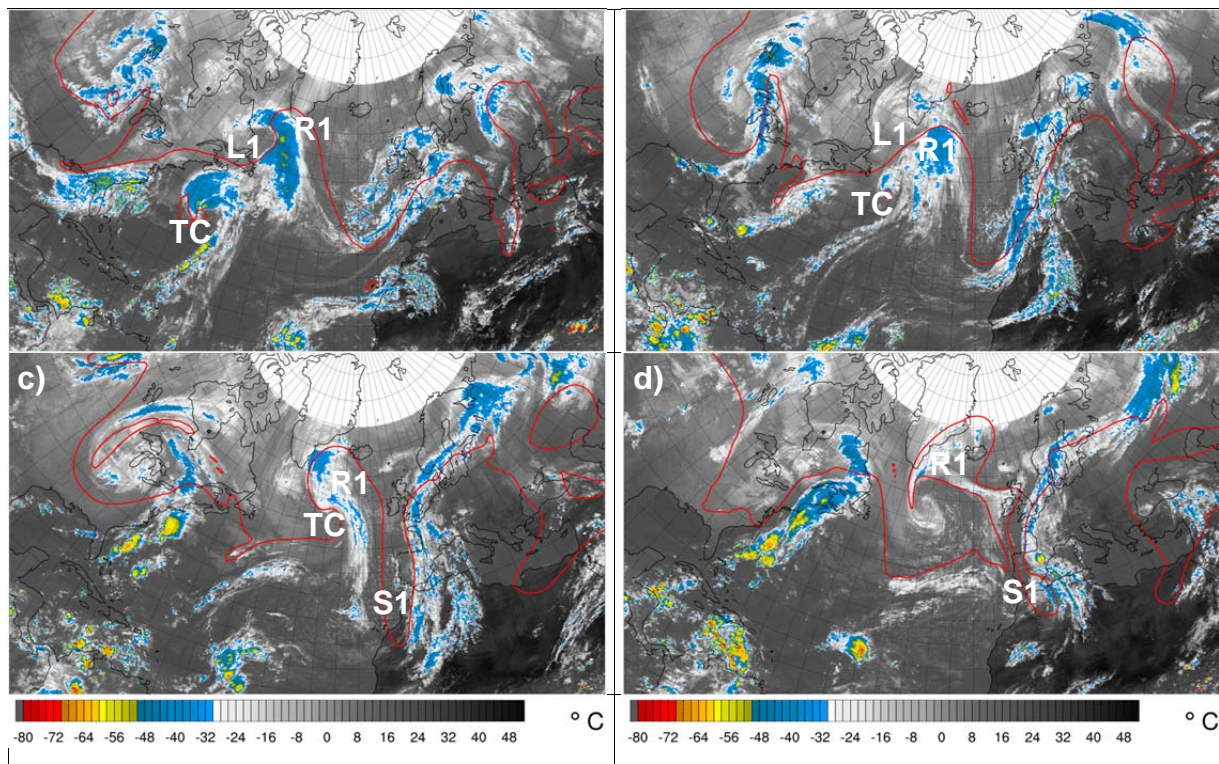


Figure 7.1 GridSat-B1 brightness temperature (shading in °C) and ERA-Interim 2PVU contour at 330 K from (a) 17 October 1200 UTC to (d) 20 October 1200 UTC.

Presumably in response to the amplification of R1 a remarkable PV streamer (S1) developed over the eastern North Atlantic (**Fehler! Verweisquelle konnte nicht gefunden werden.**c, d). Thunderstorms that developed on the eastern flank of this PV streamer caused heavy precipitation in Spain and southwestern France (Pantillon et al. 2014). At the same time, the strong southerly flow on the eastern flank of the PV streamer advected subtropical air masses toward central Europe. In conjunction with Foehn, new October temperature records were reached in the Alpine region (e.g. Vaduz 29°C).

b) Observation period 18 October 2012, 1200 UTC

The first observing period is designed to investigate the ridge amplification through the TC and through the extratropical low. The instrumentation of the DLR Falcon aircraft would be suitable to measure the structure of the jet in a region where the irrotational wind impinges on the midlatitude waveguide. This would allow to document the remote impact of diabatic processes on the midlatitude flow. Negative PV advection peaks along the flanks of the ridge at 340 K (Figure 7.2a). Thus, the flight heads southwestward and crosses the jet (Figure 7.3a) nearly aligned to the irrotational wind. A cross section along the flight path shows that PV advection by the irrotational wind occurs mainly in cloud free regions so that measurements with the Lidar instrumentation should be possible (Figure 7.3b).

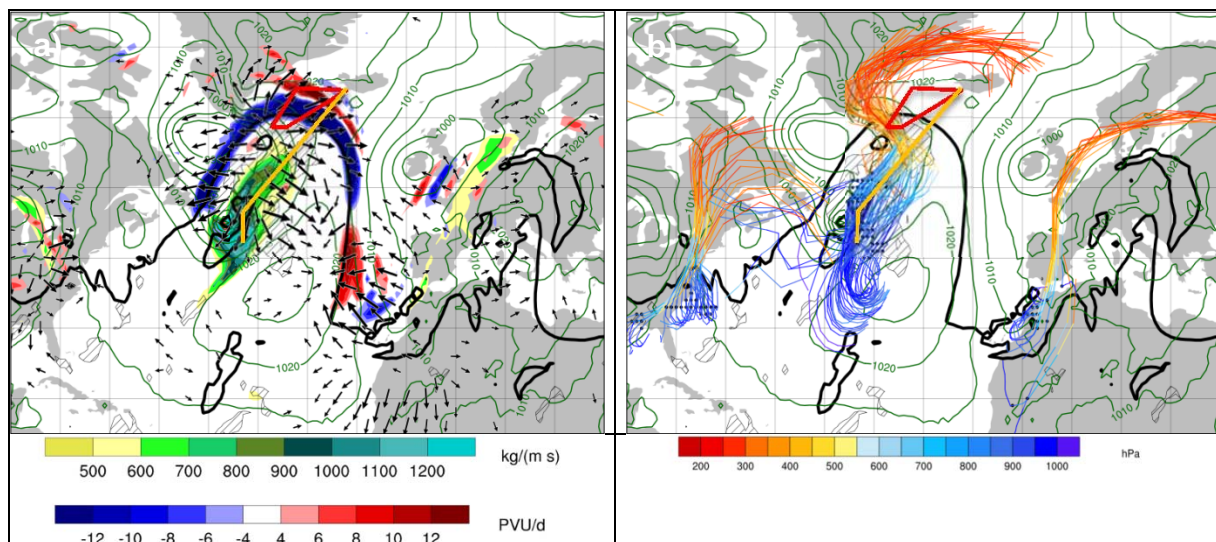


Figure 7.2 Flight path of Halo (thick orange line) and DLR Falcon (thick red line) starting on 18 October 2012, 1200 UTC. (a) PV advection by divergent wind (bluish/reddish shading in PVU/d) @ 340 K, 1000-100 hPa integrated vapour transport (greenish shading in kg/(m s)), 2 PVU contour (thick black contour) @ 340 K, divergent wind (vectors) @ 340 K, ice water content (regions where IWC > 10⁻⁵ kg/kg are hatched) @ 340 K and mean sea level pressure (green contours). (b) 48h forward and backward WCB trajectories coloured by pressure. Black dots indicate starting positions of WCB trajectories on 18 October 2012, 1200 UTC

After a short westward leg, the flight track turns northeastward and crosses the jet a second time. FL410 would be suitable to measure the winds in the region of negative PV advection which occurs between 250 to 200 hPa. A total flight distance of about 2050 km would allow to even extend slightly the flight track.

Trajectories suggest that a WCB played a crucial role in the amplification of the ridge R1 (e.g. Figure 7.2b). The instrumentation of Halo would allow to investigate the structure of the WCB related diabatic processes that contribute to the upper-level irrotational winds. Thus, the flight is designed to document the structure of the convection within the WCB and the liquid, cloud snow and rain water path. The deployment of dropsondes would further allow to estimate the water vapour transport in the region where the WCB trajectories start (see starting points in Figure 7.2b).

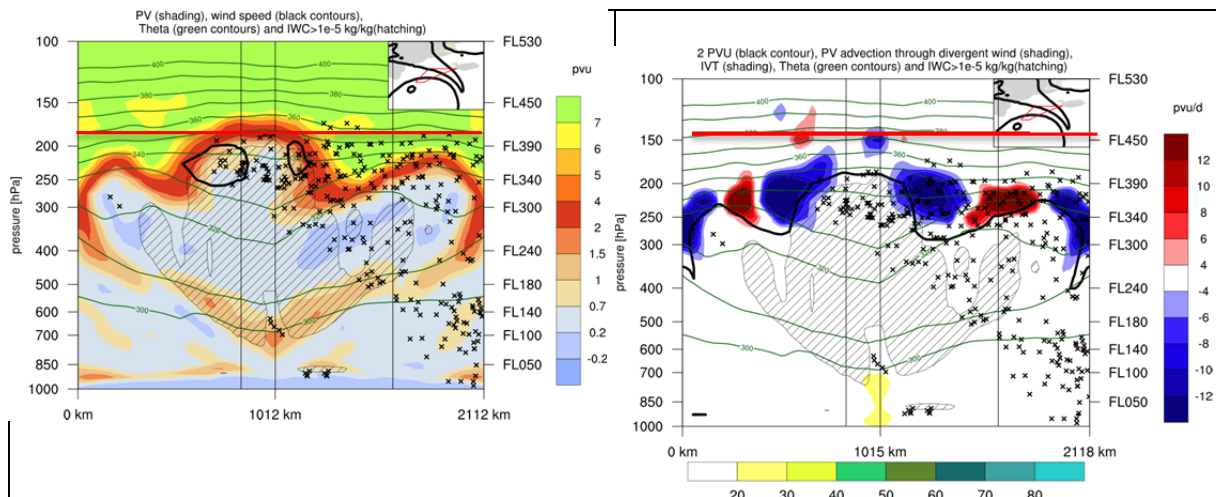


Figure 7.3 Cross section along flight path of DLR Falcon given in Figure 7.2. (a) PV (shading in PVU), potential temperature (green contours in K), wind speed (black contours starting at 50 m/s), ice water content (regions where IWC > 10⁻⁵ kg/kg are hatched), WCB intersection points. (b) as in (a) with PV advection by divergent wind (bluish/reddish shading in PVU/d), vapor transport (greenish shading) and 2PVU contour (thick black contours).

The flight heads southwestward toward ex-Rafael. After crossing the jet, Halo reaches a convectively active region as well as a region of WCB outflow as indicated by the WCB trajectory intersection points (Figure 7.4a,b). A flight close to the tropopause would allow to measure remotely

- the cloud structure in the convectively active region
- the spatial variability of the liquid, cloud snow and rain water path along the WCB-like ascending airmasses
- radiative processes in the WCB outflow region

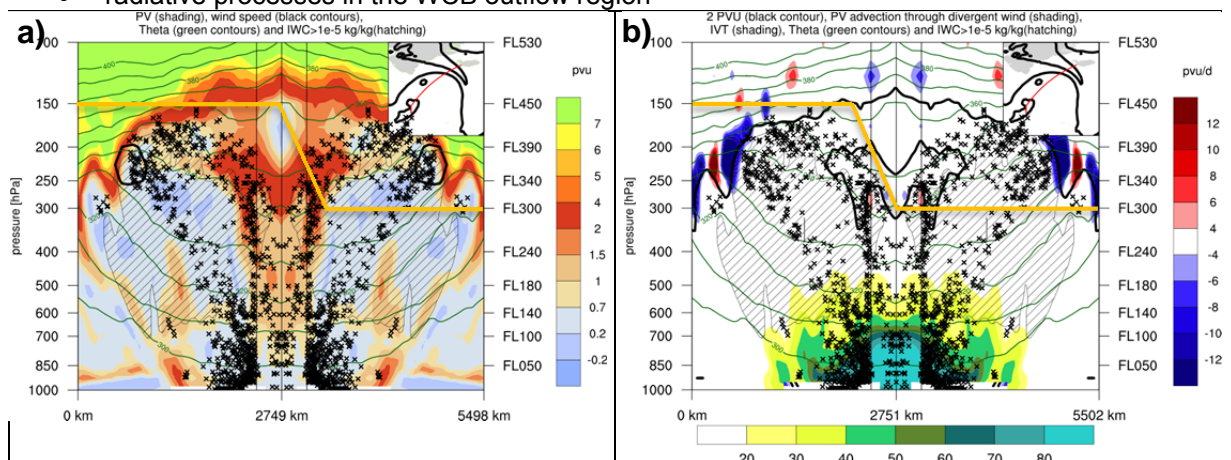


Figure 7.4 As in Figure 7.3 Cross section along flight path of DLR Falcon given in Figure 7.2. (a) PV (shading in PVU), potential temperature (green contours in K), wind speed (black contours starting at 50 m/s), ice water content (regions where IWC > 10⁻⁵ kg/kg are hatched), WCB intersection points. (b) as in (a) with PV advection by divergent wind (bluish/reddish shading in PVU/d), vapor transport (greenish shading) and 2PVU contour (thick black contours).

However, the dense cloud cover would not allow to measure profiles of water vapour and the water vapour transport with WALES. Thus, reaching its southernmost point Halo would descend to lower altitudes at which the deployment of dropsondes would be allowed. Sonde that are dropped from FL300 would capture the winds as well as information about water vapour which would provide information about the water vapour transport in the region of WCB inflow (see WCB intersection points between 1000 to 700 hPa and WCB starting points in Figure 7.2b). Despite the relatively low flight level the total distance of about 5500 km should be reachable with HALO.

An example of a 24-h adjoint sensitivity calculation valid at 1200 UTC 18 October 2012 is shown in Figure 7.5. The water vapor sensitivity is a maximum near a strong gradient in the water vapor flux at 850-hPa is shown in Figure 7.5a. This region was well sampled by the Falcon and is coincident with a WCB. The adjoint optimal perturbation for potential vorticity valid at the same time is shown in Figure 7.5b. Once again the HALO and to some degree Falcon, sample important regions of sensitivity.

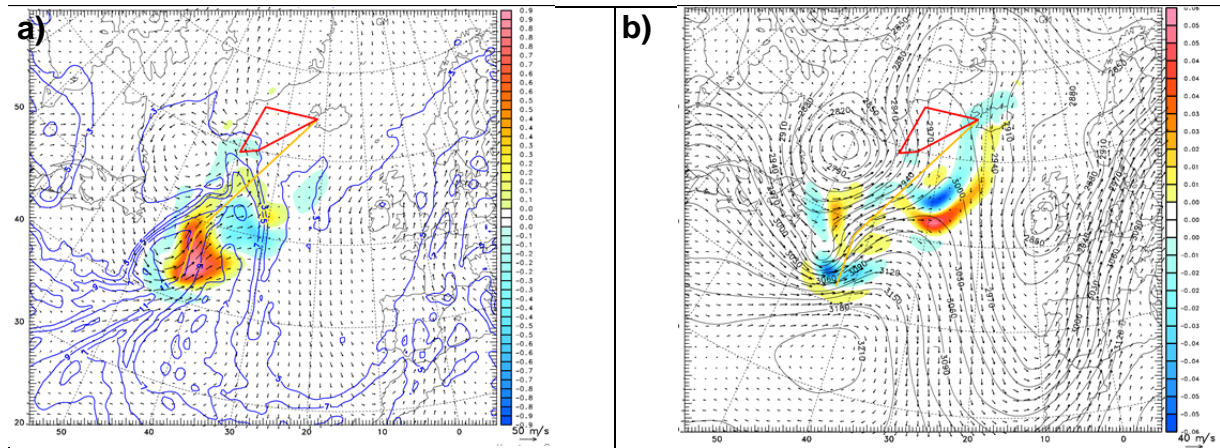


Figure 7.5 Adjoint valid at 1200 UTC 18 October 2012 for the (a) wind vectors, water vapor (every 2 g/kg), and water vapor sensitivity (color shading) at 850-hPa and (b) wind vectors, geopotential height (every 30 m), and adjoint optimal potential vorticity perturbations (color shading every 0.01 PVU) for a 24-h sensitivity calculation. In this example the response function is centered on the maximum wind speed in the southerly low-level jet at 1200 UTC 19 October. The HALO (yellow) and Falcon (red) tracks are shown

c) Observation period 19 October 2012, 1200 UTC

The WCB trajectories in Figure 7.2b suggest that the WCB outflow was located east of Greenland on 19 October 2012, 1200 UTC. The second observation period aims to reach this WCB outflow region, i.e. it aims to sample air masses that had been intensively investigated 24 hours before by Halo. According to the satellite image (Figure 7.1c) and according to mean sea level pressure (Figure 7.6a), ex-Rafael and the extratropical cyclone L1 have not merged on 19 October, 1200 UTC. Thus, the second observation period is also designed to investigate the convective nature of the two systems which still contribute to an upper-level divergent flow. This divergent outflow mainly impinges on the western flank of ridge R1 (Figure 7.6b). This region of negative PV advection by the irrotational wind would be hardly reachable with the DLR Falcon. Thus, the second observation period is designed to be performed by Halo.

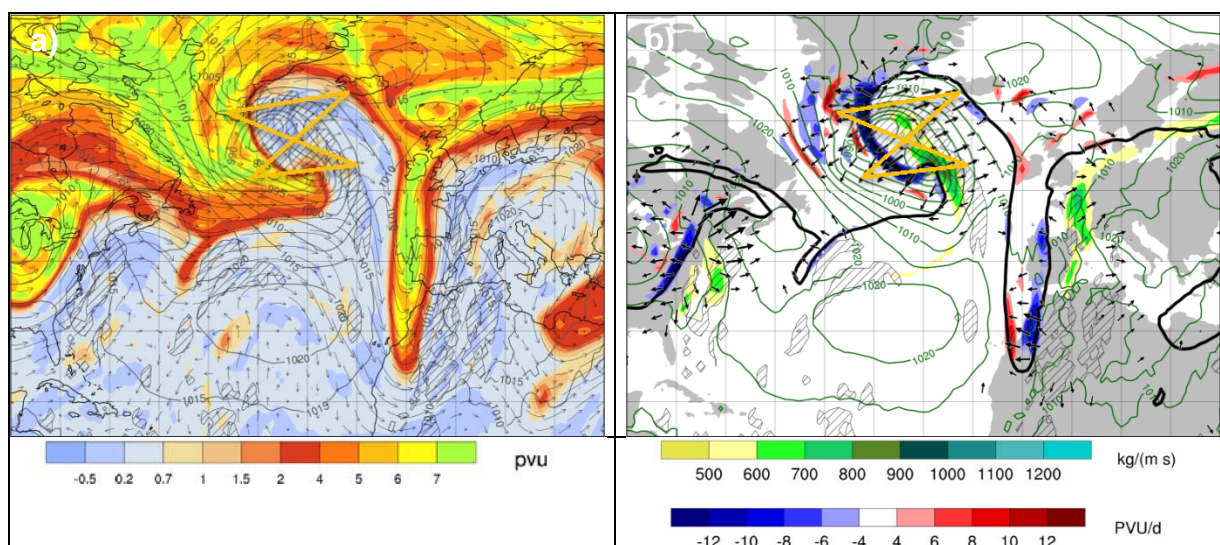


Figure 7.6 Flight path of Halo (thick orange line) starting on 19 October 2012, 1200 UTC. (a) PV (shading in PVU) @ 340 K, ice water content (regions where IWC > 10^{-5} kg/kg are hatched) @ 340 K and mean sea level pressure (gray contours), (b) as in Figure 7.2a.

The flight path initially crosses ridge R1 in southwesterly directions and reaches a region of WCB outflow as indicated by the WCB trajectory intersection points (Figure 7.8). The HAMP would allow measuring the liquid, cloud snow and rain water path in the convectively active region between ex-Rafael and the extratropical low. Depending on the flight level, Halo-SR could provide information about radiative processes associated with the extended upper-level cirrus shield.

After crossing the midlatitude jet, the flight path heads eastward and crosses ex-Rafael. Ex-Rafael is characterized by a PV tower that extends up to about 400 hPa (Figure 7.8a). The proposed flight path would allow investigating the structure of the convection east of ex-Rafael which developed in a region of strong low-level vapour transport Figure 7.8b). The vertical cross section indicates that convection still contributes significantly to negative PV advection through upper-level irrotational winds.

The last two legs of the flight would be suitable to sample the convective structure and paths of liquid, cloud snow and rain water in a region of WCB like ascent. An important aspect of NAWDEX will be the Lagrangian measurement approach, i.e. flights will be designed to measure the same air masses at several different times. Therefore, we calculated trajectories from the flight track on 19 October 2012, 1200 UTC at 310 K 48 hours backward and forward in time. The trajectories indicate that the flight on 19 October reached air masses that originated from a region of the Halo flight on 18 October 2012, 1200 UTC (Figure 7.9Figure 7.7). The pressure along the trajectories shows that the air parcels ascended between the two flights in the region of WCB like ascent.

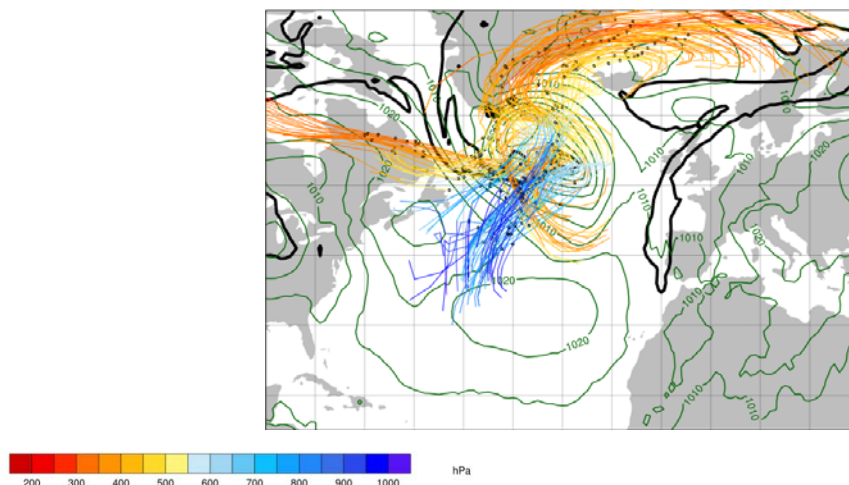


Figure 7.9

Figure 7.7 48h forward and backward trajectories started along flight track and coloured by pressure. Black dots indicate positions of trajectories on 18 October 2012, 1200 UTC and 20 October 2012, 1200 UTC.

The flight on 19 October 2012, 1200 UTC exhibits a total length of about 6300 km.

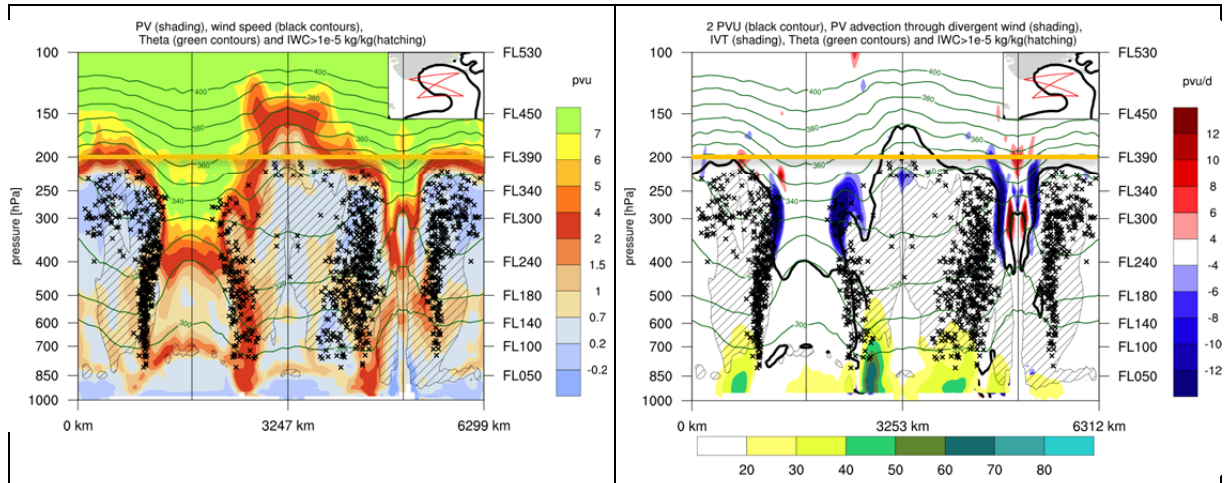


Figure 7.8 As in Figure 7.4, but on 19 October 2012, 1200 UTC.

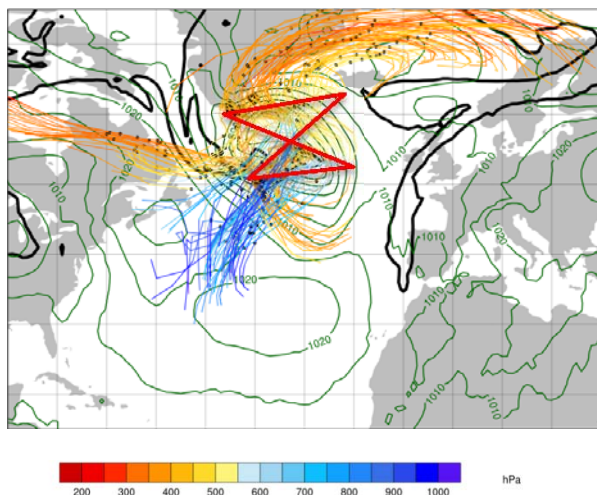


Figure 7.9

d) Air traffic during observation periods

The flight plans outlined above do not consider any air traffic so far. In order to get an impression of the air traffic at both flight times, we retrieved AMDAR data and overlayed coordinates at which data were measured on the PV charts Figure 7.9). Between 18 October 2012, 1200 and 1800 UTC several westbound flights crossed the region of the planned flight. In the northern part of the ridge the air traffic was less dense. The flight path of Halo should be practicable since FL450 on the southward leg and FL300 on the northward leg should avoid the main traffic. 24 hours later the westbound flights followed a similar track. Again, air traffic was less dense over the northern part of the ridge/tropospheric streamer. Since this flight is designed to measure remotely the convective structure and the spatial variability of liquid, cloud snow and rain water paths, this flight could be even performed at a higher FL than FL390.

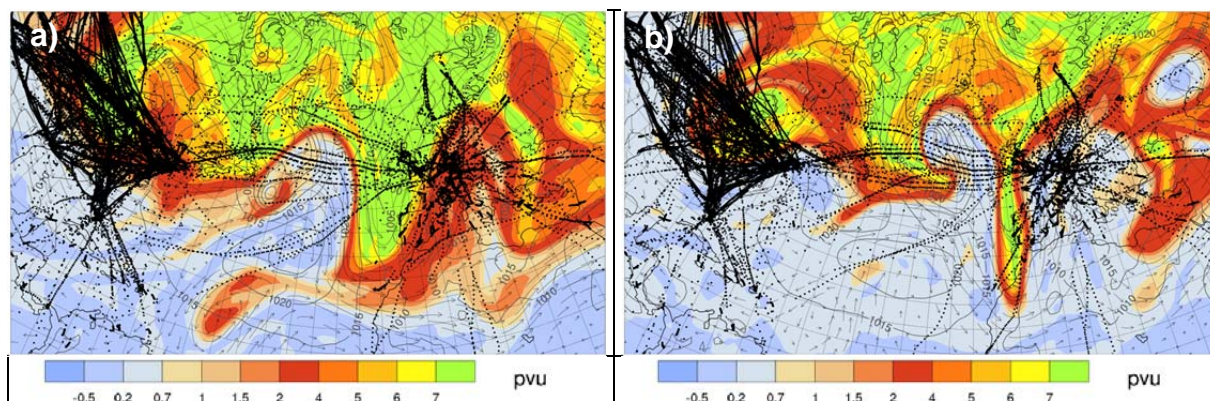


Figure 7.10 PV (shading in PVU), wind (vectors) at 340 K, mean sea level pressure (gray contours) and coordinates of AMDAR reports between 18 October 2012, 1200 and 1800 UTC (black dots). (b) same as in (a), but for 19 October 2012, 1200 to 1800 UTC.

7.1.1 The central North Atlantic case

a) Synoptic setup

On 19 September 2013, the synoptic situation was characterized by a ridge over eastern North America (R1), a weak trough over New Foundland (T1) and a disturbance over the central North Atlantic (L1). Deep convection over eastern North America contributed to an amplification of R1 which lead to a strong northerly flow component on the eastern flank of R1 (Figure 7.11a).

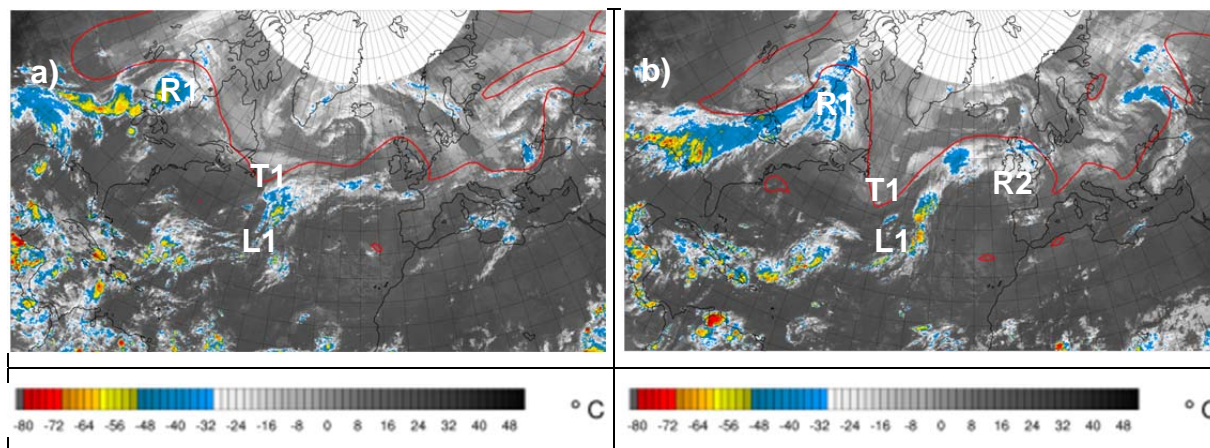


Figure 7.11 GridSat-B1 brightness temperature (shading in °C) and ERA-Interim 2PVU contour at 330 K on (a) 20 September 0000 UTC and (b) 21 September 0000 UTC.

This northerly flow was presumably conducive to a deepening of T1 which provided upper-level forcing for an intensification of the convection associated with L1. Between 20 and 21 September, WCB-like ascent developed ahead of T1. The upper-level divergent outflow associated with the WCB-like ascent slowed down the eastward progression of the upstream trough and contributed to the amplification of R2 over the eastern North Atlantic (Figure 7.11b).

b) Observation period 21 September 2013, 0000 UTC

The observation period is designed to document the structure of the upper-level PV gradient during the amplification of R2 through upper-level divergent outflow. The upper-level divergent outflow impinges to the south of Iceland on the midlatitude waveguide. Negative PV advection indicates an amplification of the ridge (Figure 7.12a). In addition, PV frontogenesis defined as

$$\left(\frac{d}{dt}\right)\left(\frac{\partial PV}{\partial x}\right) = -\left\{\left(\frac{\partial PV}{\partial x}\right)\left(\frac{\partial u}{\partial x}\right) + \left(\frac{\partial PV}{\partial y}\right)\left(\frac{\partial v}{\partial x}\right)\right\}$$

suggests that the upper-level divergent wind has a considerable impact on the temporal evolution of the PV gradient (Figure 7.12b). To document the structure of the PV gradient simultaneous flights by DLR-Falcon and Halo are required.

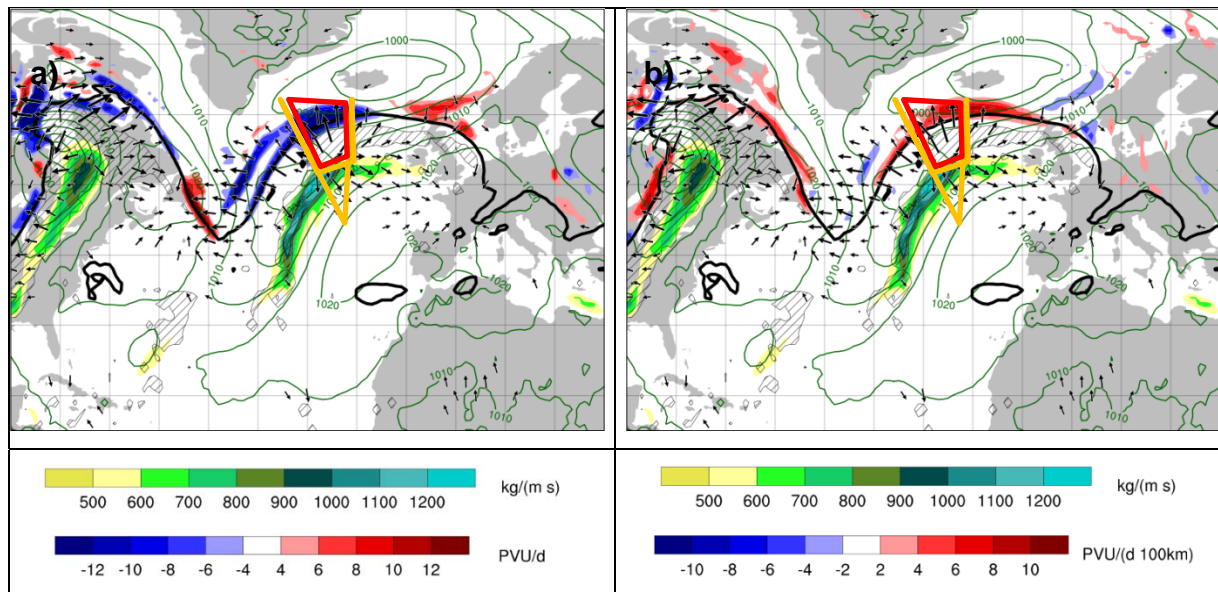


Figure 7.12 Flight path of Halo (thick orange line) and DLR Falcon (thick red line) starting on 21 September 2013, 0000 UTC. (a) PV advection by divergent wind (bluish/reddish shading in PVU/d) @ 330 K, 1000-100 hPa integrated vapour transport (greenish shading in kg/(m s)), 2 PVU contour (thick black contour) @ 330 K, divergent wind (vectors) @ 330 K, ice water content (regions where IWC > 10⁻⁵ kg/kg are hatched) @ 330 K and mean sea level pressure (green contours). (b) As in (a), but for PV frontogenesis by divergent wind (bluish/reddish shading in PVU/(d 100km)) @ 330 K.

The flight tracks of both aircraft head initially southward and cross the waveguide to the south of Iceland in a region of negative PV advection and PV frontogenesis by the divergent wind. The instrumentation of both aircraft would allow measuring the wind speed in the region of the jet via lidar observations on board of the DLR Falcon as well as vertical temperature gradients via HALO-SR on board of Halo. Under the assumption that variations of winds along the jet are small compared to across-jet variations PV can be approximated as $Q \cong \left(\frac{1}{\rho} \left(f - \frac{\partial u}{\partial y}\right) \frac{\partial \theta}{\partial z} + \frac{\partial u}{\partial z} \frac{\partial \theta}{\partial y}\right)$ where f is the Coriolis parameter. The y-coordinate points in the across-jet direction and x-coordinate points along the jet. Thus, the instrumentation of both aircraft would allow a PV estimation solely based on observed quantities. After crossing the midlatitude jet, both aircraft turn westward and northward to document the structure of the PV gradient a second time. The flight track of the DLR-Falcon turns eastward back to Iceland due to flight range limitations.

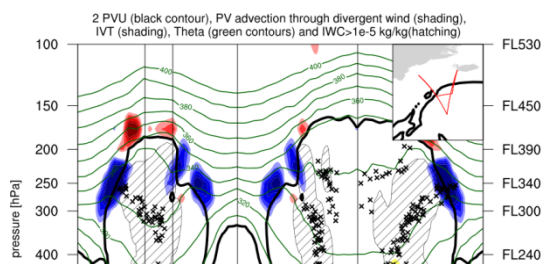


Figure 7.13 Cross section along flight path of Halo given in Figure 7.11. (a) PV advection by divergent wind (bluish/reddish shading in PVU/d), vapor transport (greenish shading), potential temperature (green contours in K), ice water content (regions where IWC > 10⁻⁵ kg/kg are hatched), WCB intersection points and 2PVU contour (thick black contours).

The flight range of Halo allows two more flight legs. The first of these two legs turns southward, crosses the jet and reaches a convectively active region. Measurements with HAMP would allow to measure the cloud structure in the convectively



active region. Dropsondes could be deployed to investigate the low-level vapour transport. Depending on the flight level, HALO-SR could provide valuable information about radiative processes in a region of WCB outflow as indicated by the WCB trajectory intersection points (Figure 7.13). The final northward leg would allow to document the vapour transport and cloud structure at a different location.

7.2 Observation examples

The following section shows observations of recent campaigns with a comparable payload installed onboard HALO and Falcon that however were taken with different focus. It demonstrates the capability of the instruments in situations comparable to NAWDEX.

7.2.1 Radar observations near frontal clouds

During the NARVAL campaign in 2012, the payload that will be flown during NAWDEX was used for the first time. With the aim to measure postfrontal precipitation events NARVAL performed long range flights from Iceland. In the course of these missions, several frontal cloud systems were passed that offer possibilities for NAWDEX preparatory studies. The campaign over the North-Atlantic showed a high data coverage although flying at lower levels (~ 8 km) beneath commercial trans-Atlantic air traffic.

On 12 January the clouds of an occluded cyclone located south of Iceland was observed. Close to Iceland the frontal clouds were passed (see red circles in Figure 7.14).

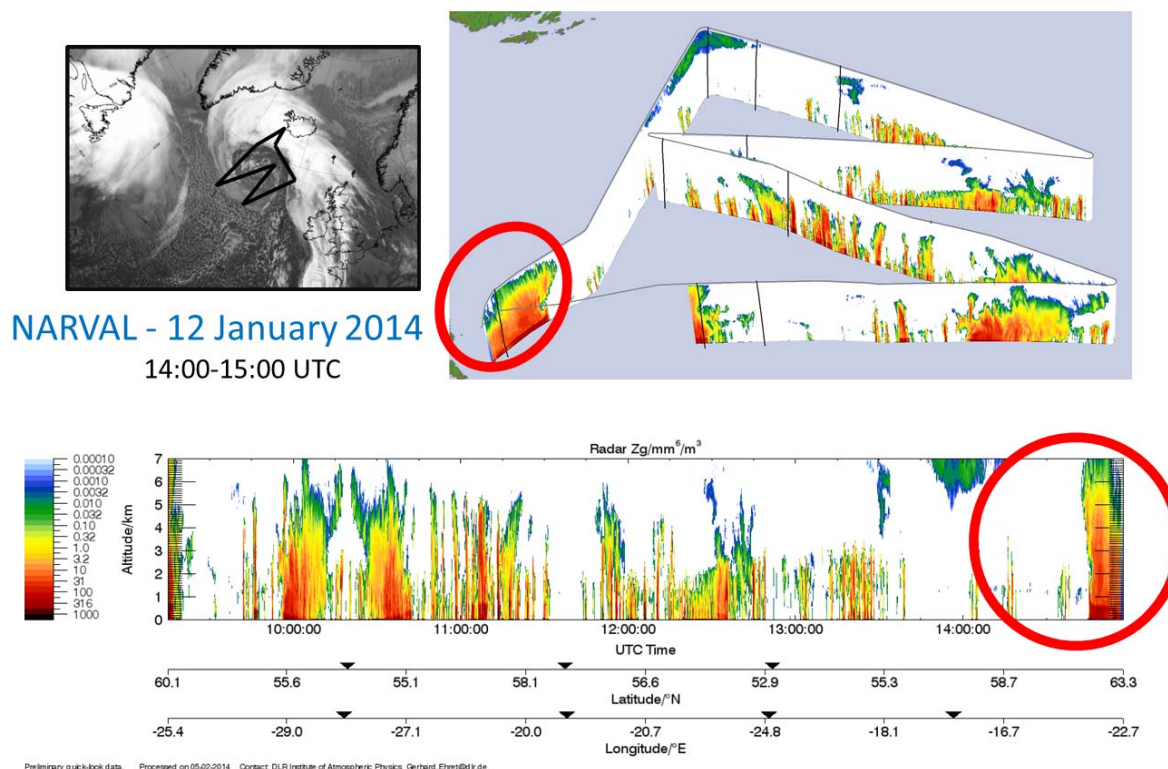


Figure 7.14 Measurement example of the NARVAL mission on 12 January 2014. Satellite image and radar reflectivity along the flight track from HAMP.

Several modelling studies showed a large uncertainty in the model representation of mixed-phase clouds. For the preparation of NAWDEX it is planned to use existing NARVAL data for frontal clouds to

investigate the benefit of radar, lidar and radiometer observations to investigate the representation of microphysical processes along WCBs. This will help to find optimal flight strategies for NAWDEX.

7.2.2 Humidity observations in the outflow of a WCB

During the ML-CIRRUS campaign in 2014 a series of HALO observations were conducted to observe mid-latitude natural and aircraft-induced cirrus clouds. A part of the observations focused on lidar observations of humidity from high levels. One double flight mission over the UK on 11 April 2014 focused on natural cirrus clouds. Trajectory calculations showed that moist air masses are related to a WCB ascent over the western Atlantic. It could be demonstrated that the DIAL is able to observe the water vapour structure inside optically thin cirrus clouds down to about 5 km altitude. Additionally dry layers related to stratospheric air could be observed. Based on this case we want to study the representation of humidity near tropopause in relation to WCB processes.

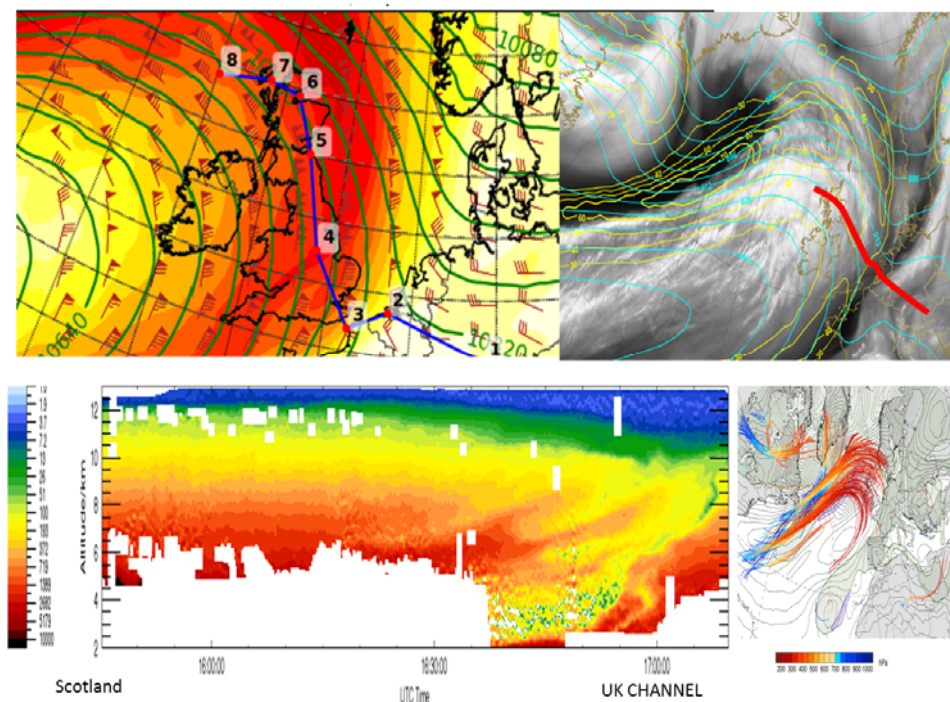


Figure 7.15 Summary slide of ML-Cirrus observations on 11 April 2014: Upper left: 300 hPa geopotential height and wind speed showing upper level ridge over the Atlantic and increased northerly winds over the UK. Upper right: WV Satellite image shows cirrus clouds being advected over the UK. Red line shows flight path of HALO. Lower left: Water vapour mixing ratio as measured by the WALES water vapour lidar. Cross section extends from the northernmost point in Scotland to the Netherlands. Lower right: Lagranto trajectory forecasts shows ascending WCB airmasses arriving over the UK at about the time of the flight

7.2.3 Jet stream wind observations during WindVal

During the WindVAL campaign the DLR Falcon was equipped with the NAWDEX wind lidar payload. One of the aims was to test the wind lidars in situations of strong horizontal and vertical gradients. After the passage of a cold front related to a cyclone south of Iceland a flight to Scotland was performed to observe increased Jetstream wind speeds in clear air.

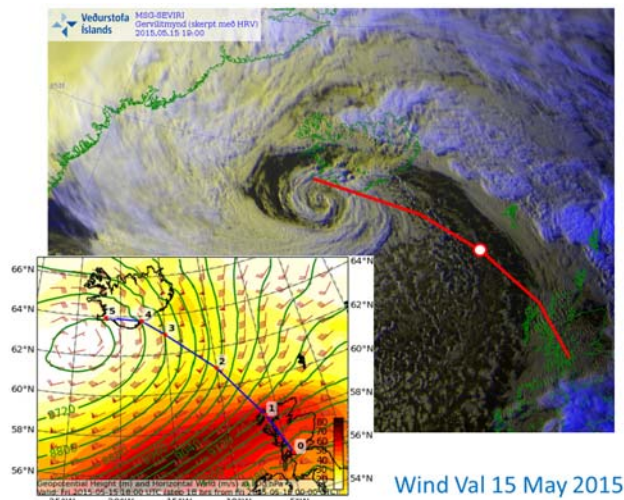


Figure 7.16 Large Panel: Satellite Image from the Icelandic Met Service showing a surface cyclone on 15 May 2015 @ 19 UTC south of Iceland. A flight (red line) was performed to Scotland and back. The white dot marks the position of the Falcon. Small panel: ECMWF forecast of 18 UTC geopotential height and wind field at 300 hPa showing an arriving jet stream over the Atlantic that was intersected on the way to Scotland.

The observations of horizontal wind speeds (see Figure 7.17) show strong wind velocities of up to 70 m s^{-1} related to the jet stream. The symmetry in the cross section results from the flight to Scotland and back on the same track. This was the maximum range of the aircraft.

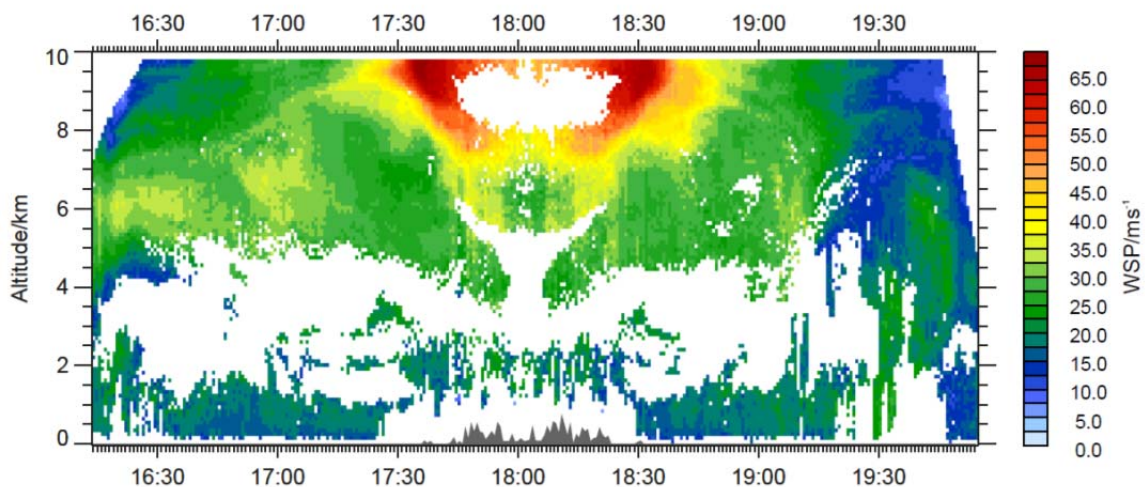


Figure 7.17 Wind speeds observed by the 2 micron Doppler wind lidar on 15 May 2015 on a flight from Iceland to Scotland and back.

The potential Vorticity at 330 K shows that a sharp gradient of PV was intersected close to Scotland. In this area the ECMWF forecast shows predicted advection of PV with the divergent wind.

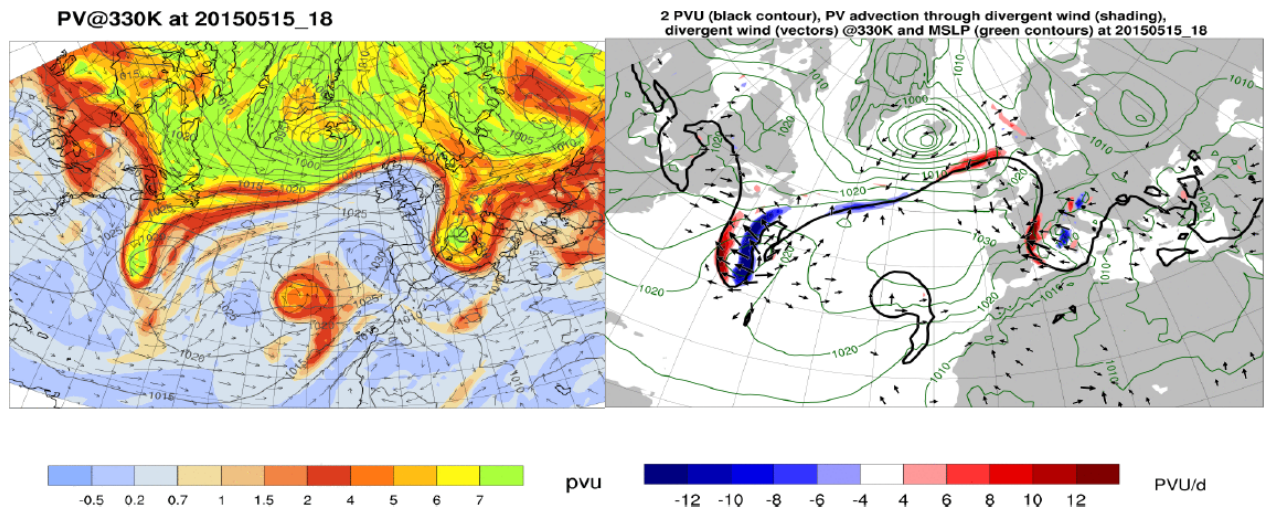


Figure 7.18 ECMWF FC (+18 h) for 15 May 2015 at 18 UTC: Left panel: PV (shading in PVU), wind (vectors) at 330 K and mean sea level pressure (gray contours). Right panel: PV advection by divergent wind (bluish/reddish shading in PVU/d) @ 330 K, 2 PVU contour (thick black contour) @ 330 K, divergent wind (vectors) @ 330 K and mean sea level pressure (green contours).

The campaign has shown that a new data analysis method for the 2 micron wind lidar horizontal wind speeds has significantly improved the data coverage in clear and clean air masses. Iceland has proven to be a good location to enter the NA jet stream with the range of the Falcon.

For the preparation of NAWDEX the two jet stream missions flown during WindVal are planned to investigate the representation of Jetstream winds near the tropopause. Additionally we want to apply the diagnostics for divergent wind for this cases and investigate what temperature information is needed to estimate PV from observations.

7.3 Climatology

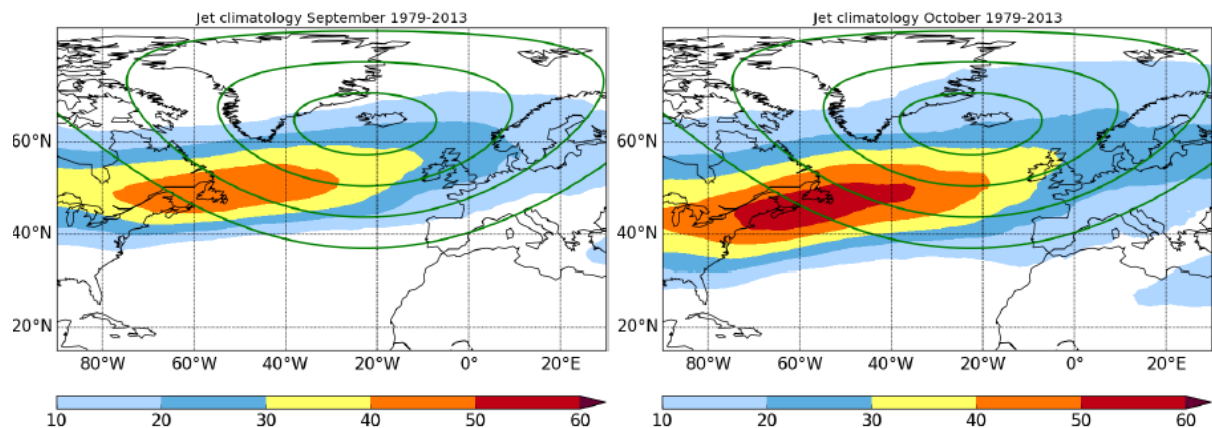


Figure 7.19 Occurrence frequency (%) that the mean wind speed between 400 to 100 hPa exceeds 30 m s⁻¹ based on 40 year (1973 – 2013) ERA reanalysis data.

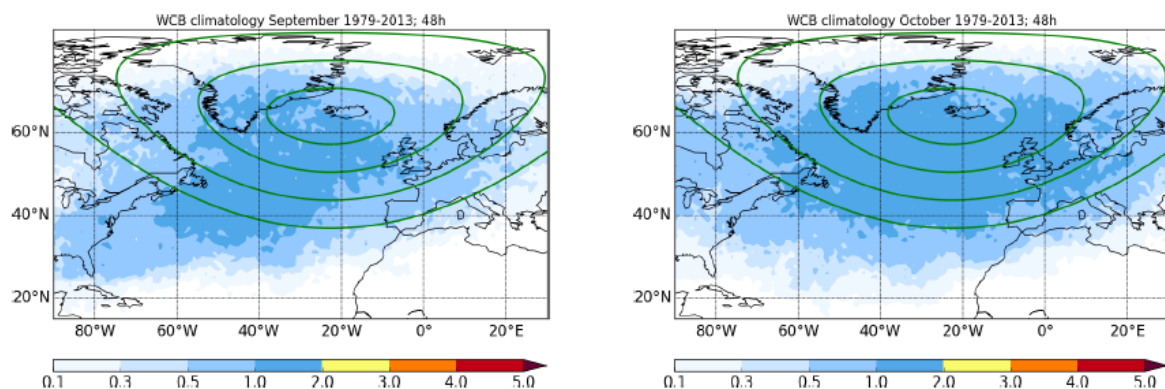


Figure 7.20 Figure 7.16 Occurrence frequency of WCB trajectories 48 hours after starting time based on 40 year (1973 – 2013) ERA reanalysis data.

7.4 Dry run

From 28 September to 9 October a dry run was performed that was based on daily weather briefings conducted via web conference. One year in advance of the campaign we used the weather situation to practice weather discussions, flight planning, decision making and coordination of observations. The available forecast products were tested and missing diagnostics are identified.

In the 2 week period

- 4-5 “NAWDEX weather events” were used for flight planning
- one „optimal case“ provided the possibility for potential observations of the the whole chain from ascending WCB airmasses to the interaction with the waveguide and formation of HIW downstream.
- we observed tropical systems that affected predictability in the early stage of the planning phase
- we had several possibilities to perform repeated flights in the proximity of Iceland due to blocking situation over Europe and Scandinavia
- we have seen that inflows appeared to be at the maximum range of the aircraft. Some situations may require stopovers even with HALO
- we observed very high outflows of WCB airmasses which requires maximum altitude operation
- the formation of pos. PV anomalies with quasi-lagrangian flights came up as an interesting scientific goal that also as it connects with the ground-based observations
- a long period of blocking high over Europe and little HIW downstream was observed

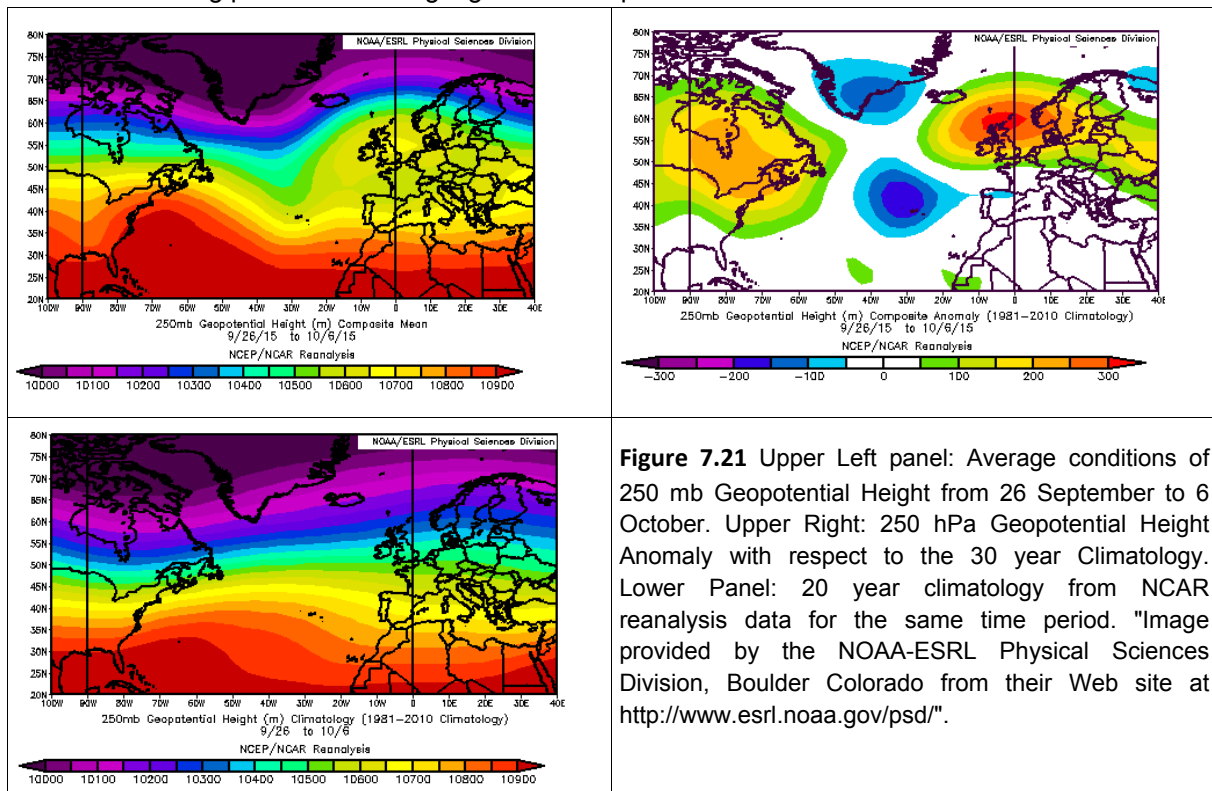


Figure 7.21 Upper Left panel: Average conditions of 250 mb Geopotential Height from 26 September to 6 October. Upper Right: 250 hPa Geopotential Height Anomaly with respect to the 30 year Climatology. Lower Panel: 20 year climatology from NCAR reanalysis data for the same time period. "Image provided by the NOAA-ESRL Physical Sciences Division, Boulder Colorado from their Web site at <http://www.esrl.noaa.gov/psd/>".

Figure 7.21 that shows the mean and anomaly for the 2week dryrun period for the 250 hPa Geopotential Height. The plots show the dominant high pressure over the UK causing the Jetstream to be deflected far to the north. This provided excellent conditions for “local” flights to observe upper level PV- features near Iceland. However, Europe was cut from High Impact Weather due to the large scale blocking.

7.4.1 Summary of NAWDEX dry run cases (28 September to 9 October 2015)

In the following, we provide a description of the dry run cases. These descriptions are based on the daily weather briefings during the NAWDEX dry run which were held by scientists from 9 institutions. The weather briefings are available at <http://www.pa.op.dlr.de/nawdex/dryrun.html>. As long as not otherwise specified operational ECMWF analysis and forecast data were used. The plots were created using exactly those tools at DLR and ETH Zurich which will be available during NAWDEX. For brevity some of the plots are not shown. If marked with a “*” the plots can be reproduced with the interactive cross section tool at <http://www.crosstool.ethz.ch/>.

1 (Pre-) Dry run case: Cyclogenesis over central North Atlantic/massive ridge building and anticyclonic wave breaking over western Europe

The first case of the NAWDEX dry run provided a perfect synoptic setup to address almost all primary objectives.

a) Synoptic situation from 26 to 29 September

A broad trough over the western North Atlantic and a weak ridge over the eastern North Atlantic characterized the synoptic situation on 26 September (Figure 7.22a). In the following days the western North Atlantic trough deepened and moved slowly eastward in response to a ridge building over North America. In a region of upper-level forcing a low pressure system started to develop ahead of the broad trough on 27 September (Figure 7.22b). The development of the low pressure system was presumably favoured by moist air masses emerging from the subtropics as indicated by high values of integrated water vapor (Figure 7.22d).

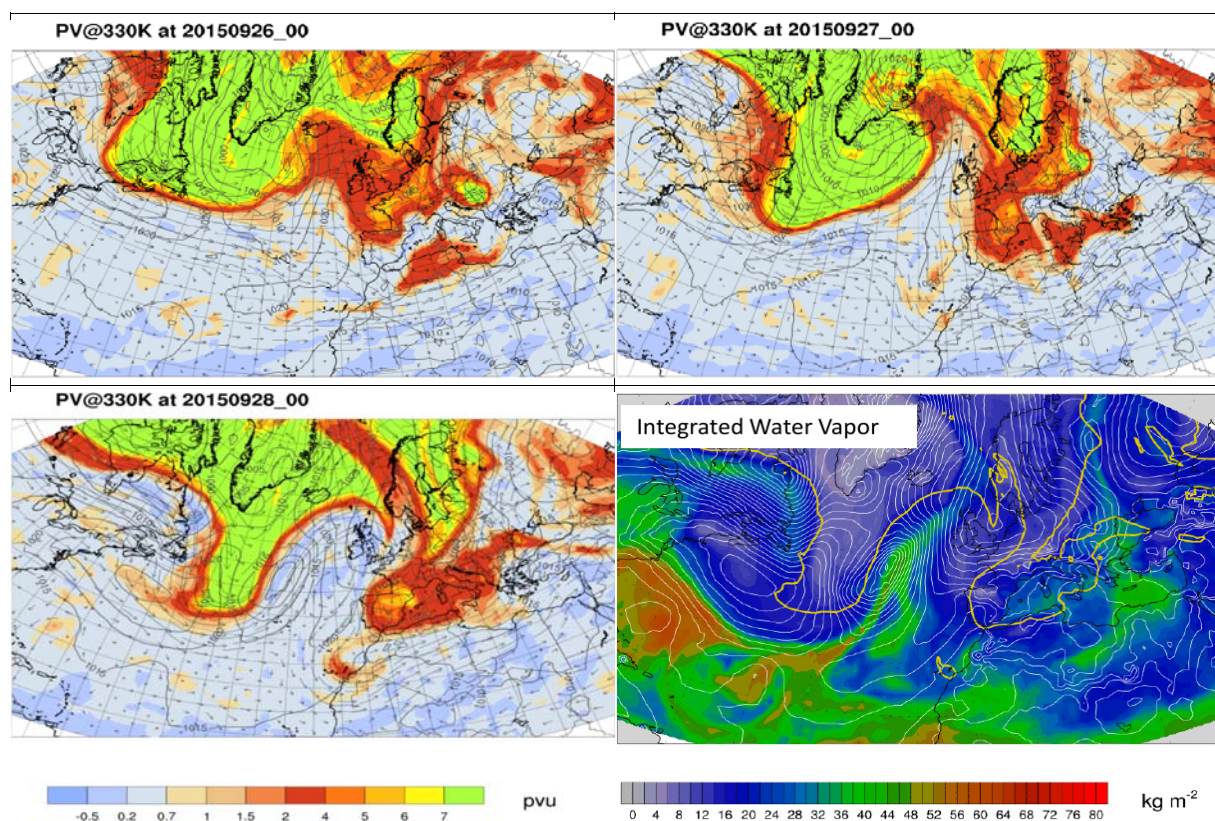


Figure 7.22 Synoptic evolution of PV (shading in PVU) @ 330 K, winds (vectors) @ 330 K, and mean sea level pressure (grey contours) from 26 to 28 September. Plot at bottom right gives integrated water vapor (shading), 2 PVU (yellow contour) @ 330 K and mean sea level pressure on 28 September.

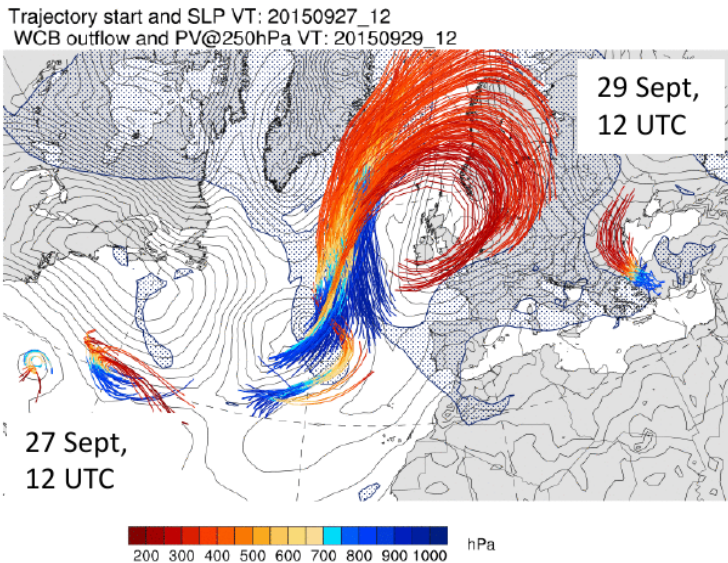


Figure 7.23 WCB trajectories starting on 27 September 12 UTC (around time of first flight). Trajectories are colored by pressure. Grey contours denote mean sea level pressure. Hatching indicates region where PV > 2 PVU at outflow time, i.e. on 29 September 12 UTC. Red ellipse marks inflow region of WCB.

Already at early stages of the development of the low pressure system diabatic processes presumably contributed to the erosion of the eastern flank of the upstream trough as well as to a ridge building over the eastern North Atlantic. On the one hand the diabatic processes enhanced upper-level divergent winds which impinged on the eastern flank of the upstream trough and thus slowed down the eastward propagation of the trough and thinned it gradually (not shown*). On the other hand diabatic processes associated with a massive WCB (Figure 7.21) led to cross-isentropic transport of low PV air which potentially contributed to the ridge building over the eastern Atlantic extending to Iceland on 28 September (Figure 7.22). This ridge building was further accelerated by upper-level divergent winds that impinged on the wave guide in the crest of the ridge (not shown*).

The upper-level ridge amplified further until 29 September and finally broke anticyclonically over western Europe. The development of a quite stationary high pressure system over western Europe was linked to this wave breaking event. The low pressure system which initially contributed to the ridge amplification crossed Iceland on 29 September and passed northward along the Norwegian coast.

b) Description of flights on 27 and 28 September

Since the inflow and outflow region of the WCB contributing to the ridge amplification were predicted to be within the range of the HALO aircraft (and partially within range of the DLR-Falcon), we decided to perform Lagrangian flights during the first days of the dry run. Actually, the synoptic development was close to the ideal setup illustrated in section 5.6.4 of this campaign implementation plan.

A first flight by HALO was designed to investigate the moisture structure in the boundary layer of the WCB inflow region and mixed phase clouds within the WCB (Figure 7.24 & Figure 7.25) addressing the primary objective described in section 3.2.1. Since most of the flight was forecast to be in clouds (Figure 7.25), LIDAR measurements with WALES were only partly possible (Table 4.7). However, a curtain of dropsondes allowed to measure wind speed and moisture in order to obtain information about the

low-level moisture transport in the WCB inflow region information about the cloud structure, and liquid, cloud snow and rain water path (Table 4.4) within the ascending air masses.

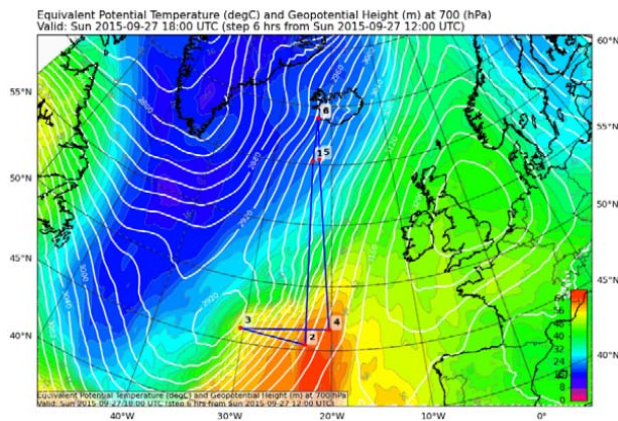


Figure 7.24 Equivalent potential temperature (shading) and geopotential height at 700 hPa (white contours) on 27 October 18 UTC, i.e. at around the time of first flight. Blue line denotes suggested flight track.

From a flight restrictions perspective, dropsondes are not allowed in the Gander Oceanic/Shanwick Oceanic corridors at levels of the NAT tracks or above. Hence, the flight was performed below the minimum level of NAT tracks at FL 280 (or below). Even at that relatively low and therefore fuel consuming flight level HALO easily reached the WCB inflow region.

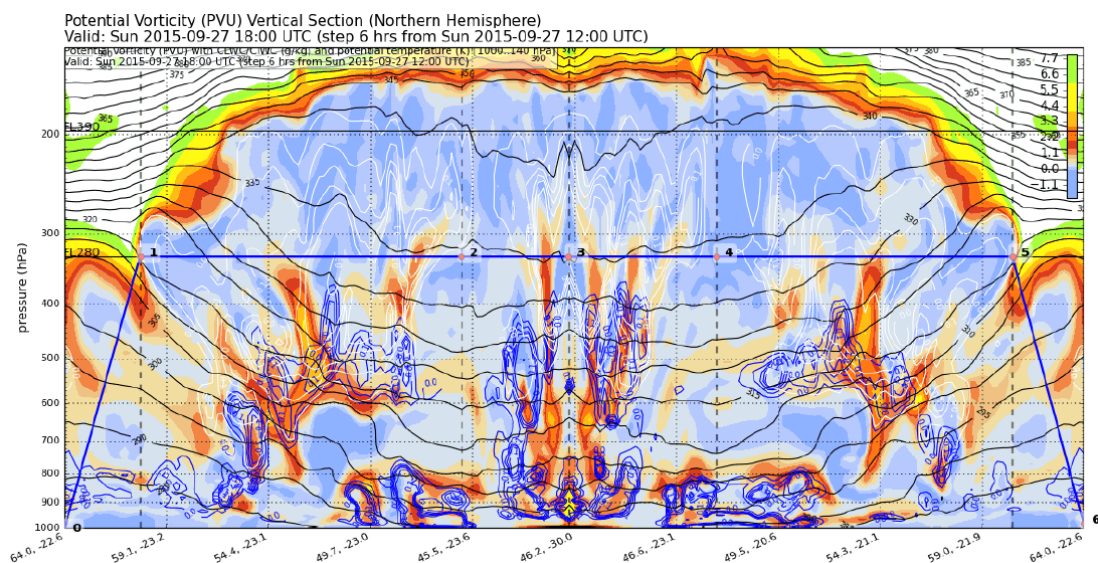


Figure 7.25. Cross section of PV (shading), potential temperature (black contours), cloud liquid water content (blue contours) and cloud ice water content (white contours) along proposed flight track on 27 September.

The synoptic situation was perfectly designed to perform Lagrangian flights into the WCB outflow region about 24 hours later. Since the WCB outflow and the wave guide were located exactly over Iceland, coordinated flights of HALO and the DLR-Falcon were possible on 28 September.

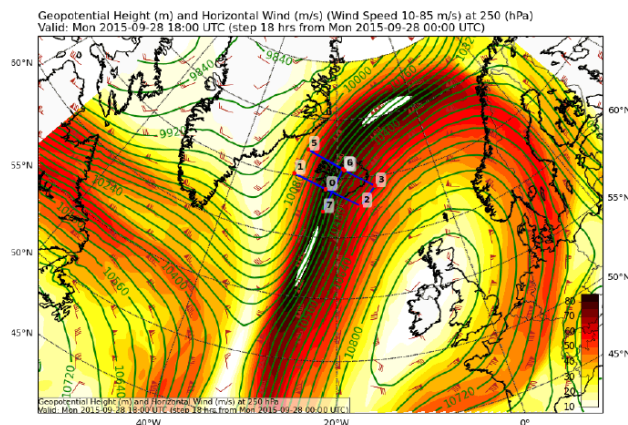


Figure 7.26 250 hPa wind speed (shading), geopotential height (green contours) and wind (barbs) on 28 September 1800 UTC. Blue line indicates proposed coordinated flight tracks of DLR-Falcon and HALO.

The flight plans were designed as a zig-zag pattern over Iceland crossing the midlatitude jet four times (Figure 7.26 & Figure 7.27). Beside the Lagrangian aspect (section 3.2.8), the flights were designed to measure the dynamic and thermodynamic structure across the wave guide (section 3.2.3), the moisture and cloud structure in the tropopause region (section 3.2.6), and to quantify possible analysis errors in a region region where divergent winds impinge on the PV gradient (not shown*). The instrumentation of HALO flying on FL 390 allowed to measure the moisture and cloud structure in the tropopause region (WALES) as well as profiles of temperature and moisture (HAMP). A simultaneous flight with the DLR-Falcon (FL 360) allowed measurements of winds speed with the Doppler wind lidar (section 4.2.2). Thus, information about the upper-level jet structure can be used to quantify analysis errors, in particular in terms of upper-level PV. Since the flights were performed in radar controlled air space the dropping of sondes were allowed.

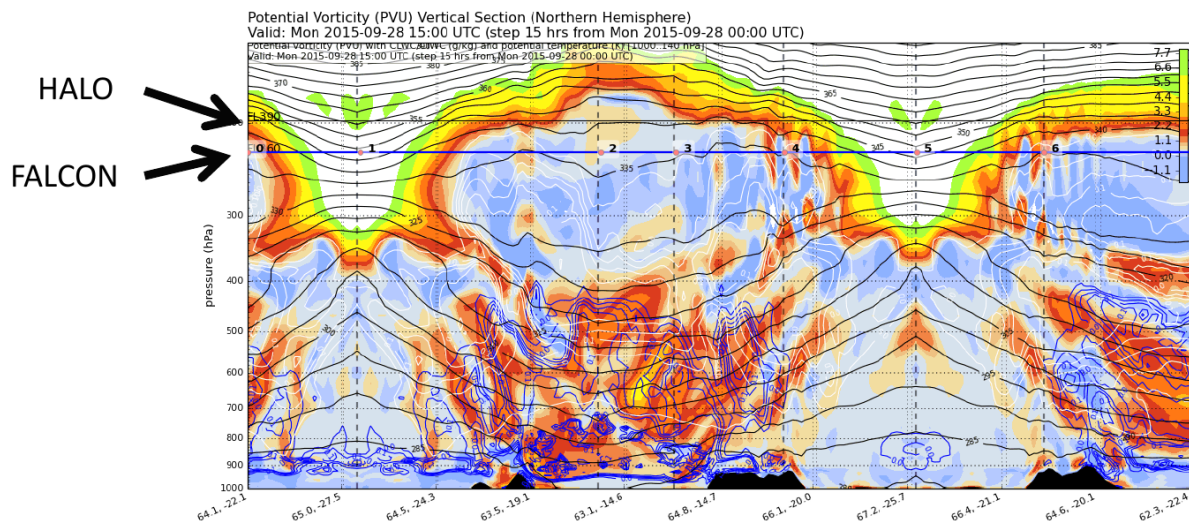


Figure 7.27 Same as in Fig. 21, but for proposed flight on 28 September.

With an estimated flight time of around four hours, the flight with HALO could have been extended southeastward toward the center of the upper-level anticyclone which was located over Ireland. This way aircraft based measurements could have provided additional information to the ground-based

observations over the UK. Since the center of the upper-level anticyclone was predicted to remain quite stationary over the UK (not shown*), intense observations of the structure and evolution of the upper-level PV (PV lense) would have been possible.

2. Dry run case: Strong zonal jet located over Iceland

a) Synoptic situation 30 September to 04 October

The highly amplified flow during the first case of the NAWDEX dry run was followed by a rather zonal flow over the North Atlantic during the first days of October (Figure 7.28). A relatively strong jet was located over Iceland on the northern flank of the quite stationary anticyclone that developed out of an anticyclonic RWB during the first event of the NAWDEX dry run.

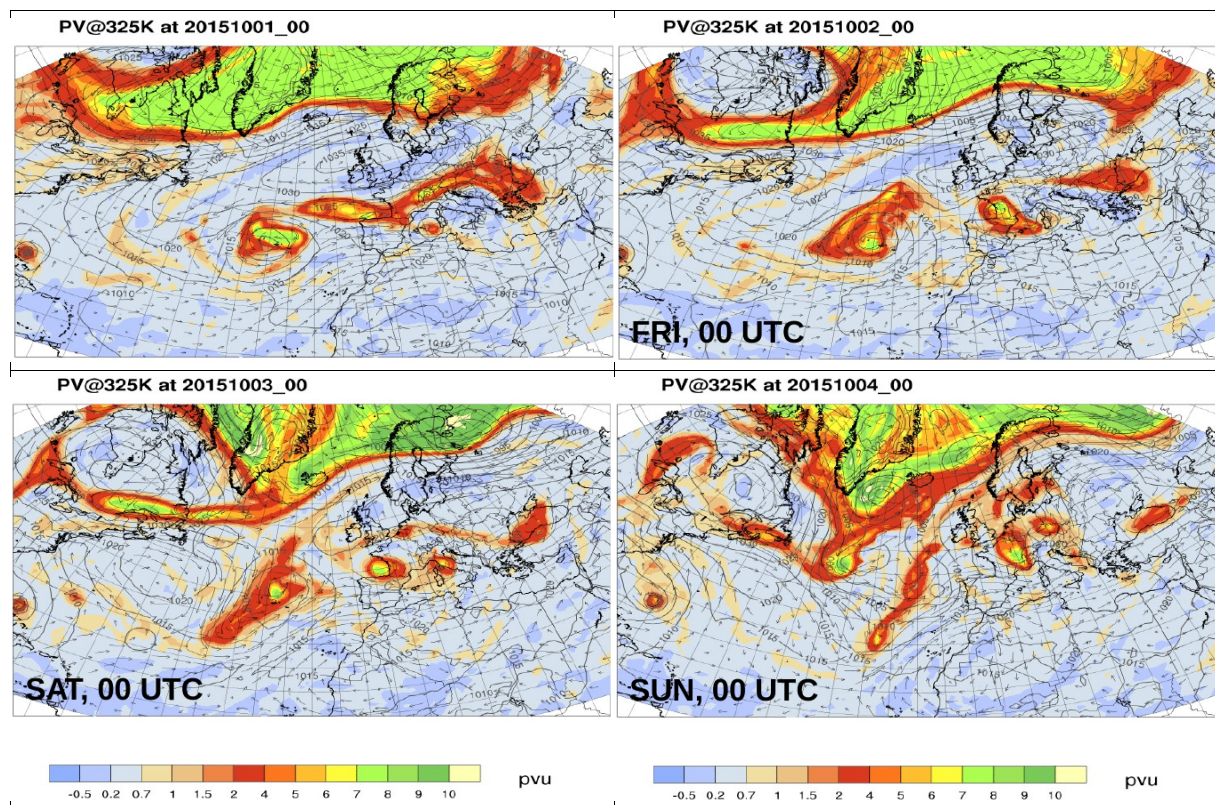


Figure 7.28 As in Figure 7.22, but from 1 to 4 October.

The zonal jet provided optimal conditions for coordinated flights of DLR-Falcon and HALO. Similar to the proposed flight on 28 September coordinated flights in controlled air space enabled us to perform measurements across the jet.

b) Description of flight on 01 October

A proposed flight pattern for 1 October 1200 UTC is indicated Figure 7.29a. With a total flight distance of about 3000 km coordinated flights with the DLR-Falcon and HALO were possible. On 1 October a shallow low pressure system developed north of Iceland in a region of strong moisture flux (Figure 7.29). At the same time, (presumably) diabatically enhanced upper-level divergent winds impinged on the wave guide slightly north of Iceland and contributed to a weak northward deflection of the jet (cf. Figure 7.28). The flight pattern was designed to perform measurements along and across the wave guide, and in a region of strong low-level moisture flux. This way the flight contributed to the following main objectives

- moisture structure in the boundary layer (section 3.2.1), remote sensing measurements of low-level moisture flux not possible all the time due to cloud cover
- structure of mixed phase clouds in developing low-pressure system (section 3.2.2)
- structure of the upper-level PV (section 3.2.3)
- moisture and cloud structure in tropopause region (3.2.6), it should be noted that the outflow height for this event was above FL390 → even for HALO difficult to reach
- quantification of analysis errors in lower- and upper-troposphere (3.2.7)

The flight of HALO could have been extended southward to the center of the upper-level PV lense and its associated anticyclonic circulation. The center of the anticyclone was still located over the UK so that simultaneous airborne and ground-based measurements would have been possible.

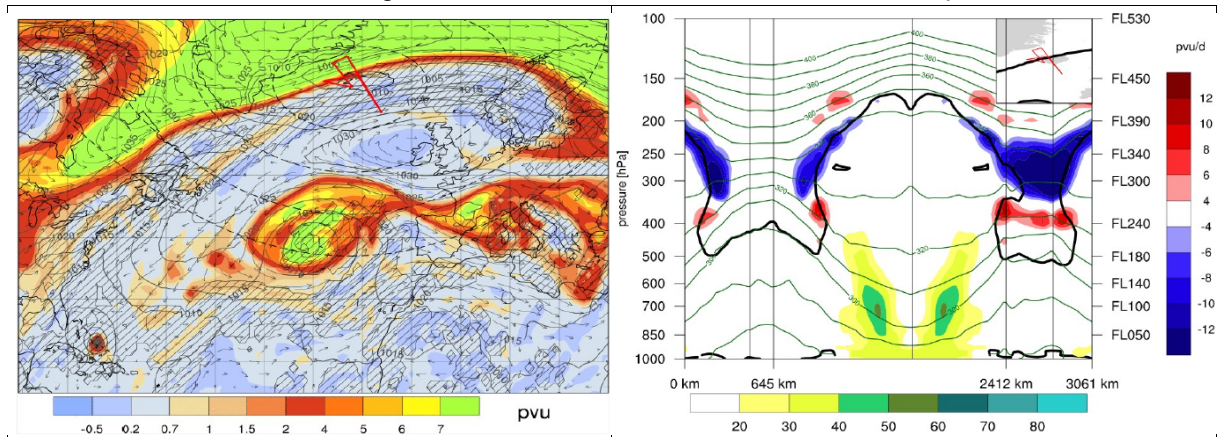


Figure 7.29 a) As in **Figure 7.22**, but on 01 October 1200 UTC. Red line over Iceland indicates proposed flight pattern. b) Vertical cross section along proposed flight pattern. Moisture flux (greenish shading), PV advection by divergent wind (bluish, reddish shading), 2 PVU (black contour), potential temperature (green contours).

Similar flights as the one proposed would have been possible during the following two days. These were characterized by a similar upper-level flow situation. However, cloud diabatic processes were much weaker. This way, a comparison of the upper-level PV structure in regions with strong cloud diabatic heating and with weak cloud diabatic heating might have been of interest in terms of analysis errors. Since a further cyclogenesis and WCB activity was predicted to occur over the North Atlantic we skipped this flight option.

3. Dry run case: Cyclogenesis west of Greenland and WCB over the eastern North Atlantic

a) Synoptic situation

Already on 03 October, 1200 UTC the mean sea level pressure field indicated a cyclogenesis event east of Greenland (Figure 7.28c). This low pressure system intensified quite rapidly ahead of an upper-level trough to a mean sea level pressure of less than 985 hPa on 4 October 0000 UTC (Figure 7.28d). At the same time, a WCB inflow region was located southeast of this cyclone. The WCB trajectories were predicted to move straight north, to ascend over Iceland and to have their outflow north of Iceland on 05 October. As for the first dry run case, this synoptic setup was perfectly designed to perform Lagrangian measurements along the WCB. Downstream of the WCB, a high amplitude ridge developed which extended to about 75N on 5 October.

b) Description of flight on 4 October

The first flight was designed to perform measurements with HALO in the WCB inflow region on 4 October 0000 UTC (Figure 7.30a). At this time, the WCB inflow region was located west of Ireland and thus within reach for HALO. The flight strategy and the primary objectives of that flight were quasi identical to the flight on 27 September. Dropsondes allowed us to obtain information about the boundary moisture structure in the WCB inflow region. In addition, HAMP and WALES provided information about the cloud structure in the WCB inflow region and along the WCB. Since one of the primary objectives of this period was to perform Lagrangian flights we calculated 48 forward trajectories from the flight track to obtain information about the location of airmasses 24 hours after the first flight. Figure 7.30b shows that air masses which were measured during the first flight were expected to be located north of Iceland and between 500 to 400 hPa about 24 hours later (Figure 7.30b). Hence, we decided to perform a second flight on 5 October

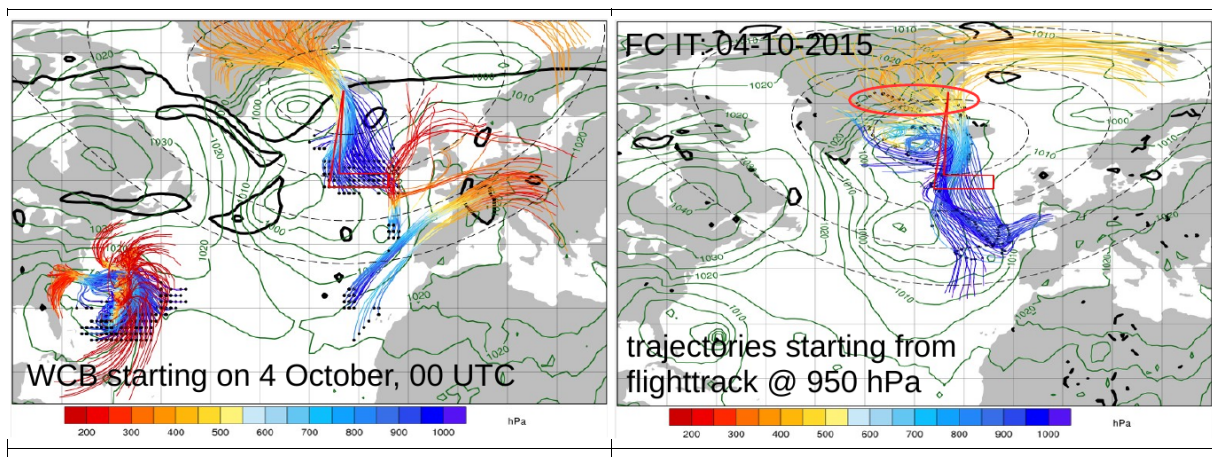


Figure 7.30 WCB trajectories starting on 4 October (colored by pressure), 2 PVU (black contour) and mean sea level pressure (green contours). Red line south of Iceland indicates proposed flight pattern on 4 October. b) as in a), but now showing 48 forward and backward trajectories starting from the flight track at 950 hPa. Red ellipse marks region where air masses are expected to be located 24 hours after the flight on 4 October.

c) Description of flight on 5 October

Similar to the first dry run event, the synoptic situation on 5 October was ideally setup to perform coordinated flights with the DLR-Falcon and HALO. The major advantage of the synoptic setup was that all flights could be conducted in radar controlled air space. This way a certain flexibility concerning the flight level as well as the dropping of sondes ensured to optimize the flight patterns according to the primary objectives of NAWDEX. The proposed flight pattern crossed the jet as well as the ascending WCB air masses twice (Figure 7.31). This way we were able to address many of the NAWDEX primary objectives

- mixed phase clouds in WCB with a focus on across WCB variations of liquid, cloud snow and rain water path (section 3.2.2)
- structure and across jet variation of upper-level PV (section 3.2.3)
- quantification of analysis errors across the midlatitude jet (section 3.2.7)
- Lagrangian Tracking of airmasses (section 3.2.8)

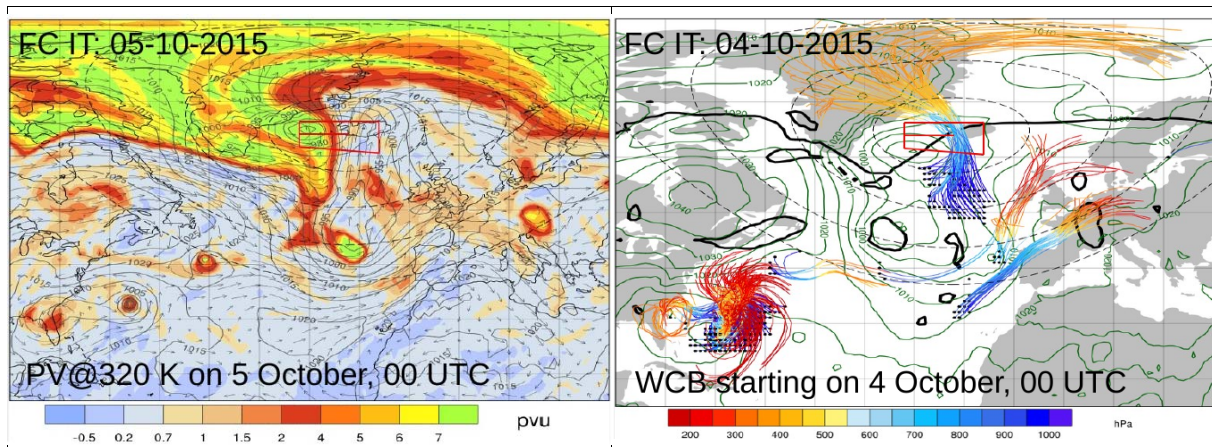


Figure 7.31. a) PV@320K (shading), wind@320K (vectors), mean sea level pressure (gray contours) on 5 October 0000 UTC. b) as in Fig. 9a. Red lines close to Iceland indicate proposed flight pattern.

Depending on the rest periods of the pilots a second flight with the HALO could have been possible on 05 October. This flight could have sampled the cloud structure and moisture variation in the WCB outflow region. Since the outflow of the WCB was relatively low, HALO should have easily reached the outflow height of the WCB at about 400 hPa.

4. Dry run case: ET of Joaquin, downstream PV streamer and severe precipitation over the Mediterranean

a) Synoptic situation

After a period of a relatively far northward position of the midlatitude wave guide, the jet over the Atlantic shifted southward in response to a cyclonic wave breaking over the North Atlantic during the second week of the dry run. In addition, the last days of the NAWDEX dry run were strongly impacted by the ET of Hurricane Joaquin.

Hurricane Joaquin recurved east of North America and approached a highly amplified midlatitude flow on 06 October. At this day, Joaquin was located south of Nova Scotia. Air masses ascended WCB-like to the east of the cyclone center and were transported rapidly into downstream regions. While weather prediction systems struggled to predict Joaquin's track around recurvature time, forecasts were relatively consistent in showing an eastward track of Joaquin across the Atlantic. However, several ensemble prediction systems showed track variations toward the end of Joaquin's life cycle over the eastern North Atlantic. In some scenarios Joaquin moved toward Scotland and in other scenarios Joaquin moved toward the Iberian Peninsula. Forecasts that were initialized on 6 October clearly show this track uncertainty (Figure 7.32).

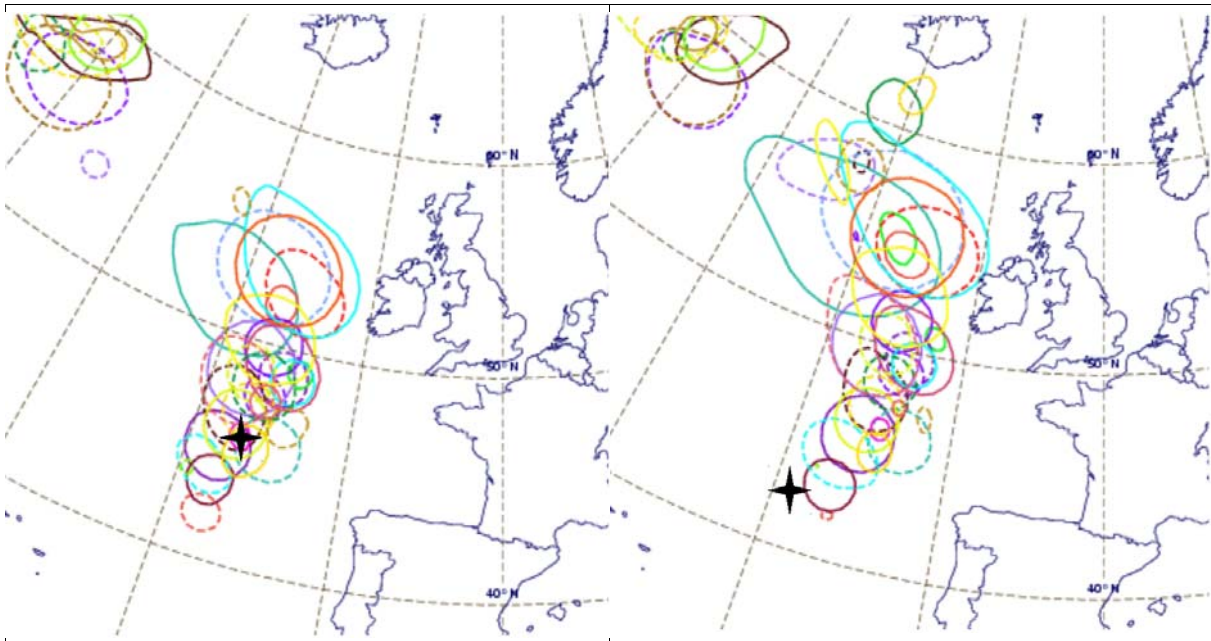


Figure 7.32 96h ECMWF EPS forecasts of MSLP 990-hPa isolines valid on 10 October 2015 0000 UTC. Black star denotes location of Joaquin in deterministic forecast. b) Same as in a), but 102h Météo-France ensemble forecast. Plots provided by Gwendal Revère

In addition, the intensity of WCBs (measured by the number of trajectories ascending more than 600 hPa in 48h) ascending to the east of Joaquin showed substantial variations across the ensemble members which were initialized on 6 October 0000 UTC. For example, ensemble member 29 did not show an indication of WCB-like ascending airmasses on 8 October, 1200 UTC (Figure 7.33a). In contrast, in ensemble member 34 a relatively strong WCB developed (Figure 7.33b). The difference in WCB activity between the two ensemble members suggests that in member 34 a more pronounced downstream anticyclone evolved in response to diabatic processes and the reduction of upper-level PV. This in turn affected presumably the track of Joaquin. The stronger anticyclone in member 34 induced a southerly flow on its western flank which steered Joaquin northward (Figure 7.33d). This did not happen in ensemble member 29. Here, Joaquin moved on a more southward track toward the Iberian peninsula (Figure 7.33c). The analysis suggests that the correct representation of the intensity of diabatic processes to the east of Joaquin was essential for an accurate prediction of Joaquin's track.

The deterministic forecast as well as the EPS forecasts initialized on 6 October indicated a WCB inflow region west of the Azores (and east of Joaquin) on 8 October. This forecast finally verified. Joaquin crossed the North Atlantic to the North of the Azores and a quite intense WCB developed east of Joaquin's center. The WCB air masses ascended rapidly to above 300 hPa into a weak ridge over the eastern Atlantic and the Iberian peninsula. Above the region of strongest ascent, upper-level divergent winds impinged on the midlatitude wave guide and contributed to an amplification of this ridge.

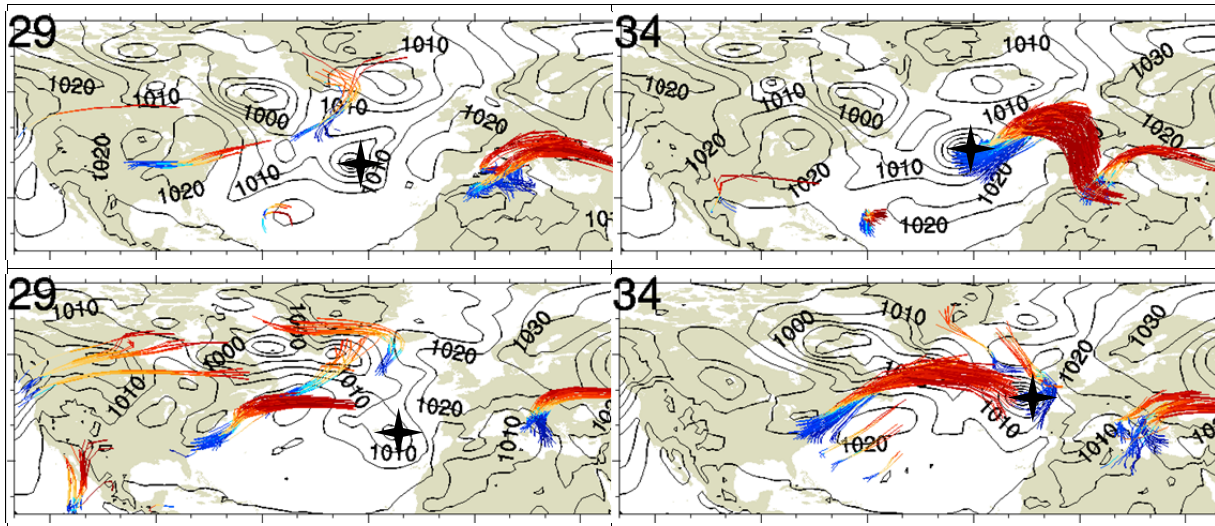


Figure 7.33 MSLP (black contours) and WCB trajectory forecasts initialized on 6 October 2015 0000 UTC and valid on (a, b) 08 October 2015 1200 UTC and (c, d) 10 October 0000 UTC.. (a, c) ensemble member 29, (b, d) ensemble member 34. Black stars denote location of Joaquin.

A relatively narrow trough formed to the east of this ridge as part of the downstream development. Ahead of this trough a further WCB developed over the Mediterranean region on 10 October. This WCB and embedded convection caused severe precipitation over Italy and the Balkan peninsula (only in German: http://www.wettergefahren-fruehwarnung.de/Ereignis/20151013_e.html).

b) Description of flight on 8 October

The inflow region of the WCB immediately to the east of Joaquin on 8 October would have definitely not been within reach from Iceland. Hence, we considered a transfer flight of HALO from Iceland to the Azores (flight time about 4-5 hours). As such a transfer flight would spend several flight hours, its realization would certainly depend on the previous progress of the field campaign. As this situation was quite promising concerning the NAWDEX primary objectives, we planned Lagrangian flights into the inflow and outflow of WCB-like ascending air masses.

The first flight was scheduled for 08 October 1200 UTC. At this time, the WCB inflow region was located east of the Azores. The flight on 8 October aimed to investigate the moisture structure in the boundary layer of the WCB inflow region. Following the proposed flight track in Figure 7.34b, we measured in the inflow region of WCB-like ascending trajectories which reached levels above 300 hPa about 24 to 48 hours later. Since the airspace around the Azores is radar controlled airspace various flight levels - in addition to the chosen one - might have been possible.

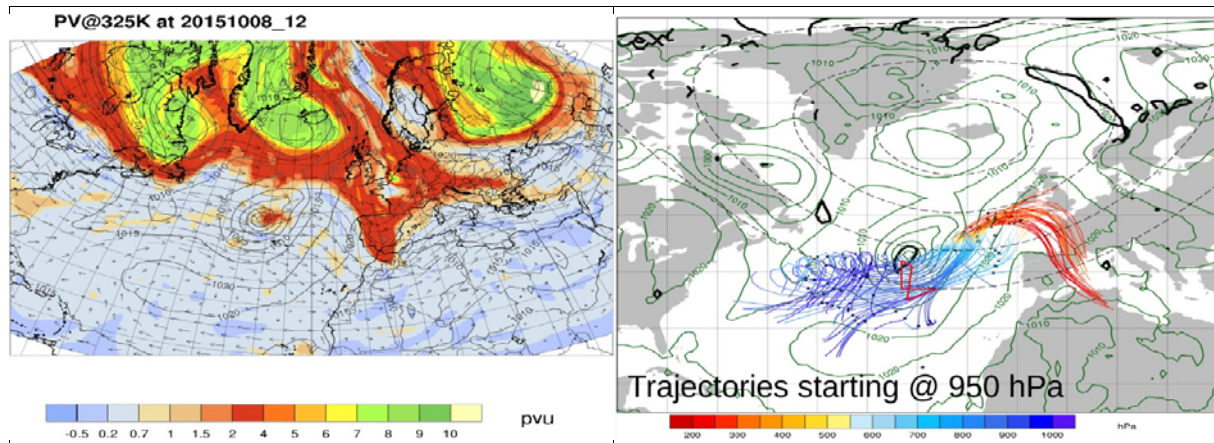


Figure 7.34 a) PV@325K (shading), wind@325K (vectors), mean sea level pressure (gray contours) on 8 October 1200 UTC. b) as in Fig. 9a. Red lines close to the Azores indicate proposed flight pattern.

c) Description of flight on 9 October

The last flight of the NAWDEX dry run was designed to measure air masses in the WCB outflow region which had been sampled in the WCB inflow region on 8 October. Thus, we designed a flight pattern from the Azores in northeasterly directions. On the first leg of the flight, we sampled air masses in the subtropical jet which had not experienced lifting during the previous 24 hours. Shortly after crossing Joaquin's center we reached air masses which ascended in the WCB to the east of Joaquin. Backward trajectories from the flight track reveal that we sampled air masses which started to ascend 24 hours previously east of the Azores. This flight addressed several main NAWDEX objectives

- mixed phase clouds along/across WCB like ascending air masses (Fig. 15)
- diabatic effects on cyclonic systems (section 3.2.4) since we crossed the center of “ex”-Joaquin
- moisture and cloud structure in tropopause region (section 3.2.6)
- quantification of analysis errors (section 3.2.7)
- Lagrangian tracking of disturbances (section 3.2.8)

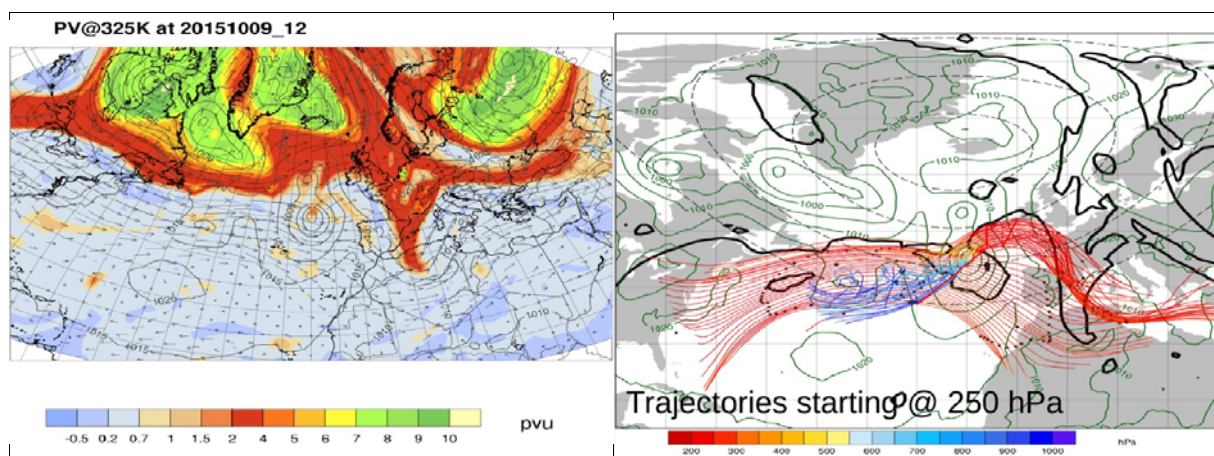


Figure 7.35 As in Fig. 7.30, but on 9 October 1200 UTC.

As the airmasses ascending to the east of Joaquin were rapidly moving eastward, a return flight to the Azores was not possible

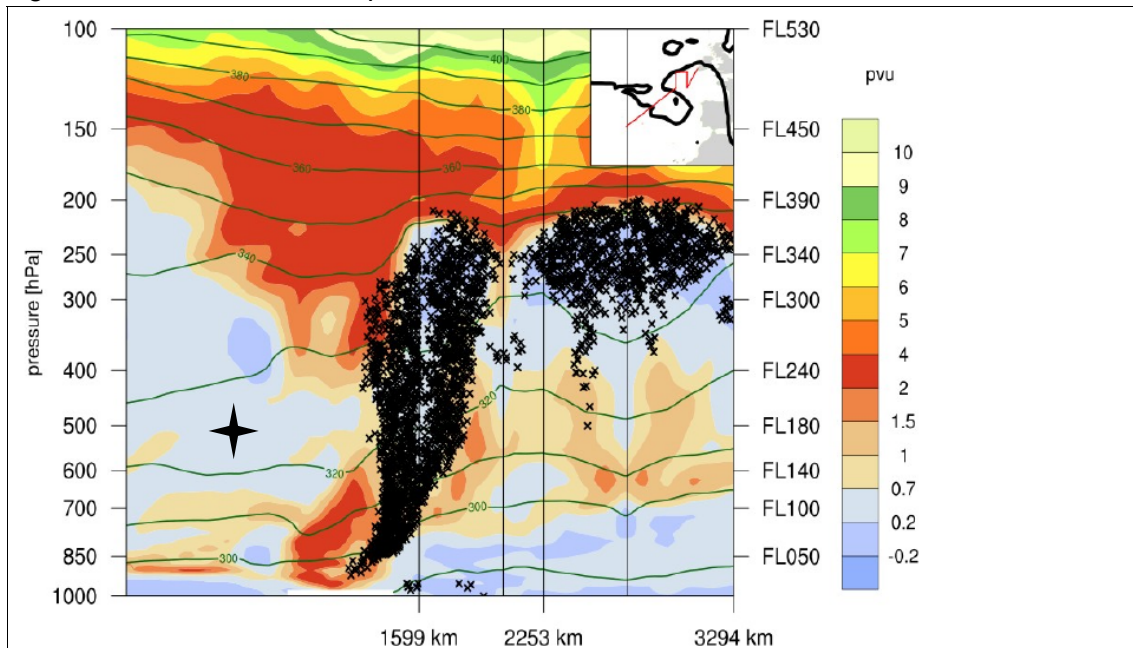


Figure 7.36 Cross section of PV (shading), potential temperature (green contours) and WCB trajectories intersecting with the cross section (black crosses) along flight track on 9 October 1200 UTC. Black star indicates location of remnant PV tower of Joaquin.

7.4.2 Summary

Lessons learned - General flight planning:

- Iceland is the right location to access the North Atlantic
- discussion between the partners works very well. overall we have common objectives and a common language, which is very helpful then for the real, likely more stressful, flight planning
- the strategy to fly low for upstream flights and high in radar controlled air space over Iceland worked well for the dry run cases
- ADBOBE Connect was a valuable instrument for the dryrun.
- communication by videoconferencing works, but is not as good as when being together in a room - several of us should be physically in Iceland during the campaign (and of course others can join via video).

Aims addressed during dry run

- moisture structure in the boundary layer *
- Mixed phase clouds **
- Upper level PV ***
- Diabatic effects on cyclonic systems *
- Impacts of tropopause waveguide uncertainty on HIW events xx
- Moisture and cloud structure in tropopause region */xx
- Quantification of analysis errors
- Lagrangian Tracking of disturbances

Lessons learned - Flight planning tools

- worked fine and allowed a sophisticated weather discussion
- We saw that some additional **ENS information** (e.g. Spaghetti plots) are needed
 - ETH Spaghetti of 2PV contour implemented
 - Gwendals spaghetti of surface pressure very helpful. Operational?
- Do we see **PV Anomalies on the stratospheric side of the jetstream** and can we see radiative impact on observed airmasses? Same for PV lenses.
 - Johns RDF trajectories would be valuable to see potential changes in Theta
 - Trajectories from flight track with time series of theta, pressure, thetaE to see heating from different diabatic processes?
- **Adjoint sensitivity** calculations are an interesting tool. Target box can be shifted to regions of HIW during NAWDEX.
- **Interest** in a demonstration of **Met3D** by Marc Rautenhaus in upcoming weeks
 - **A workshop will be organized by CRC waves to weather in spring 2016 for a scientific discussion, in-depth filing of flight strategies for discussed cases**
- What else do we need?

8 Forecasting products

For the planning of the flights a set of automatic products and flexible tools are required. Part of the forecasting tools was already developed during T-NAWDEX-Falcon and will be adapted. Here we give only a short overview..

8.1 NWP Forecasts

8.1.1 Mission support system (MSS)

The MSS allows an interactive planning of flight routes in the context of ECMWF's operational forecasts. Various products can be visualized for desired geographical sections and vertical levels. The tool calculates cross sections along planned flight routes. It also contains a flight performance calculation for HALO and Falcon. Further information can be found in Rautenhaus et al. 2012.

- Web-Map-Service-based system; Python client runs on all systems
- DLR server operational with ECMWF forecasts: <http://mss.pa.op.dlr.de>
→ further data sources can be integrated
- Support for predefined maps, vertical sections, flight profiles, flight performance
→ required forecast products need to be defined in advance

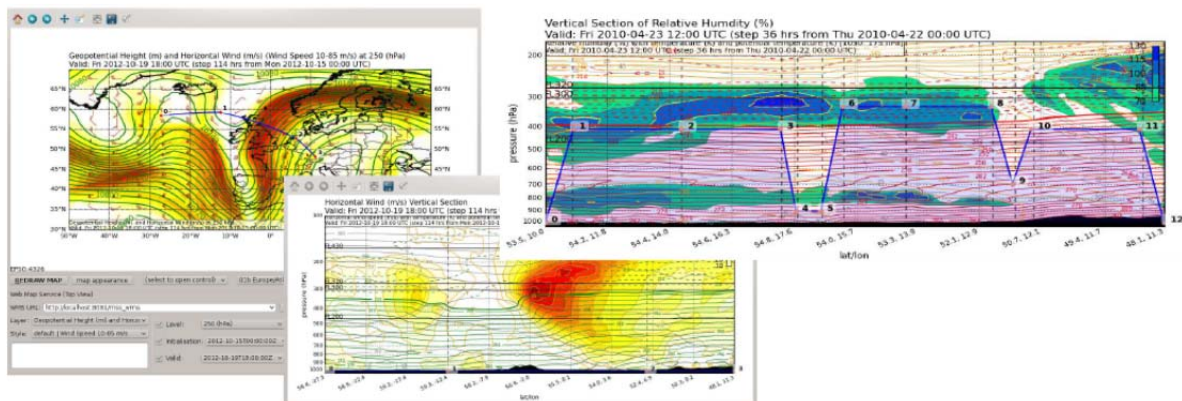
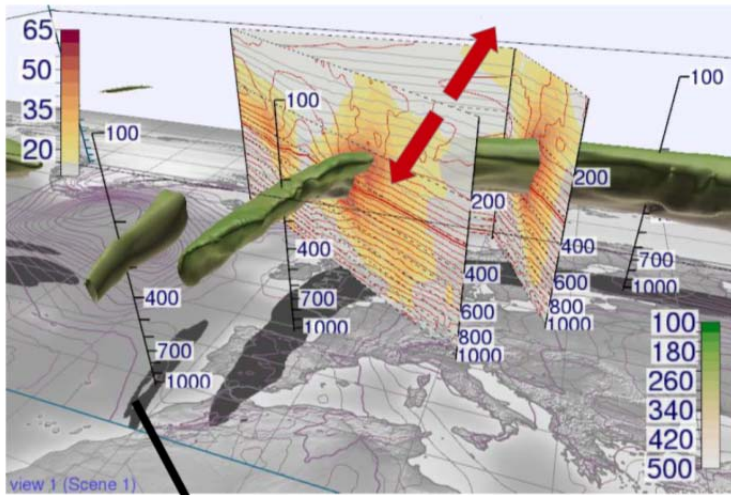


Figure 8.1 Examples of flight planning images created with the MSS. Left image shows 300 hPa Geopotential Height and Winds. Blue line shows planned flight track. Middle panel shows cross sections of wind and potential temperature along the flight track. Right Panel shows cross section of simulated relative humidity with a planned flight profile

8.1.2 Met 3D

Met-3D is a recent development to improve forecasting for flight planning by use of ensemble uncertainty information and advanced 3D exploration techniques (Rautenhaus 2015a,b). Unlike MSS the Ensemble data has to be stored locally.



- Met.3D open-source repository: <https://bitbucket.org/wxmetvis/met.3d>
- Currently optimised for ECMWF data but other model data possible
- Requires data on-site → check internet bandwidth at campaign site and remote visualization options
- Work in progress: Interactive Skew–T–Diagrams / LAGRANTO integration / integrated flight performance with real-time visual feedback
- NAWDEX: store high-res ensemble data set for analysis and visualization research
- Future plans in DFG Waves to weather:
 - Uncertainty visualization, feature-based ensemble visualization (detection & visualization of 3D jet & cyclonic & ... features)
 - Analysis of NAWDEX data sets in context of operational products

8.1.3 Trajectory calculations and additional products

Using the latest ECMWF forecasts, different charts are provided via a web page:

- WCB probability calculated from WCB trajectories in all 51 ensemble forecast members
- WCB trajectories from the deterministic forecast (Figures 7.19, 7.23, 7.25)
- PV and wind, and divergent wind, advection of PV with the divergent wind, and water vapour transport at various isentropic levels (Figure 7.31)
- surface sensible and latent heat flux

A special feature is the cross section tool which simply allows to draw linked cross sections in different directions to plan the legs of the research flights. There, the variables mentioned in the 3rd bulled point can be shown (Figures 7.20, 7.21, 7.24). Of further relevance are the origin and the track of the air masses to be measured. An online tool calculates forward and backward trajectories from an arbitrary flight route drawn in the horizontal plot from bullet point 3. The forecast products can be extended by further variables and charts on request.

8.2 Satellite products

8.3 Additional links to forecast products



9 References

- Agusti-Panareda A, Thorncroft CD, Craig GC, Gray SL. 2004. The extratropical transition of hurricane Irene (1999): A potential-vorticity perspective. *Q. J. R. Meteorol. Soc.*, **130**: 1047–1074.
- Bhawar R, Di Girolamo P, Summa D, Flamant C, Althausen D, Behrendt A, Kiemle C, Bosser P, Cacciani M, Champollion C et al., 2011: The water vapour intercomparison effort in the framework of the convective and orographically induced precipitation study: airborne-to-ground-based and airborne-to-airborne lidar systems. *Q. J. R. Meteorol. Soc.*, **137**: 325–348.
- Boettcher M, Wernli H. 2011. Life Cycle Study of a Diabatic Rossby Wave as a Precursor to Rapid Cyclogenesis in the North Atlantic—Dynamics and Forecast Performance. *Mon. Wea. Rev.*, **139**, 1861–1878.
- Bony S, Stevens B, Frierson DM, Jakob C, Kageyama M, Pincus R, Shepherd TG, Sherwood SC, Siebesma AP, Sobel A, Watanabe M, Webb MJ. 2015. Clouds, circulation and climate sensitivity. *Nature Geoscience*, **8**: 261–268.
- Browning KA, Hardman ME, Harrold TW, Pardoe CW. 1973. Structure of rainbands within a mid-latitude depression. *Q. J. R. Meteorol. Soc.*, **99**: 215–231.
- Čampa J, Wernli H. 2012. A PV Perspective on the Vertical Structure of Mature Midlatitude Cyclones in the Northern Hemisphere. *J. Atmos. Sci.*, **69**, 725–740.
- Carlson TN. 1980. Airflow through midlatitude cyclones and the comma cloud pattern. *Mon. Wea. Rev.*, **108**: 1498–1509.
- Cavallo SM, Hakim GJ. 2010. Composite Structure of Tropopause Polar Cyclones. *Mon. Wea. Rev.*, **138**: 3840–3857.
- Cavallo SM, Hakim GJ. 2012. Radiative impact on tropopause polar vortices over the Arctic. *Mon. Wea. Rev.*, **140**: 1683–1702.
- Chaboureaud J-P, Claud C. 2006. Satellite-based climatology of Mediterranean cloud systems and their association with large-scale circulation, *J. Geophys. Res.*, **111**, D01102
- Chaboureaud J-P, Pantillon F, Lambert D, Richard E, Claud C. 2012. Tropical transition of a Mediterranean storm by jet crossing. *Q. J. R. Meteorol. Soc.*, **138**: 596–611.
- Chagnon J, Gray S, Methven J. 2013. Diabatic processes modifying potential vorticity in a North Atlantic cyclone. *Q. J. R. Meteorol. Soc.*, **139**: 1270–1282.
- Cordeira JM, Ralph FM, Moore BJ. 2013. The development and evolution of two atmospheric rivers in proximity to western North Pacific tropical cyclones in October 2010. *Mon. Wea. Rev.*, **141**: 4234–4255.
- Davis CA, Stoelinga MT, Kuo YH. 1993. The integrated effect of condensation in numerical simulations of extratropical cyclogenesis. *Mon. Wea. Rev.*, **121**: 2309–2330.
- Davies HC, Didone M. 2013. Diagnosis and Dynamics of Forecast Error Growth. *Mon. Wea. Rev.*, **141**: 2483–2501.
- Dirren S, Didone M., Davies HC. 2003. Diagnosis of “forecast-analysis” differences of a weather prediction system. *Geophys. Res. Lett.*, **30**: 2060. doi:10.1029/2003GL017986
- Done J, Craig G, Gray S, Clark P, Gray M, 2006: Mesoscale simulations of organized convection: Importance of convective equilibrium. *Q. J. R. Meteorol. Soc.*, **132**: 737–756.
- Doyle, J.D., C. Amerault, C.A. Reynolds, P. Alex Reinecke, 2014: Initial condition sensitivity and predictability of a severe extratropical cyclone using a moist adjoint. *Mon. Wea. Rev.*, **142**, 320–342
- Ehrlich A, Bierwirth E, Wendisch M, Gayet JF, Mioche G, Lampert A, Heintzenberg, J, 2008. Cloud phase identification of Arctic boundary-layer clouds from airborne spectral reflection measurements: Test of three approaches, *Atmos. Chem. Phys.*, **8**, 7493–7505, DOI: 10.5194/acp-8-7493-2008
- Errico, RM, 1997: What is an adjoint model? *Bull. Amer. Meteor. Soc.*, **78**: 2577–2591.
- Ewald F, Kölling T, Baumgartner A, Zinner T, Mayer B. 2015. Design and characterization of specMACS, a multipurpose hyperspectral cloud and sky imager. *Atmos. Meas. Tech. Discuss.*, **8**, 9853–9925, doi:10.5194/amtd-8-9853-2015, 2015
- Forster PM, Shine KP. 1997. Radiative forcing and temperature trends from stratospheric ozone changes. *J. Geophys. Res.*, **102**: 10841–10855.
- Fricke C, Ehrlich A, Jäkel E, Bohn B, Wirth M, Wendisch M. 2014. Influence of local surface albedo variability and ice crystal shape on passive remote sensing of thin cirrus, *Atmos. Chem. Phys.*, **14**, 1943–1958.
- Grams CM, Wernli H, Boettcher M, Campa J, Corsmeier U, Jones SC, Keller JH, Lenz CJ, Wiegand L. 2011. The key role of diabatic processes in modifying the upper tropospheric wave guide: a North Atlantic case-study. *Q. J. R. Meteorol. Soc.*, **137**: 2174–2193.
- Gray S, Dunning C, Methven J, Masato G, Chagnon J. 2014. Systematic model forecast error in Rossby wave structure. *Geophys. Res. Lett.*, **41**: 2979–2987.
- Hartmann, D. L., et al., 1989: Potential vorticity and mixing in the south polar vortex during spring. *J. Geophys. Res. Atmos.*, **94**: 11 625–11 640.
- Klippertz P, Martin JE. 2005. Tropical plumes and extreme precipitation in subtropical and tropical West Africa. *Q. J. R. Meteorol. Soc.*, **131**: 2337–2365.
- Keil C, Heinlein F, Craig GC. 2013. The convective adjustment time-scale as indicator of predictability of convective precipitation. *Q. J. R. Meteorol. Soc.*, **140**: 480–490.

- Kew SF, Sprenger M, Davies HC. 2010. Potential Vorticity Anomalies of the Lowermost Stratosphere: A 10-Yr Winter Climatology. *Mon. Wea. Rev.*, **138**: 1234–1249.
- Kiemle C, Brewer WA, Ehret G, Hardesty RM, Fix A, Senff C, Wirth M, Poberaj G, LeMone MA. 2007. Latent heat flux profiles from collocated airborne water vapor and wind lidars during IHOP_2002. *J. Atmos. Oceanic Technol.*, **24**: 627–639.
- Kiemle C, Wirth M, Fix A, Rahm S, Corsmeier U, Di Girolamo P. 2011. Latent heat flux measurements over complex terrain by airborne water vapour and wind lidars. *Q. J. R. Meteorol. Soc.*, **137**: 190–203.
- Klepp C, Ament F, Bakan S, Hirsch L, Stevens. 2014. NARVAL Campaign Report, Reports on Earth System Science, Max-Planck-Institut für Meteorologie, available at http://www.mpimet.mpg.de/fileadmin/publikationen/Reports/WEB_BzE_164_last.pdf
- Kuo YH, Shapiro MA, Donall EG. 1991. The interaction between baroclinic and diabatic processes in a numerical simulation of a rapidly intensifying extratropical marine cyclone. *Mon. Wea. Rev.*, **119**: 368–384.
- Joos H, Forbes R. 2015. Impact of different IFS microphysics on a warm conveyor belt and the downstream flow evolution. *Q. J. R. Meteorol. Soc.*, in preparation.
- Joos H, Wernli W. 2012. Influence of microphysical processes on the potential vorticity development in a warm conveyor belt: a case-study with the limited-area model COSMO. *Q. J. R. Meteorol. Soc.*, **138**: 407–418.
- Langland, R. H., M. A. Shapiro, and R. Gelaro, 2002: Initial condition sensitivity and error growth in forecasts of the 25 January 2000 east coast snowstorm. *Mon. Wea. Rev.*, **130**, 957–974.
- Langland, R., R. Gelaro, G. Rohaly, and M. Shapiro, 1995: Evaluation of physical processes in an idealized extratropical cyclone using adjoint sensitivity. *Quart. J. Roy. Meteor. Soc.*, **121**, 1349–1386.
- Madonna E, Wernli H, Joos H, Martius O. 2014. Warm Conveyor Belts in the ERA-Interim Dataset (1979–2010). Part I: Climatology and Potential Vorticity Evolution. *J. Climate*, **27**: 3–26.
- Magnusson L, Källén E. 2013. Factors influencing skill improvements in the ECMWF forecasting system. *Mon. Wea. Rev.*, **141**: 3142–3153.
- Martínez-Alvarado O, Joos H, Chagnon J, Boettcher M, Gray SL, Plant RS, Methven J, Wernli H. 2014. The dichotomous structure of the warm conveyor belt. *Q.J.R. Meteorol. Soc.*, **140**: 1809–1824. doi: 10.1002/qj.2276
- Martínez-Alvarado O, Plant RS. 2014. Parametrized diabatic processes in numerical simulations of an extratropical cyclone. *Q. J. R. Meteorol. Soc.*, **140**: 1742–1755.
- Martius O, Zenklusen E, Schwierz C, Davies HC. 2006. Episodes of Alpine heavy precipitation with an overlying elongated stratospheric intrusion: A climatology. *Int. J. Climatol.* **26**: 1149–1164.
- Martius O, Schwierz C, Davies HC. 2010. Tropopause-Level Waveguides. *J. Atmos. Sci.*, **67**: 866–879.
- Massacand AC, Wernli H, Davies HC. 2001. Influence of upstream diabatic heating upon an alpine event of heavy precipitation. *Mon. Wea. Rev.*, **129**: 2822–2828.
- Mech M, Orlandi E, Crewell S, Ament F, Hirsch L, Hagen M, Peters G, Stevens B. HAMP – the microwave package on the High Altitude and Long range research aircraft (HALO). 2014. *Atmos. Meas. Tech.*, **7**(12):4539–4553.
- Melchionna S, Bauer M, and Peters G: A new algorithm for the extraction of cloud parameters using multipeak analysis of cloud radar data – First application and preliminary results, *Meteorol. Z.*, **17**, 613–620, 2008.
- Moore RW, Montgomery MT, Davies HC. 2008. The integral role of a diabatic Rossby vortex in a heavy snowfall event. *Mon. Wea. Rev.*, **136**: 1878–1897.
- Pomroy HR, Thorpe AJ. 2000. The evolution and dynamical role of reduced upper-tropospheric potential vorticity in intensive observing period one of FASTEX. *Mon. Wea. Rev.*, **128**: 1817–1834.
- Paffrath U, Lemmerz C, Reitebuch O, Witschas B, Nikolaus I, Freudenthaler V. 2009. The airborne demonstrator for the direct-detection Doppler wind lidar ALADIN on ADM-Aeolus: II. Simulations and Rayleigh receiver radiometric performance. *J. Atmos. Ocean. Tech.*, **26**: 2516–2530.
- Parker DJ, Thorpe AJ. 1995. Conditional convective heating in a baroclinic atmosphere: a model of convective frontogenesis. *J. Atmos. Sci.*, **52**: 1699–1711.
- Rasp S. 2015. High-Resolution Trajectory Analysis of Vertical Motions in Different Weather Situations. MSc Dissertation, Ludwig-Maximilians-Universität München.
- Rautenhaus M, Bauer G, Dörnbrack A. 2012. A web service based tool to plan atmospheric research flights, *Geosci. Model Dev.*, **5**: 55–71, doi:10.5194/gmd-5-55-2012
- Rautenhaus M, Kern M, Schäfler A, Westermann R. 2015. 3-D visualization of ensemble weather forecasts – Part 1: The visualization tool Met.3D (version 1.0), *Geosci. Model Dev.*, **8**, 2329–2353, doi:10.5194/gmd-8-2329-2015, 2015.
- Rautenhaus M, Grams, C M, Schäfler A, Westermann R. 2015. 3-D visualization of ensemble weather forecasts – Part 2: Forecasting warm conveyor belt situations for aircraft-based field campaigns, *Geosci. Model Dev.*, **8**, 2355–2377, doi:10.5194/gmd-8-2355-2015, 2015.
- Reitebuch O, Lemmerz C, Nagel E, Paffrath U, Durand Y, Endemann M, Fabre F, Chaloupy M. 2009. The airborne demonstrator for the direct-detection Doppler wind lidar ALADIN on ADM-Aeolus: I. Instrument design and comparison to satellite instrument. *J. Atmos. Ocean. Tech.*, **26**: 2501–2515.
- Riemer M, Jones SC. 2010. The downstream impact of tropical cyclones on a developing baroclinic wave in idealized scenarios of extratropical transition. *Q. J. R. Meteorol. Soc.*, **136**: 617–637.
- Richardson D, Bidlot J, Ferranti L, Ghelli A, Haiden T, Hewson T, Janousek M, Prates F, Vitart F. 2012: Verification statistics and evaluations of ECMWF forecasts in 2011–2012. ECMWF Technical Memorandum, 688.

- Rodwell, M. J., Magnusson L, Bauer P, Bechtold P, Bonavita M, Cardinali C, Diamantakis M, Earnshaw P, Garcia-Mendez A, Isaksen L, Källén E, Klocke D, Lopez P, McNally T, Persson A, Prates F, Wedi N. 2013. Characteristics of occasional poor medium-range weather forecasts for Europe. *Bull. Amer. Meteor. Soc.*, 94: 1393-1405.
- Rossa AM, Wernli H, Davies HC. 2000. Growth and decay of an extratropical cyclone's PV-tower. *Meteorol. Atmos. Phys.*, 73: 139–156.
- Schäfler A, Dörnbrack A, Kiemle C, Rahm S, Wirth M. 2010. Tropospheric water vapour transport as determined from airborne lidar measurements. *J. Atmos. Oceanic Technol.*, 27: 2017–2030.
- Schäfler A, Boettcher M, Grams CM, Rautenhaus M, Sodemann, Wernli H. 2014. Planning of aircraft measurements within a warm conveyor belt. *Weather*, 69: 161–166. doi: 10.1002/wea.2245
- Schäfler A, Harnisch F. 2015. Impact of the inflow moisture on the evolution of a Warm Conveyor Belt. *Q.J.R. Meteorol. Soc.*, 141: 299–310. doi: 10.1002/qj.2360
- Schwierz C, Dirren S, Davies HV. 2004. Forced Waves on a Zonally Aligned Jet Stream. *J. Atmos. Sci.*, 61: 73–87
- Selz T, Craig GC. 2015. Upscale error growth in a high-resolution simulation of a summertime weather event over Europe. *Mon. Wea. Rev.*, 143: 813-827.
- Shapiro MA. 1978. Further evidence of the mesoscale and turbulent structure of upper level jet stream-frontal zone systems. *Mon. Wea. Rev.*, 106: 1100-1111.
- Torn, R. D., G. J. Hakim, 2009: Initial Condition Sensitivity of Western Pacific Extratropical Transitions Determined Using Ensemble-Based Sensitivity Analysis. *Mon. Wea. Rev.*, 137, 3388-3406.
- Vaughan, G., S. J. Pepler, and D. S. McKenna, 1996: Aircraft measurements of potential vorticity and Richardson number in baroclinic zones. *Quart. J. Roy. Meteor. Soc.*, 122: 721–735.
- Weissmann M, Busen R, Dörnbrack, A Rahm S, Reitebuch O. 2005. Targeted Observations with an Airborne Wind Lidar. *J. Atmos. Ocean. Tech.*, 22: 1706-1719.
- Wendisch M, Pöschl U, Andreae MO, Machado LAT, Albrecht R, et al. 2015. The ACRIDICON-CHUVA campaign to study tropical deep convective clouds and precipitation using the new German research aircraft HALO. Submitted to *Bull. Am. Meteorol. Soc*
- Werner F, Siebert H, Pilewskie P, Schmeissner T, Shaw RA, Wendisch M. 2013. New airborne retrieval approach for trade wind cumulus properties under overlying cirrus, *J. Geophys. Res. Atmospheres*, 118, 3634-3649.
- Wernli H, Davies HC. 1997. A Lagrangian-based analysis of extratropical cyclones. I. The method and some applications. *Q. J. R. Meteorol. Soc.*, 123: 1677–1706.
- Wernli H. 1997. A Lagrangian-based analysis of extratropical cyclones. II. A detailed case-study. *Q. J. R. Meteorol. Soc.*, **123**: 467–489.
- Wernli H, Dirren S, Liniger M, Zillig M. 2002. Dynamical aspects of the life-cycle of the winter storm 'Lothar', *Q. J. R. Meteorol. Soc.*, **128**: 405-429.
- Wirth M, Fix A, Mahnke P, Schwarzer H, Schrandt F, Ehret G. 2009. The airborne multi-wavelength water vapor differential absorption lidar WALES: system design and performance. *Appl. Phys. B*, **63**: XX-XX
- Zierl B, Wirth V. 1997. The influence of radiation on tropopause behavior and stratosphere-troposphere exchange in an upper tropospheric anticyclone. *J. Geophys. Res.*, **102**: 23883– 23894.
- Zhu H, Thorpe A. 2006. Predictability of Extratropical Cyclones: The Influence of Initial Condition and Model Uncertainties. *J. Atmos. Sci.*, **63**: 1483–1497.
- Zhang F, Bei N, Rotunno R, Snyder C Epifanio CC. 2007. Mesoscale predictability of moist baroclinic waves: Convection-permitting experiments and multistage error growth dynamics. *J. Atmos. Sci.*, 64: 3579-3594.